



KUNGL
TEKNISKA
HÖGSKOLAN



Numerical approximations of time domain
boundary integral equation for wave propagation

Andreas Atle

Stockholm 2003

Licentiate Thesis
Stockholm University
Department of Numerical Analysis and Computer Science

Akademisk avhandling som med tillstånd av Kungl Tekniska Högskolan framläggas till offentlig granskning för avläggande av filosofie licentiatexamen tisdagen den 28 oktober 2003 kl 14.45 i D31, Lindstedtsvägen 3, Kungl Tekniska Högskolan, Stockholm.

ISBN 91-7283-599-0

TRITA-0320

ISSN 0348-2952

ISRN KTH/NA/R-03/20-SE

© Andreas Atle, October 2003

Universitetsservice US AB, Stockholm 2003

Abstract

Boundary integral equation techniques are useful in the numerical simulation of scattering problems for wave equations. Their advantage over methods based on partial differential equations comes from the lack of phase errors in the wave propagation and from the fact that only the boundary of the scattering object needs to be discretized. Boundary integral techniques are often applied in frequency domain but recently several time domain integral equation methods are being developed.

We study time domain integral equation methods for the scalar wave equation with a Galerkin discretization of two different integral formulations for a Dirichlet scatterer. The first method uses the Kirchhoff formula for the solution of the scalar wave equation. The method is prone to get unstable modes and the method is stabilized using an averaging filter on the solution. The second method uses the integral formulations for the Helmholtz equation in frequency domain, and this method is stable. The Galerkin formulation for a Neumann scatterer arising from Helmholtz equation is implemented, but is unstable.

In the discretizations, integrals are evaluated over triangles, sectors, segments and circles. Integrals are evaluated analytically and in some cases numerically. Singular integrands are made finite, using the Duffy transform.

The Galerkin discretizations uses constant basis functions in time and nodal linear elements in space. Numerical computations verify that the Dirichlet methods are stable, first order accurate in time and second order accurate in space. Tests are performed with a point source illuminating a plate and a plane wave illuminating a sphere.

We investigate the On Surface Radiation Condition, which can be used as a medium to high frequency approximation of the Kirchhoff formula, for both Dirichlet and Neumann scatterers. Numerical computations are done for a Dirichlet scatterer.

ISBN 91-7283-599-0 • TRITA-0320 • ISSN 0348-2952 • ISRN KTH/NA/R-03/20-SE

Acknowledgments

I wish to thank my advisor, Prof. Björn Engquist, for his support, guidance and encouragement throughout this work.

I would also like to thank all my good friends and colleagues at NADA for making NADA a nice place to work at.

Financial support has been provided by the Parallel and Scientific Computing Institute (PSCI), Vetenskapsrådet (VR) and NADA, and is gratefully acknowledged.

Contents

1	Introduction	1
1.1	Dirichlet surface	3
1.2	Neumann surface	4
1.3	Outline	4
2	Integral equations using Kirchoff formula	7
2.1	The scalar wave equation	7
2.1.1	Dirichlet problem	9
2.1.2	Neumann problem	10
2.1.3	Robin problem	10
2.2	Maxwell's equations	10
2.2.1	The electromagnetic potentials	12
2.2.2	Integral representation of the potentials	13
2.2.3	Integral representation of charges	14
2.2.4	Integral representation of the fields	14
3	Variational formulations from frequency domain	15
3.1	Functional analysis	15
3.2	Basis functions in space and time	16
3.3	Variational formulation, Dirichlet case	17
3.4	Variational formulation, Neumann case	18
3.5	Point representation on triangle plane	19
3.6	Integrals over time	22
3.7	Dirichlet discretization	23
3.8	Neumann discretization	24
3.9	Integrals J_p^ω	26
3.9.1	Case when $\omega = 0$	26
3.9.2	Case when $\omega > 0$	27

4	Quadrature	29
4.1	Background	29
4.2	Integration of a triangle	29
4.2.1	Local coordinates on a triangle	29
4.2.2	Case $\omega = 0$	30
4.2.3	Case $\omega > 0$	37
4.3	Integration of a circle sector	38
4.3.1	Local coordinates on a circle sector	38
4.3.2	Elimination of ϕ	38
4.3.3	Case $\omega = 0$	39
4.3.4	Case $\omega > 0$	40
4.4	Integration of a circle	41
4.5	Integration of a circle segment	41
4.5.1	Local coordinates on a circle segment	42
5	Stabilization	45
5.1	Background	45
5.2	Stability analysis for a finite object	46
6	Marching On in Time method	49
6.1	Matrix structure in MOT	49
6.2	Assembly of matrix block \mathbf{A}_u	50
6.2.1	First selection of admissible time differences	51
6.2.2	Find domain on K'	52
6.2.3	Circle intersecting a triangle	53
7	Numerical experiments on Kirchhoff integral equation	55
7.1	Test case with a plate	55
7.2	Stability of Dirichlet plate	56
7.3	Order of accuracy in time of Dirichlet plate	57
7.4	Order of accuracy in space of Dirichlet plate	59
7.5	Test case with a Dirichlet sphere	60
8	Numerical experiments on variational formulation from FD	63
8.1	Dirichlet plate, with various ω	63
8.2	Stability of Dirichlet plate, with $\omega = 0$	64
8.3	Stability of Dirichlet sphere, with $\omega = 0$	65
8.4	Time order of Dirichlet plate, with $\omega = 0$	66
8.5	Order of accuracy in space of Dirichlet plate, with $\omega = 0$	66
8.6	Dirichlet sphere, with $\omega = 0$	68
8.7	Instability of Neumann sphere, with $\omega = 0$	68

9 On Surface Radiation condition	71
9.1 On Surface Radiation Condition (OSRC)	72
9.2 Dirichlet problem	73
9.3 Neumann problem	73
9.4 Dirichlet test case on sphere	74
9.4.1 Numerical experiments	75
A Numerical Integration	77
A.1 Numerical integration	77
A.1.1 Numerical integration over an interval	77
A.1.2 Numerical integration over a triangle	79
A.1.3 Numerical integration over a square	80
A.1.4 L^2 -norm calculations using basis functions	82
Bibliography	83

List of Figures

1.1	Scattering problem.	1
2.1	Computational domain	8
3.1	Time integral contribution	24
4.1	Forbidden domain for a triangle.	33
6.1	Fix a point on triangle K (left) to get a strip over triangle K' (right)	51
6.2	Triangle plane cuts out a circle of a sphere	52
6.3	Integration of a strip over triangle K'	53
6.4	$P\mathbf{r}$ outside (inside) K' to left (right). $\#ni$ is the number of triangle nodes inside the circle. $\#is$ is the number of intersection points.	54
7.1	Triangulated plate with 11×11 nodes (left) and sphere with 92 nodes (right).	56
7.2	Potential at different times for 17×17 plate, with $CFL = 0.5$. . .	57
7.3	Scattered field for a 17×17 plate for $CFL = 1$ (top) and $CFL = 0.5$ (bottom). The scale is different for the first two columns.	58
7.4	Scattered field for a Dirichlet sphere, with pulse width $T = 40$. The dotted curves are the analytical solutions.	61
8.1	Computation on a 9×9 plate, for various ω	64
8.2	Long time error of u^{sc} on test case with a plate with 9×9 nodes and $CFL = 0.5$	65
8.3	Scattered field after 10000 iterations on a test case with a sphere with 92 nodes and $CFL = 0.5$. The dotted curve is the analytical solution.	66
8.4	Scattered field for a Dirichlet sphere, with pulse width $T = 40$. The dotted curves are the analytical solutions.	69
8.5	Scattered field for a Dirichlet sphere, with pulse width $T = 5$. The dotted curves are the analytical solutions.	70

9.1 OSRC solution vs MOT solution of the scattered field for different observation points \mathbf{r} . Upper left: $\mathbf{r} = (0,0,10)$, Upper right: $\mathbf{r} = (10,0,0)$, Lower left: $\mathbf{r} = (0,10,0)$, Lower right: $\mathbf{r} = (-10,0,0)$	76
A.1 Parametrization of triangle	79

List of Tables

- 7.1 Eigenvalues of the corresponding one-step method for different CFL-numbers, with and without stabilization filter. *) indicates that the scheme is unstable. 58
- 7.2 Order of accuracy in time of Dirichlet 11×11 plate (left) and a 17×17 plate (right). 59
- 7.3 Spatial order of Dirichlet plate. 59

- 8.1 Multiplicity of eigenvalue 1 on 9×9 plate for different CFL numbers. 65
- 8.2 Order of accuracy in time of Dirichlet 11×11 plate (left) and a 17×17 plate (right). 67
- 8.3 Order of accuracy in space of Dirichlet plate. 67

Chapter 1

Introduction

Scattering problems arise in many applications, for example in acoustics and electromagnetics. In a scattering problem, an external field u^{inc} illuminates a scatterer and creates a potential on the surface Γ of the scatterer and the potential depends on the characteristics of the scatterer. The potential determines the scattered field u^{sc} in the exterior of the scatterer. We want to find the total field in the exterior of the scatterer consisting both of the incoming field and the scattered field.

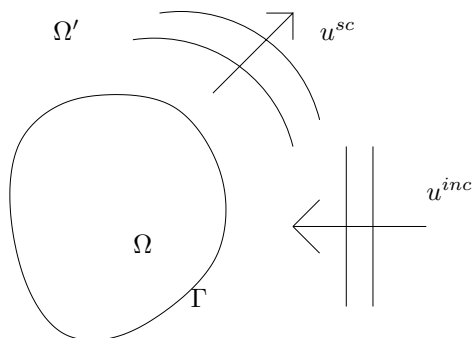


Figure 1.1. Scattering problem.

One way of solving acoustic scattering problems is to solve the wave equation in time domain (TD), for the scattered field,

$$\nabla^2 u^{sc} - \frac{1}{c^2} \frac{\partial^2 u^{sc}}{\partial t^2} = -g(\mathbf{r}, t), \quad (1.1)$$

$$u^{sc}(\mathbf{r}, t) = 0, \quad t \leq 0, \quad (1.2)$$

with boundary conditions on the surface Γ with normal n ,

$$u^{inc} + u^{sc} = 0, \quad \text{for a Dirichlet surface} \quad (1.3)$$

$$\frac{\partial u^{inc}}{\partial n} + \frac{\partial u^{sc}}{\partial n} = 0, \quad \text{for a Neumann surface.} \quad (1.4)$$

There are many ways of solving these equations, e.g. finite difference, finite elements, finite volumes, etc. A drawback with these methods is that the whole space around a scatterer needs to be discretized.

The scattering problem may alternatively be solved in frequency domain (FD), where the solution is a time harmonic wave satisfying

$$u(\mathbf{r}, t) = \hat{u}(\mathbf{r})e^{ikt}. \quad (1.5)$$

The ansatz (1.5) solves the scalar Helmholtz equation [20],

$$\nabla^2 \hat{u} + k\hat{u} = 0, \quad (1.6)$$

with boundary conditions (1.3) and (1.4).

Electromagnetic scattering problems are solved with vector Helmholtz equations [21]. The classical way of solving the Helmholtz equation is to use the method of moments (MM), [13]. Only the surface of the scatterer needs to be discretized in order to obtain the potential on the scatterer. The potential determines the scattered field in all exterior points. In acoustics, we consider Dirichlet (or sound soft) as well as Neumann (or sound hard) scatterers. The acoustic scattering problem for a Dirichlet scatterer is to find the time harmonic potential Φ that solves

$$-\hat{u}^{inc}(\mathbf{r}) = \int_{\Gamma} \frac{e^{ikR}}{4\pi R} \hat{\Phi}(\mathbf{r}') d\Gamma', \quad \forall \mathbf{r} \in \Gamma. \quad (1.7)$$

If we want to get a solution for a broad band of frequencies, for example transients, the method of moments becomes expensive. We want to solve for all frequencies at the same time, without discretizing the whole space around the scatterer. This can be done with the Time Domain Integral Equations (TDIE). For the Dirichlet scatterer, we obtain the retarded potential integral equation (RPIE)

$$-u^{inc}(\mathbf{r}, t) = \int_{\Gamma} \frac{\Phi(\mathbf{r}', t - R/c)}{4\pi R} d\Gamma', \quad \forall \mathbf{r} \in \Gamma. \quad (1.8)$$

When the integrals are discretized, it is possible to get a matrix scheme, in which we can step forward in time. This scheme is called Marching On in Time (MOT). Another application of TDIE is when we want to solve a scattering problem in the scatterer resonance region, where the method of moments is known to break down. TDIE originates from the early sixties, back to Friedman and Shaw [11] and has increased in popularity in recent years. The reason why they have been less popular in the past is that the TDIE has problems with instabilities. In a work by Isabelle Terrasse [23], it is shown in which spaces the solution of Maxwell's

equations lives in, in the case of a PEC-scatterer. Numerical schemes based on the Marching On in Time method often suffers from instabilities. Michielssen [25] claims that the instabilities comes from that high frequencies that are not resolved by the numerical schemes. Michielssen [25] has proposed to use bandlimited basis functions in time (BLIFs), developed by Knab [17]. The BLIFs filters out the high frequencies, which are the reason for the instabilities. One drawback with the BLIF basis functions is that they are several timesteps wide. This means that marching scheme becomes implicit. To make the scheme explicit, one can use a predictor-corrector scheme, which predicts the future solution to get the present solution. Another approach is to solve for all times, using an iterative solver. In analogy with the frequency domain solvers, the bottleneck of the marching method is a matrix-vector multiplication. The complexity of the matrix-vector multiplication can be reduced using a plane wave expansion of the field, which is done in the PWTD method, developed by Michielssen et.al. [10].

1.1 Dirichlet surface

In the Dirichlet case one can derive a Fredholm integral equation of the first kind, from the Kirchhoff representation of the scattered field. This approach leads to a stepping scheme with an eigenvalue close to -1. A problem with stability arises as the eigenvalues leaves the unit circle at -1. The stability properties has been studied by Davies [5] in case of the second type of Fredholm integral equation. For the case of the Fredholm IE of the first kind, there exists averaging techniques to make the method more stable, see [24], [6]. In order to avoid those instabilities for the Dirichlet case, we use variational formulations proposed by Bamberger and Ha Duong in [1]. The integral equations in frequency domain has a well known behavior [20]. Bamberger and Ha Duong gives a variational formulation in frequency domain that is continuous and coersive. By taking the inverse Laplace transform, they get a retarded potential formulation, where these properties are preserved. Therefore we expect a discretization of their variational formulations to be stable. Our contribution is an implementation of a marching method for a Dirichlet scatterer in acoustics, for two different variational formulations. In the Kirchhoff approach, we use stabilization techniques to avoid numerical instabilities. In the computation of the integral kernels, integral evaluations are needed over four different shapes; triangles, circle sectors, circle segments and circles. Most of those integrals are computed analytically. Some of the integrals are computed numerically with high order adaptive methods. Both variational formulations yields a solution which is first order in time and second order in space. The order is verified by numerical computations.

1.2 Neumann surface

In the case of a Neumann boundary, there exists formulations that resemble a Fredholm integral equation of the second kind, [3], [7], which is known to have good convergence properties. These methods are not true Fredholm integral equations of the second kind, because the integral kernel contains time derivatives. They can also be considered as Volterra types of integral equations. We therefore cannot expect the equations to have the nice properties of the Fredholm equation of the second kind. We use the variational formulations proposed by Bamberger and Ha Duong in [2]. Their variational equation is both coersive and continuous as in the Dirichlet case. Recently, Ha Duong, Ludwig and Terrasse, published a review article on an Acoustic Marching On in Time solver, see [12]. The implementation of a Neumann scatterer using formulations in [2] is presented but the scheme is unstable. One possible reason for the instability is that we use less regular basis functions in time, than what is proposed in the variational formulation, but this causes no problem in the Dirichlet case. Another possibility is that an error is introduced when the integration order is changed.

1.3 Outline

In chapter 2, we derive the classical integral representations of the acoustic and electromagnetic scattering problems, using the Kirchhoff formula. A variational formulation is obtained for a Dirichlet scatterer in acoustics.

In chapter 3, we use variational formulations arising from the Helmholtz equation in frequency domain. By taking the inverse Laplace transform we obtain variational formulations for Dirichlet and Neumann scatterers. We introduce basis function in space and time and get the discretized variational formulations.

In chapter 4, we evaluate the necessary integrals over four different shapes, triangle, sector, segment and circle. In the triangle case, integrals with singular integrands are transformed with the Duffy transform. In the three other cases, there are no problems with singularities.

In chapter 5, we discuss how to stabilize the Kirchhoff formulation for a Dirichlet scatterer. This is done by filtering techniques, which moves the eigenvalues at -1 to origo.

In chapter 6, we explain the time stepping procedure and the assembly procedure. An algorithm for the assembly process is given. We discuss how to find the domain of integration which are the triangles, sectors etc. in chapter 4.

In chapter 7 we do numerical experiments on the Kirchhoff formulations. We test the stabilizing filter for a Dirichlet scatterer. We conclude that the filter is necessary in order to get a stable scheme. We verify that the method is first order accurate in time and second order accurate in space, in the case of a point source illuminating a plate. We also perform tests with a plane wave illuminating a sphere. The solution is compared with an analytical solution.

In chapter 8 we do numerical experiments on the variational formulation for a Dirichlet scatterer arising from formulations in frequency domain. We examine a parameter ω that appears in the variational formulations and conclude that the best choice is $\omega = 0$. This choice is stable in long time calculations. Furthermore, most integrals has an analytic expression, which make the assembly process faster. The largest eigenvalue of the corresponding one-step method is a multiple eigenvalue 1 (up to 14 digits). We run the method 10000 time steps and there are no sign of instability. We perform the same tests as in chapter 7, to check the order, point source solution and plane wave solution.

In chapter 9 we look at On Surface Radiation Condition (OSRC), which can be used as a high frequency approximation of the MOT method. A numerical test with low frequency is performed, with the solution to the MOT method as a reference solution. The OSRC solution resembles the MOT solution.

Chapter 2

Integral equations using Kirchhoff formula

In this chapter we will explain how to get an integral representation of the scattered field for the Acoustic equation as well as for the Maxwell equation. In section 2.1, the Kirchhoff formula is introduced for the solution of the scalar wave equation. The Kirchhoff formula is used to get an integral representation that couples the incoming and the scattered field on the boundary of the scatterer. The coupling depends on the material properties of the scatterer. When we have a sound soft scatterer, then we obtain a Dirichlet boundary condition. If we have a sound hard scatterer, then we get a Neumann boundary condition. One can also think of objects that are neither sound soft nor hard, but something in between. We then get a Robin boundary condition. The integral formulation is given for these three cases. In the following chapters we will only consider the Dirichlet and Neumann cases. In section 2.2, we show how an integral formulation can be derived for the Maxwell's equations. The electric and magnetic fields are written as a combination of potentials. These potentials are solutions to the inhomogeneous wave equation and can be represented by the Kirchhoff integrals.

2.1 The scalar wave equation

Consider the 3D wave equation for the pressure u and sound speed c ,

$$\nabla^2 u - \frac{1}{c^2} \frac{\partial^2 u}{\partial t^2} = -g(\mathbf{r}, t), \quad (2.1)$$

$$u(\mathbf{r}, t) = 0, \quad t \leq 0, \quad (2.2)$$

where $\mathbf{r} = (x, y, z)$ is the spatial coordinate. Let Ω be a closed domain bounded by a regular surface Γ and let $\Omega' = \mathbb{R}^3 \setminus \Omega$ be the exterior domain. Suppose that

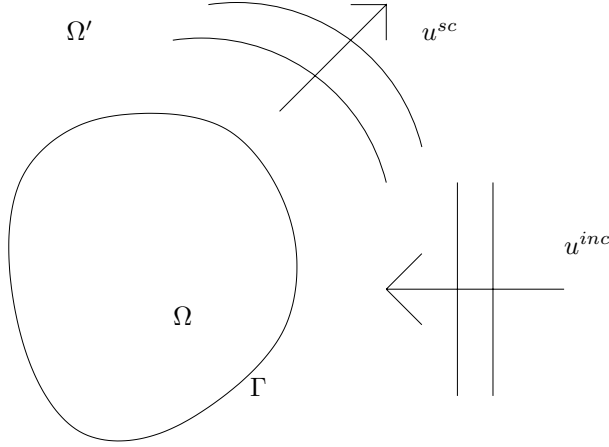


Figure 2.1. Computational domain

u is scalar function which has two continuous derivatives in Ω and Γ . Using the fundamental solution of the wave equation yields the Kirchoff formula [22]

$$4\pi u(\mathbf{r}, t) = \int_{\Omega} \frac{1}{R} g^* dv' + \int_{\Gamma} \left\{ \frac{1}{R} \frac{\partial u^*}{\partial n} - \frac{\partial R^{-1}}{\partial n} u^* + \frac{1}{cR} \frac{\partial R}{\partial n} \frac{\partial u^*}{\partial t} \right\} d\Gamma' \quad (2.3)$$

where

$$g^*(\mathbf{r}', t) = g(\mathbf{r}', t - R/c), \quad R = |\mathbf{r} - \mathbf{r}'|, \quad (2.4)$$

and n is the outwards normal.

The field can be divided into an incoming part u^{inc} and a scattered part u^{sc} . The total field u^{tot} is the sum of the two parts. For a given incoming field $u^{inc}(\mathbf{r}, t)$, we want to compute the scattered field in $\Omega' \times \mathbb{R}^+$.

$$\nabla^2 u^{inc} - \frac{1}{c^2} \frac{\partial^2 u^{inc}}{\partial t^2} = -g(\mathbf{r}, t), \quad \text{in } \mathbb{R}^3 \times \mathbb{R}^+, \quad (2.5)$$

$$\nabla^2 u^{sc} - \frac{1}{c^2} \frac{\partial^2 u^{sc}}{\partial t^2} = 0, \quad \text{in } \Omega' \times \mathbb{R}^+. \quad (2.6)$$

Define the function $\tilde{u}(\mathbf{r}, t)$ in $\mathbb{R}^3 \times \mathbb{R}$

$$\tilde{u} = \begin{cases} -u^{inc}, & \text{in } \Omega \times \mathbb{R}^+, \\ u^{sc}, & \text{in } \Omega' \times \mathbb{R}^+. \end{cases} \quad (2.7)$$

The equation for \tilde{u} away from Γ are

$$\tilde{u} = \frac{1}{4\pi} \int_{\Gamma} \left\{ \frac{1}{R} \left[\frac{\partial \tilde{u}^*}{\partial n} \right] - \frac{\partial}{\partial n} \left(\frac{1}{R} \right) [\tilde{u}^*] + \frac{1}{cR} \frac{\partial R}{\partial n} \frac{\partial}{\partial t} [\tilde{u}^*] \right\} d\Gamma', \quad (2.8)$$

where $[\tilde{u}] = \tilde{u}^{int} - \tilde{u}^{ext}$ and $\tilde{u}^{int}, \tilde{u}^{ext}$ are the solutions to the interior and exterior problem respectively. To get a unique solution to this problem, we need a boundary condition on Γ . There are at least three possible boundary conditions, namely Dirichlet, Neumann and Robin boundary condition. The Dirichlet and Neumann boundary condition corresponds to a sound-soft and sound-hard object, respectively. The Robin boundary condition corresponds to an object that is neither sound-soft or sound-hard, but something in between.

2.1.1 Dirichlet problem

Consider a Dirichlet problem, that has $u^{tot} = 0$ on the boundary. This is equivalent to $[\tilde{u}] = 0$ on the boundary and the integral equation can be written

$$\tilde{u} = P^D \left(\left[\frac{\partial \tilde{u}}{\partial n} \right] \right) \triangleq \frac{1}{4\pi} \int_{\Gamma} \frac{1}{R} \left[\frac{\partial \tilde{u}^*}{\partial n} \right] d\Gamma', \quad (2.9)$$

or equivalently, with $J = \left[\frac{\partial \tilde{u}}{\partial n} \right]$,

$$-u^{inc}(\mathbf{r}, t) = P^D(J)(\mathbf{r}, t), \quad \forall (\mathbf{r}, t) \in \Gamma \times \mathbb{R} \quad (2.10)$$

$$u^{sc}(\mathbf{r}, t) = P^D(J)(\mathbf{r}, t), \quad \forall (\mathbf{r}, t) \in \Omega' \times \mathbb{R}. \quad (2.11)$$

A solution of the Dirichlet problem consists of two steps. We want to find a solution of equation (2.10). This can be done by multiplying with test functions J^t and solve to get the potential J . Let $V^1(\mathbf{r})$ be the space of linear functions in space and $W^0(t)$ be the space of constant functions in time. We obtain the variational formulation 1.

Variational formulation 1 (Dirichlet). Find $J \in V^1(\mathbf{r}) \times W^0(t)$ such that

$$-\iint u^{inc} J^t d\Gamma dt = \iint P^D(J) J^t d\Gamma dt, \quad \forall J^t \in V^1(\mathbf{r}) \times W^0(t). \quad (2.12)$$

The potential can then be used to compute the scattered field u^{sc} outside the scatterer in equation (2.11).

2.1.2 Neumann problem

Consider a Neumann problem, that has $\frac{\partial u^{tot}}{\partial n} = 0$ on the boundary. This is equivalent to $[\frac{\partial \tilde{u}}{\partial n}] = 0$ on the boundary and the integral equation can be written

$$\tilde{u} = P^N([\tilde{u}]) \triangleq \frac{1}{4\pi} \int_{\Gamma} -\frac{\partial}{\partial n} \left(\frac{1}{R} \right) [\tilde{u}^*] + \frac{1}{cR} \frac{\partial R}{\partial n} \frac{\partial}{\partial t} [\tilde{u}^*] d\Gamma', \quad (2.13)$$

or equivalently

$$-u^{inc}(\mathbf{r}, t) = P^N([\tilde{u}]) (\mathbf{r}, t), \quad \forall (\mathbf{r}, t) \in \Gamma \times \mathbb{R} \quad (2.14)$$

$$u^{sc}(\mathbf{r}, t) = P^N([\tilde{u}]) (\mathbf{r}, t), \quad \forall (\mathbf{r}, t) \in \Omega' \times \mathbb{R}. \quad (2.15)$$

A solution of the Neumann problem consists of two steps. The solution of equation (2.14) yields $[\tilde{u}]$. A variational formulation of the Neumann problem can be found in [7]. This can be used to compute the scattered field u^{sc} outside the scatterer in equation (2.15).

2.1.3 Robin problem

In the case when the scatterer surface is neither Dirichlet nor Neumann, we can have a Robin boundary condition on Γ . For a given α ,

$$\frac{\partial u^{tot}}{\partial n} + \alpha u^{tot} = -f, \quad \text{on } \Gamma. \quad (2.16)$$

If $J = [\frac{\partial \tilde{u}}{\partial n}]$ and $M = [\tilde{u}]$, then the general problem can be written

$$\tilde{u} = P^D(J) + P^N(M), \quad (2.17)$$

$$J + \alpha M = f, \quad \text{on } \Gamma. \quad (2.18)$$

There is also an impedance formulation of the problem, which can be found in [12].

2.2 Maxwell's equations

We will not implement a numerical algorithm for the Maxwell's equations in this paper, but we will comment on how to extend our method to solve electromagnetic problems. Consider a closed object Ω with a boundary Γ , where the normal direction is directed outwards. Suppose that the Maxwell's equations are satisfied in

both the interior Ω and in the exterior Ω' . This means that the electric field \mathbf{E} and the magnetic field \mathbf{H} satisfies the Maxwell's equations

$$\nabla \times \mathbf{E} + \frac{\partial \mathbf{B}}{\partial t} = \mathbf{0}, \quad (2.19)$$

$$\nabla \times \mathbf{H} - \frac{\partial \mathbf{D}}{\partial t} = \mathbf{J}, \quad (2.20)$$

$$\nabla \cdot \mathbf{B} = 0, \quad (2.21)$$

$$\nabla \cdot \mathbf{D} = \rho_e, \quad (2.22)$$

where $\mathbf{D} = \varepsilon \mathbf{E}$ and $\mathbf{B} = \mu \mathbf{H}$. The electrical current is denoted \mathbf{J} and the electric charges is denoted ρ_e . It is also assumed that $\mathbf{J}|_{\Omega} = \mathbf{0}$ and $\rho_e|_{\Omega} = 0$. Define the incoming field $\mathbf{E}^{inc} \in \mathbb{R}^3 \times \mathbb{R}$ and the scattered field $\mathbf{E}^{sc} = \mathbf{E} - \mathbf{E}^{inc} \in \Omega' \times \mathbb{R}$ to be the solutions of

$$\nabla \times \mathbf{E}^{inc} + \frac{\partial \mathbf{B}^{inc}}{\partial t} = \mathbf{0}, \quad (2.23)$$

$$\nabla \times \mathbf{H}^{inc} - \frac{\partial \mathbf{D}^{inc}}{\partial t} = \mathbf{J}, \quad (2.24)$$

$$\nabla \cdot \mathbf{B}^{inc} = 0, \quad (2.25)$$

$$\nabla \cdot \mathbf{D}^{inc} = \rho_e \quad (2.26)$$

and

$$\nabla \times \mathbf{E}^{sc} + \frac{\partial \mathbf{B}^{sc}}{\partial t} = \mathbf{0}, \quad (2.27)$$

$$\nabla \times \mathbf{H}^{sc} - \frac{\partial \mathbf{D}^{sc}}{\partial t} = \mathbf{0}, \quad (2.28)$$

$$\nabla \cdot \mathbf{B}^{sc} = 0, \quad (2.29)$$

$$\nabla \cdot \mathbf{D}^{sc} = 0, \quad (2.30)$$

together with the initial data

$$\mathbf{E}^{sc} = \mathbf{H}^{sc} = \mathbf{B}^{sc} = \mathbf{D}^{sc} = \mathbf{0}, \quad \text{when } t \leq 0 \quad (2.31)$$

Define the distribution $\tilde{\mathbf{E}}$ as

$$\tilde{\mathbf{E}} = \begin{cases} \mathbf{E}^{sc}, & \text{in } \Omega' \times \mathbb{R} \\ -\mathbf{E}^{inc}, & \text{in } \Omega \times \mathbb{R} \end{cases} \quad (2.32)$$

Now consider the homogeneous Maxwell's equations for both the interior and exterior problem. Using distribution theory, the Maxwell's equations in $\mathbb{R}^3 \times \mathbb{R}$ become

$$\nabla \times \tilde{\mathbf{E}} + \frac{\partial \tilde{\mathbf{B}}}{\partial t} = [\mathbf{n} \times \tilde{\mathbf{E}}] \delta_{\Gamma}, \quad (2.33)$$

$$\nabla \times \tilde{\mathbf{H}} - \frac{\partial \tilde{\mathbf{D}}}{\partial t} = [\mathbf{n} \times \tilde{\mathbf{H}}] \delta_{\Gamma}, \quad (2.34)$$

$$\nabla \cdot \tilde{\mathbf{B}} = [\mathbf{n} \cdot \tilde{\mathbf{B}}] \delta_{\Gamma}, \quad (2.35)$$

$$\nabla \cdot \tilde{\mathbf{D}} = [\mathbf{n} \cdot \tilde{\mathbf{D}}] \delta_{\Gamma}, \quad (2.36)$$

where $[f] = f^e - f^i$ and δ_Γ is the indicator function for the boundary Γ . We can identify

$$-\tilde{\mathbf{M}} = [\mathbf{n} \times \tilde{\mathbf{E}}], \quad (2.37)$$

$$\tilde{\mathbf{J}} = [\mathbf{n} \times \tilde{\mathbf{H}}], \quad (2.38)$$

$$\tilde{\rho}_m = [\mathbf{n} \cdot \tilde{\mathbf{B}}], \quad (2.39)$$

$$\tilde{\rho}_e = [\mathbf{n} \cdot \tilde{\mathbf{D}}], \quad (2.40)$$

to obtain a more familiar form of Maxwell's equations. The perfectly electric conductor (PEC) boundary conditions are

$$[\mathbf{n} \times \tilde{\mathbf{E}}] = 0 \quad \text{and} \quad [\mathbf{n} \cdot \tilde{\mathbf{H}}] = 0, \quad \text{i.e.} \quad \tilde{\mathbf{M}} = \mathbf{0} \quad \text{and} \quad \tilde{\rho}_m = 0. \quad (2.41)$$

In this case, the Maxwell's equations in $\mathbb{R}^3 \times \mathbb{R}$ are

$$\nabla \times \tilde{\mathbf{E}} + \frac{\partial \tilde{\mathbf{B}}}{\partial t} = \mathbf{0}, \quad (2.42)$$

$$\nabla \times \tilde{\mathbf{H}} - \frac{\partial \tilde{\mathbf{D}}}{\partial t} = \tilde{\mathbf{J}}, \quad (2.43)$$

$$\nabla \cdot \tilde{\mathbf{B}} = 0, \quad (2.44)$$

$$\nabla \cdot \tilde{\mathbf{D}} = \tilde{\rho}_e. \quad (2.45)$$

2.2.1 The electromagnetic potentials

A solution to Maxwell's equations can be divided into two parts, a perfect electric conductor (PEC) where $\tilde{\mathbf{M}} = \mathbf{0}$, $\tilde{\rho}_e = 0$ and a perfect magnetic conductor (PMC), where $\tilde{\mathbf{J}} = \mathbf{0}$ and $\tilde{\rho}_m = 0$. The total field is the sum of the two parts. Consider first the PEC case where $\tilde{\mathbf{M}} = \mathbf{0}$ and $\tilde{\rho}_m = 0$. Introduce the vector potential \mathbf{A} (or \mathbf{A}_0) by

$$\tilde{\mathbf{B}} = \nabla \times \mathbf{A} = \nabla \times \mathbf{A}_0. \quad (2.46)$$

\mathbf{A} is unique up to the gradient of a scalar function,

$$\mathbf{A} = \mathbf{A}_0 - \nabla \Theta. \quad (2.47)$$

Next let the scalar potential Φ (or Φ_0) be defined by

$$\nabla \Phi = -\tilde{\mathbf{E}} - \frac{\partial \mathbf{A}}{\partial t}, \quad \nabla \Phi_0 = -\tilde{\mathbf{E}} - \frac{\partial \mathbf{A}_0}{\partial t}, \quad (2.48)$$

where $\Phi = \Phi_0 + \frac{\partial \Theta}{\partial t}$. To specify Θ , introduce the Lorenz gauge [14],[22],

$$\nabla \cdot \mathbf{A} + \frac{1}{c^2} \frac{\partial \Phi}{\partial t} = 0. \quad (2.49)$$

This specifies Θ and we have reduced the Maxwell's equations (2.42)-(2.45) to wave equations,

$$\nabla^2 \mathbf{A} - \frac{1}{c^2} \frac{\partial^2 \mathbf{A}}{\partial t^2} = -\mu \tilde{\mathbf{J}}, \quad (2.50)$$

$$\nabla^2 \Phi - \frac{1}{c^2} \frac{\partial^2 \Phi}{\partial t^2} = -\frac{1}{\varepsilon} \tilde{\rho}_e. \quad (2.51)$$

Consider now the PMC case, where $\tilde{\mathbf{J}} = \mathbf{0}$ and $\tilde{\rho}_e = 0$. Introduce the potentials \mathbf{F} and Ψ ,

$$\tilde{\mathbf{D}} = -\nabla \times \mathbf{F}, \quad \nabla \Psi = -\tilde{\mathbf{H}} - \frac{\partial \mathbf{F}}{\partial t}, \quad (2.52)$$

and the Lorenz gauge

$$\nabla \cdot \mathbf{F} + \frac{1}{c^2} \frac{\partial \Psi}{\partial t} = 0, \quad (2.53)$$

to get

$$\nabla^2 \mathbf{F} - \frac{1}{c^2} \frac{\partial^2 \mathbf{F}}{\partial t^2} = -\varepsilon \tilde{\mathbf{M}}, \quad (2.54)$$

$$\nabla^2 \Psi - \frac{1}{c^2} \frac{\partial^2 \Psi}{\partial t^2} = -\frac{1}{\mu} \tilde{\rho}_m. \quad (2.55)$$

The fields can now be written as the sum of the PEC part and the PMC part, i.e.

$$\tilde{\mathbf{E}}(\mathbf{r}, t) = -\nabla \Phi - \frac{\partial \mathbf{A}}{\partial t} - \frac{1}{\varepsilon} \nabla \times \mathbf{F}, \quad (2.56)$$

$$\tilde{\mathbf{H}}(\mathbf{r}, t) = -\nabla \Psi - \frac{\partial \mathbf{F}}{\partial t} + \frac{1}{\mu} \nabla \times \mathbf{A}. \quad (2.57)$$

2.2.2 Integral representation of the potentials

The potentials are solutions to the wave equation, and the Kirchhoff formula yields an integral representation

$$\Phi(\mathbf{r}, t) = \frac{1}{\varepsilon} \int_{\Gamma} \frac{\rho_e(\mathbf{r}', t - R/c)}{4\pi R} d\Gamma', \quad (2.58)$$

$$\Psi(\mathbf{r}, t) = \frac{1}{\mu} \int_{\Gamma} \frac{\rho_m(\mathbf{r}', t - R/c)}{4\pi R} d\Gamma', \quad (2.59)$$

$$\mathbf{A}(\mathbf{r}, t) = \mu \int_{\Gamma} \frac{\mathbf{J}(\mathbf{r}', t - R/c)}{4\pi R} d\Gamma', \quad (2.60)$$

$$\mathbf{F}(\mathbf{r}, t) = \varepsilon \int_{\Gamma} \frac{\mathbf{M}(\mathbf{r}', t - R/c)}{4\pi R} d\Gamma'. \quad (2.61)$$

2.2.3 Integral representation of charges

Until now, we need to calculate both $\tilde{\mathbf{J}}$ and $\tilde{\rho}_e$ (and $\tilde{\mathbf{M}}$, $\tilde{\rho}_m$). We can express both $\tilde{\rho}_e$ in $\tilde{\mathbf{J}}$ and $\tilde{\rho}_m$ in $\tilde{\mathbf{M}}$. Define

$$\nabla_{\Gamma} \cdot (\mathbf{n} \times \mathbf{H}_{i,e}) = -\mathbf{n} \cdot (\nabla \times \tilde{\mathbf{H}}_{i,e})|_{\Gamma}, \quad (2.62)$$

where \mathbf{H}_i is the interior field and \mathbf{H}_e is the exterior field. Now one can show conservation of charges on Γ

$$\nabla_{\Gamma} \cdot \tilde{\mathbf{J}} + \frac{\partial \tilde{\rho}_e}{\partial t} = 0, \quad \nabla_{\Gamma} \cdot \tilde{\mathbf{M}} + \frac{\partial \tilde{\rho}_m}{\partial t} = 0. \quad (2.63)$$

Since $\tilde{\mathbf{E}} = \tilde{\mathbf{H}} = \tilde{\mathbf{B}} = \tilde{\mathbf{D}} = \mathbf{0}$ when $t \leq 0$, also $\tilde{\mathbf{J}} = \tilde{\mathbf{M}} = \mathbf{0}$, $\tilde{\rho}_e = \tilde{\rho}_m = 0$ when $t \leq 0$, so we can write

$$\tilde{\rho}_e(\mathbf{r}, t) = -\int_0^t \nabla_{\Gamma} \cdot \tilde{\mathbf{J}}(\mathbf{r}, \tau) d\tau, \quad (2.64)$$

$$\tilde{\rho}_m(\mathbf{r}, t) = -\int_0^t \nabla_{\Gamma} \cdot \tilde{\mathbf{M}}(\mathbf{r}, \tau) d\tau. \quad (2.65)$$

2.2.4 Integral representation of the fields

Our goal is to express the electric and magnetic field in the potentials on the scatterer. We can write Φ and Ψ as

$$\Phi(\mathbf{r}, t) = -\frac{1}{\varepsilon} \int_{\Gamma} \frac{\int_0^{t-R/c} \nabla_{\Gamma} \cdot \tilde{\mathbf{J}}(\mathbf{r}', \tau) d\tau}{4\pi R} d\Gamma', \quad (2.66)$$

$$\Psi(\mathbf{r}, t) = -\frac{1}{\mu} \int_{\Gamma} \frac{\int_0^{t-R/c} \nabla_{\Gamma} \cdot \tilde{\mathbf{M}}(\mathbf{r}', \tau) d\tau}{4\pi R} d\Gamma'. \quad (2.67)$$

If we define $\mathbf{P}^1(\mathbf{K})$ and $\mathbf{P}^2(\mathbf{K})$ as

$$\mathbf{P}^1(\mathbf{K}) = \frac{1}{\varepsilon} \nabla \int_{\Gamma} \frac{\int_0^{t-R/c} \nabla_{\Gamma} \cdot \mathbf{K}(\mathbf{r}', \tau) d\tau}{4\pi R} d\Gamma' - \mu \frac{\partial}{\partial t} \int_{\Gamma} \frac{\mathbf{K}(\mathbf{r}', t-R/c)}{4\pi R} d\Gamma' \quad (2.68)$$

$$\mathbf{P}^2(\mathbf{K}) = -\nabla \times \int_{\Gamma} \frac{\mathbf{K}(\mathbf{r}', t-R/c)}{4\pi R} d\Gamma', \quad (2.69)$$

the equations for $\tilde{\mathbf{E}}$ and $\tilde{\mathbf{H}}$ can be written as

$$\tilde{\mathbf{E}} = \mathbf{P}^1(\tilde{\mathbf{J}}) + \mathbf{P}^2(\tilde{\mathbf{M}}), \quad (2.70)$$

$$\tilde{\mathbf{H}} = \frac{\varepsilon}{\mu} \mathbf{P}^1(\tilde{\mathbf{M}}) - \mathbf{P}^2(\tilde{\mathbf{J}}). \quad (2.71)$$

The equations (2.70) and (2.71) can be used to get a variational formulation similar to (1).

Chapter 3

Variational formulations from frequency domain

The variational formulations described in this chapter has been derived by Bamberger and Ha Duong in [1], [2]. They first derive the variational formulations for Helmholtz equations for one frequency. This formulation is shown to yield a unique solution for the corresponding Helmholtz problem. The formulations for the wave equation are obtained by using Parsevals identity. We will give a short review of the derivation of the variational formulation in the Dirichlet case. A more thorough derivation is given in [1] for the Dirichlet case and in [2] for the Neumann case. In section 3.1, we specify the necessary spaces, in order to understand the variational formulations. In section 3.2, we explain which basis functions are used in time and space. In sections 3.3 and 3.4 we discuss the variational formulations for the Dirichlet and Neumann cases, respectively. In section 3.5 we introduce notation for representing points on different planes. We define a K -gradient and show how it is related to the “normal” gradient. In section 3.6 time is eliminated in our variational formulations, by integration. In sections 3.7 and 3.8, we face the consequences of eliminating the time dependence for the Dirichlet and Neumann case. In section 3.9, we derive integrals, which we evaluate over triangles, circle sectors, circles and circle segments in chapter 4.

3.1 Functional analysis

In order to develop a variational formulation for the wave equation, we need to specify spaces, in which the variational formulation is valid. To define Sobolev spaces in \mathbb{R}^2 , we introduce the Fourier transform in \mathbb{R}^2

$$\widehat{u}(\xi) = \frac{1}{2\pi} \int_{\mathbb{R}^2} e^{-i(\xi \cdot \mathbf{x})} u(\mathbf{x}) d\mathbf{x}. \quad (3.1)$$

Let $\mathcal{S}(\mathbb{R}^2)$ be the space of indefinitely differentiable functions, that are rapidly decreasing at infinity. (Rapidly decreasing means that all partial derivatives decrease more rapidly than any positive power of the variable). The dual space $\mathcal{S}'(\mathbb{R}^2)$ is the space of slowly increasing distributions. The Sobolev space of the scatterer boundary for $s \in \mathbb{R}$ can now be defined

$$H^s(\mathbb{R}^2) = \left\{ u \in \mathcal{S}'(\mathbb{R}^2) : \int_{\mathbb{R}^2} (1 + |\xi|^2)^s |\widehat{u}(\xi)|^2 d\xi \right\}. \quad (3.2)$$

Assuming that the scatterer boundary is infinitely differentiable, the space $H^s(\Gamma)$ is defined, by using a mapping from Γ to \mathbb{R}^2 . The assumption of the boundary can be relaxed to a piecewise Lipschitz boundary, i.e. where the mapping is a Lipschitz continuous function.

The space $\mathbf{H}_\omega^s(\mathbb{R}_+, E)$ is defined as

$$f \in \mathbf{H}_\omega^s(\mathbb{R}_+, E) \iff \begin{cases} \widehat{f} \text{ has an inverse Laplace transform and} \\ \int_{-\infty+i\omega}^{+\infty+i\omega} |k|^{2s} \|\widehat{f}(k)\|_E^2 dk < \infty. \end{cases} \quad (3.3)$$

3.2 Basis functions in space and time

Our goal is to find a solution to the wave equation, that can be written in some basis functions

$$J(\mathbf{r}, t) = \sum_{m,l} J_{ml} \Phi_m(\mathbf{r}) \tilde{\Psi}_l(t), \quad (3.4)$$

where $\Phi_m(\mathbf{r})$ are spatial basis functions and $\tilde{\Psi}_l(t)$ are basis functions in time. The scatterer Γ is triangulated. Introduce linear spatial nodal elements $\Phi_j(\mathbf{r})$ on the triangulation. The spatial elements are defined as the piecewise linear function that satisfies

$$\Phi_j(\mathbf{r}) = \begin{cases} 1, & \mathbf{r} = \mathbf{r}_j, \\ 0, & \mathbf{r} = \mathbf{r}_i, \quad i \neq j. \end{cases} \quad (3.5)$$

For a certain triangle K , we have three local spatial basis function as we denote Φ_j^K , with local indices $j = 1, 2, 3$. Let \mathbf{r}_j^K be the nodes of K . Then the point $\mathbf{r} \in K$ can be parameterized

$$\mathbf{r}(x, y) = \mathbf{r}_1^K + x(\mathbf{r}_2^K - \mathbf{r}_1^K) + y(\mathbf{r}_3^K - \mathbf{r}_1^K), \quad x, y \geq 0, \quad x + y \leq 1. \quad (3.6)$$

The local spatial basis functions are defined as

$$\Phi_1^K(\mathbf{r}(x, y)) = 1 - x - y, \quad (3.7)$$

$$\Phi_2^K(\mathbf{r}(x, y)) = x, \quad (3.8)$$

$$\Phi_3^K(\mathbf{r}(x, y)) = y. \quad (3.9)$$

We define the space

$$V_h^1(\mathbf{r}) = \{\text{Linear combinations of } \Phi_j^K(\mathbf{r})\}. \quad (3.10)$$

When we have a physical coordinate \mathbf{r} and want to calculate the spatial basis function, we need to get x and y . This can be done by solving the system (with $\mathbf{r}_j = \mathbf{r}_j^K$ and $\mathbf{r}_{ij} = \mathbf{r}_i - \mathbf{r}_j$)

$$\begin{pmatrix} \mathbf{r}_{21}^T \mathbf{r}_{21} & \mathbf{r}_{31}^T \mathbf{r}_{21} \\ \mathbf{r}_{21}^T \mathbf{r}_{31} & \mathbf{r}_{31}^T \mathbf{r}_{31} \end{pmatrix} \begin{pmatrix} x \\ y \end{pmatrix} = \begin{pmatrix} (\mathbf{r} - \mathbf{r}_1) \cdot \mathbf{r}_{21} \\ (\mathbf{r} - \mathbf{r}_1) \cdot \mathbf{r}_{31} \end{pmatrix} \quad (3.11)$$

This system has a unique solution as long as the triangle edges are non parallel.

There are different ways of choosing the basis functions in time. In [25], Weile, Shanker and Michielssen use BLIF basis functions. The BLIF functions are several time steps wide which leads to to an implicit solver. For the Dirichlet problem, we will use constant elements in time. The time basis function are defined as

$$\Psi_k(t) = \begin{cases} 1, & t \in [(k-1)\Delta t, k\Delta t), \\ 0, & \text{otherwise.} \end{cases} \quad (3.12)$$

For the Neumann problem, we need more regular basis functions, and we use the basis functions $\int_{-\infty}^t \Psi_k(\tau) d\tau$.

We define the finite dimensional spaces

$$W_h^0(t) = \{\text{Linear combinations of } \Psi_k(t)\}, \quad (3.13)$$

$$W_h^1(t) = \{\text{Linear combinations of } \int_{-\infty}^t \Psi_k(\tau) d\tau\}. \quad (3.14)$$

3.3 Variational formulation, Dirichlet case

The variational formulation for the Dirichlet problem was proposed by Bamberger and Ha Duong [1]. When deriving a variational formulation for the Dirichlet problem, we first consider the case of a single frequency k , with $\Im k > 0$. Define the single layer potential

$$(S_k \phi)(\mathbf{r}) = \frac{1}{4\pi} \int_{\Gamma} \frac{e^{ik|\mathbf{r}-\mathbf{r}'|}}{|\mathbf{r}-\mathbf{r}'|} \phi(\mathbf{r}') d\Gamma'. \quad (3.15)$$

The Dirichlet problem for a fixed frequency k is

$$S_k \phi = g, \quad (3.16)$$

where ϕ is the jump of $\frac{\partial u}{\partial n}$ over the boundary and $g = -u^{inc}$. In [1] it is shown that the variational equation that admits a unique solution for the fixed frequency k , with $\Im k > 0$ is:

Variational formulation 2 (Dirichlet problem, Helmholtz equation). Suppose that $g \in H^{1/2}(\Gamma)$. Then the variational formulation for the Helmholtz Dirichlet problem is to find $\phi \in H^{-1/2}(\Gamma)$ such that

$$\langle \psi, -ikS_k\phi \rangle = \langle \psi, -ikg \rangle, \quad \forall \psi \in H^{-1/2}(\Gamma). \quad (3.17)$$

The corresponding retarded potential to the single layer potential (3.15) is

$$(S\phi)(t, \mathbf{r}) = \frac{1}{4\pi} \int_{\Gamma} \frac{\phi(t - R/c, \mathbf{r}')}{R} d\Gamma'. \quad (3.18)$$

The Parseval identity yields the variational formulation for the time dependent problem:

Variational formulation 3 (Dirichlet problem). Suppose that $u^{inc} \in H_{\omega/2}^{3/2}(\mathbb{R}_+, H^{1/2}(\Gamma))$. The variational formulation for the Dirichlet problem is to find $J \in H_{\omega/2}^1(\mathbb{R}_+, H^{-1/2}(\Gamma))$ such that

$$\begin{aligned} & \iiint e^{-\omega t} \frac{\partial}{\partial t} J(t - R/c, \mathbf{r}')}{4\pi R} d\Gamma' J^t(t, \mathbf{r}) d\Gamma dt \\ &= - \iint e^{-\omega t} \frac{\partial}{\partial t} u^{inc}(t, \mathbf{r}) J^t(t, \mathbf{r}) d\Gamma dt, \quad \forall J^t \in H_{\omega/2}^1(\mathbb{R}_+, H^{-1/2}(\Gamma)). \end{aligned} \quad (3.19)$$

We search for solutions in the finite dimensional space $V_h^1(\mathbf{r}) \times W_{\Delta t}^0(t)$ and the basis function representation

$$J(\mathbf{r}, t) = \sum_{m,l} J_{ml} \Phi_m(\mathbf{r}) \Psi_l(t) \in V_h^1(\mathbf{r}) \times W_{\Delta t}^0(t), \quad (3.20)$$

$$J^t(\mathbf{r}, t) = \Phi_j(\mathbf{r}) \Psi_k(t) \in V_h^1(\mathbf{r}) \times W_{\Delta t}^0(t), \quad (3.21)$$

yields the discrete variational formulation

Variational formulation 4 (Dirichlet problem). Find the coefficients J_{ml} of $J \in V_h^1 \times W_{\Delta t}^0$ in (3.20) such that

$$\begin{aligned} & \sum_{m,l} J_{ml} \iint \frac{\Phi_j(\mathbf{r}) \Psi_m(\mathbf{r}')}{4\pi R} \int e^{-\omega t} \Psi_k(t) \frac{\partial}{\partial t} \Psi_l(t - R/c, \mathbf{r}') dt d\Gamma' d\Gamma \\ &= - \iint e^{-\omega t} \frac{\partial}{\partial t} u^{inc}(t, \mathbf{r}) \Phi_j(\mathbf{r}) \Psi_k(t) dt d\Gamma, \quad \forall \Phi_j(\mathbf{r}) \Psi_k(t) \in V_h^1 \times W_{\Delta t}^0. \end{aligned} \quad (3.22)$$

3.4 Variational formulation, Neumann case

The variational formulation for the Neumann problem was proposed by Bamberger and Ha Duong [2]. Following approximately the same procedure as for the Dirichlet problem, we get the variational problem

Variational formulation 5 (Neumann problem). Suppose that $\frac{\partial u^{inc}}{\partial n} \in H_{\omega/2}^3(\mathbb{R}_+, H^{-1/2}(\Gamma))$. The variational formulation for the Neumann problem is to find $J \in H_{\omega/2}^2(\mathbb{R}_+, H^{1/2}(\Gamma))$ such that

$$\begin{aligned} & \iint \int e^{-\omega t} \frac{\mathbf{n} \cdot \mathbf{n}'}{4\pi R} \frac{\partial^2}{\partial t^2} J(t - R/c, \mathbf{r}') \frac{\partial}{\partial t} J^t(t, \mathbf{r}) \\ & + e^{-\omega t} \frac{\mathbf{n}' \times \nabla' J(t - R/c, \mathbf{r}') \cdot \mathbf{n} \times \nabla \frac{\partial}{\partial t} J^t(t, \mathbf{r})}{4\pi R} d\Gamma' d\Gamma dt \\ = & - \iint \int e^{-\omega t} \frac{\partial}{\partial n} u^{inc}(t, \mathbf{r}) \frac{\partial}{\partial t} J^t(t, \mathbf{r}) d\Gamma dt, \\ & \forall J^t \in H_{\omega/2}^2(\mathbb{R}_+, H^{1/2}(\Gamma)). \end{aligned} \quad (3.23)$$

This variational formulation require the time basis functions to be more regular. Using the basis functions

$$J(\mathbf{r}, t) = \sum_{m,l} J_{ml} \Phi_m(\mathbf{r}) \int_{-\infty}^t \Psi_l(\tau) d\tau \in V_h^1(\mathbf{r}) \times W_{\Delta t}^1(t), \quad (3.24)$$

$$J^t(\mathbf{r}, t) = \Phi_j(\mathbf{r}) \int_{-\infty}^t \Psi_k(\tau) d\tau \in V_h^1(\mathbf{r}) \times W_{\Delta t}^1(t), \quad (3.25)$$

yields the discrete variational formulation

Variational formulation 6 (Neumann problem). Find the coefficients J_{ml} of $J \in V_h^1 \times W_{\Delta t}^1$ in (3.24) such that

$$\begin{aligned} & \sum_{m,l} J_{ml} \iint \frac{\mathbf{n} \cdot \mathbf{n}' \Phi_j(\mathbf{r}) \Phi_m(\mathbf{r}')}{4\pi R} \int e^{-\omega t} \Psi_k(t, \mathbf{r}) \frac{\partial}{\partial t} \Psi_l(t - R/c, \mathbf{r}') dt \\ & + \frac{\mathbf{n} \times \nabla \Phi_j(\mathbf{r}) \cdot \mathbf{n}' \times \nabla' \left(\Phi_m(\mathbf{r}') \int e^{-\omega t} \Psi_k(t) \int_{-\infty}^t \Psi_l(\tau - R/c) d\tau dt \right)}{4\pi R} d\Gamma' d\Gamma \\ = & - \iint \int e^{-\omega t} u^{inc}(t, \mathbf{r}) \Phi_j(\mathbf{r}) \Psi_k(t) dt d\Gamma, \\ & \forall \Phi_j(\mathbf{r}) \int_{-\infty}^t \Psi_k(\tau) d\tau \in V_h^1 \times W_{\Delta t}^1. \end{aligned} \quad (3.26)$$

3.5 Point representation on triangle plane

In order to obtain a useful variational formulation for the discretized problems, we need to find the domain of integration, which is a strip over a triangle. To express points on the triangle plane, different basis for each triangle are used, such that the third component of the point in the triangle plane is zero. We also need to evaluate gradients on the triangles in the triangle plane basis.

A point \mathbf{r} at an arbitrary triangle K in 3D with nodes $\mathbf{r}_1, \mathbf{r}_2$ and \mathbf{r}_3 is parameterized according to

$$\mathbf{r} = \mathbf{r}_1 + \alpha \mathbf{r}_{21} + \beta \mathbf{r}_{31}, \quad \alpha \in [0, 1], \quad \beta \in [0, 1 - \alpha]. \quad (3.27)$$

It is assumed that $\mathbf{r}_{21} = \mathbf{r}_2 - \mathbf{r}_1$ and $\mathbf{r}_{31} = \mathbf{r}_3 - \mathbf{r}_1$ are non-parallel. A basis for this triangle plane is

$$\mathbf{e}_1^K = \frac{\mathbf{r}_{21}}{|\mathbf{r}_{21}|}, \quad (3.28)$$

$$\mathbf{e}_2^K = \frac{\mathbf{r}_{31} - (\mathbf{r}_{31} \cdot \mathbf{e}_1^K) \mathbf{e}_1^K}{|\mathbf{r}_{31} - (\mathbf{r}_{31} \cdot \mathbf{e}_1^K) \mathbf{e}_1^K|}, \quad (3.29)$$

$$\mathbf{e}_3^K = \mathbf{e}_1^K \times \mathbf{e}_2^K. \quad (3.30)$$

The triangles in the scatterer are numbered s.t. \mathbf{e}_3^K is equal to the outwards normal \mathbf{n} . We define the coordinate transformation:

Definition 1 (Coordinate transformation). *The representation of a point in the triangle plane basis is written as*

$$(x_1, x_2, x_3)_K = x_1 \mathbf{e}_1^K + x_2 \mathbf{e}_2^K + x_3 \mathbf{e}_3^K. \quad (3.31)$$

Definition 2 (K-plane). *We say that a point \mathbf{r} is in the K-plane iff*

$$\mathbf{r} = (x_1, x_2, 0)_K, \quad (3.32)$$

for some parameters x_1 and x_2 .

The point $\mathbf{r} = \mathbf{r}_1 + \alpha \mathbf{r}_{21} + \beta \mathbf{r}_{31}$ on the triangle can now be written as

$$\mathbf{r} = \mathbf{r}_1 + (\alpha |\mathbf{r}_{21}| + \beta (\mathbf{r}_{31} \cdot \mathbf{e}_1^K), \beta |\mathbf{r}_{31} - (\mathbf{r}_{31} \cdot \mathbf{e}_1^K) \mathbf{e}_1^K|, 0)_K. \quad (3.33)$$

Now we define the K -gradient

Definition 3 (K-gradient). *Suppose that $\mathbf{r} = \mathbf{r}_1 + (x_1, x_2, x_3)_K$. Then the K -gradient of $\Phi(\mathbf{r})$ is defined as*

$$\nabla_K \Phi(\mathbf{r}) = \left(\frac{\partial \Phi(\mathbf{r})}{\partial x_1}, \frac{\partial \Phi(\mathbf{r})}{\partial x_2}, \frac{\partial \Phi(\mathbf{r})}{\partial x_3} \right)_K. \quad (3.34)$$

Lemma 1 (K-gradient in α and β). *Suppose we have the triangle representation $\mathbf{r} = \mathbf{r}_1 + \alpha \mathbf{r}_{21} + \beta \mathbf{r}_{31}$, where \mathbf{r} is in the K -plane. Then the K -gradient is*

$$\nabla_K \Phi(\mathbf{r}) = \left(\frac{1}{|\mathbf{r}_{21}|} \frac{\partial \Phi}{\partial \alpha}, \frac{1}{|\mathbf{r}_{31} - (\mathbf{r}_{31} \cdot \mathbf{e}_1^K) \mathbf{e}_1^K|} \left(\frac{\partial \Phi}{\partial \beta} - \frac{(\mathbf{r}_{31} \cdot \mathbf{e}_1^K)}{|\mathbf{r}_{21}|} \frac{\partial \Phi}{\partial \alpha} \right), 0 \right)_K \quad (3.35)$$

Proof. We use the chain rule

$$\nabla_K \Phi(\mathbf{r}) = \left(\frac{\partial \Phi}{\partial \alpha} \frac{\partial \alpha}{\partial x_1} + \frac{\partial \Phi}{\partial \beta} \frac{\partial \beta}{\partial x_1}, \frac{\partial \Phi}{\partial \alpha} \frac{\partial \alpha}{\partial x_2} + \frac{\partial \Phi}{\partial \beta} \frac{\partial \beta}{\partial x_2}, 0 \right)_K. \quad (3.36)$$

Rewriting the parameterization as

$$\alpha = \frac{1}{|\mathbf{r}_{21}|} \left(x_1 - \frac{x_2 (\mathbf{r}_{31} \cdot \mathbf{e}_1^K)}{|\mathbf{r}_{31} - (\mathbf{r}_{31} \cdot \mathbf{e}_1^K) \mathbf{e}_1^K|} \right) \quad (3.37)$$

$$\beta = \frac{x_2}{|\mathbf{r}_{31} - (\mathbf{r}_{31} \cdot \mathbf{e}_1^K) \mathbf{e}_1^K|}, \quad (3.38)$$

yields the derivatives

$$\frac{\partial \alpha}{\partial x_1} = \frac{1}{|\mathbf{r}_{21}|}, \quad (3.39)$$

$$\frac{\partial \beta}{\partial x_1} = 0, \quad (3.40)$$

$$\frac{\partial \alpha}{\partial x_2} = \frac{-(\mathbf{r}_{31} \cdot \mathbf{e}_1^K)}{|\mathbf{r}_{21}| |\mathbf{r}_{31} - (\mathbf{r}_{31} \cdot \mathbf{e}_1^K) \mathbf{e}_1^K|}, \quad (3.41)$$

$$\frac{\partial \beta}{\partial x_2} = \frac{1}{|\mathbf{r}_{31} - (\mathbf{r}_{31} \cdot \mathbf{e}_1^K) \mathbf{e}_1^K|}. \quad (3.42)$$

By inserting the derivatives in the chain rule we obtain the lemma. \square

The cross product of the gradient can be written in K -plane coordinates

Lemma 2 (Cross product transformation). *Suppose $\mathbf{n} = \mathbf{e}_3^K$ and $\mathbf{n}_K = (0, 0, 1)_K$. Then*

$$\mathbf{n} \times \nabla \Phi(\mathbf{r}) = (\mathbf{n}_K \times \nabla_K \Phi(\mathbf{r}))_K.$$

We get the gradient expression

$$\begin{aligned} \mathbf{n} \times \nabla \Phi(\mathbf{r}) &= (\mathbf{n}_K \times \nabla_K \Phi(\mathbf{r}))_K \\ &= \left(-\frac{\partial \Phi}{\partial x_2}, \frac{\partial \Phi}{\partial x_1}, 0 \right)_K \\ &= \left(\frac{1}{|\mathbf{r}_{31} - (\mathbf{r}_{31} \cdot \mathbf{e}_1^K) \mathbf{e}_1^K|} \left(\frac{(\mathbf{r}_{31} \cdot \mathbf{e}_1^K)}{|\mathbf{r}_{21}|} \frac{\partial \Phi}{\partial \alpha} - \frac{\partial \Phi}{\partial \beta} \right), \frac{1}{|\mathbf{r}_{21}|} \frac{\partial \Phi}{\partial \alpha}, 0 \right)_K \end{aligned} \quad (3.43)$$

where the coefficients in the expression can be precalculated. Observe that the spatial basis is linear and therefore the gradient is constant. Thus we can move the gradient of the basis functions outside the integral.

3.6 Integrals over time

In the variational formulation of both the Dirichlet and Neumann cases, integrals over time are obtained, for which we can find analytical expressions expressed in R . Define the integrals

$$I_1^\omega(R, k-l) = e^{k\omega\Delta t} \int e^{-\omega t} \Psi_k(t) \Psi_l(t - R/c) dt, \quad (3.44)$$

$$I_2^\omega(R, k-l) = e^{k\omega\Delta t} \int e^{-\omega t} \Psi_k(t) \frac{\partial}{\partial t} \Psi_l(t - R/c) dt, \quad (3.45)$$

$$I_3^\omega(R, k-l) = e^{k\omega\Delta t} \int e^{-\omega t} \Psi_k(t) \int_{-\infty}^t \Psi_l(\tau - R/c) d\tau dt, \quad (3.46)$$

where $\omega \geq 0$. Introduce the interval $\tilde{I}(u_1, u_2)$ such that

$$R \in \tilde{I}(u_1, u_2) \iff u_1 c \Delta t < R < u_2 c \Delta t. \quad (3.47)$$

If constant elements in time are used, we obtain the following integrals over time

$$I_1^\omega(R, u) = \frac{1}{\omega} \begin{cases} e^{\omega\Delta t} - e^{u\omega\Delta t} e^{-\frac{\omega}{c}R}, & R \in \tilde{I}(u-1, u) \\ e^{\omega(u+1)\Delta t} e^{-\frac{\omega}{c}R} - 1, & R \in \tilde{I}(u, u+1) \\ 0, & \text{otherwise,} \end{cases} \quad (3.48)$$

$$I_2^\omega(R, u) = \begin{cases} -e^{\omega u \Delta t} e^{-\frac{\omega}{c}R}, & R \in \tilde{I}(u-1, u) \\ e^{\omega(u+1)\Delta t} e^{-\frac{\omega}{c}R}, & R \in \tilde{I}(u, u+1) \\ 0, & \text{otherwise,} \end{cases} \quad (3.49)$$

$$I_3^\omega(R, u) = \frac{1}{\omega^2} \cdot \begin{cases} \omega\Delta t (e^{\omega\Delta t} - 1), & R \in \tilde{I}(0, u-1) \\ (\omega u \Delta t + 1) e^{\omega\Delta t} - \omega\Delta t - \frac{\omega}{c} e^{\omega\Delta t} R - e^{\omega u \Delta t} e^{-\frac{\omega}{c}R}, & R \in \tilde{I}(u-1, u) \\ -\omega\Delta t (u+1) - 1 + \frac{\omega}{c} R + e^{\omega(u+1)\Delta t} e^{-\frac{\omega}{c}R}, & R \in \tilde{I}(u, u+1) \\ 0, & \text{otherwise,} \end{cases} \quad (3.50)$$

where \tilde{I} is defined in (3.47).

Taking the limit $\omega \rightarrow 0$ produces

$$I_1^0(R, u) = \begin{cases} (1-u)\Delta t + \frac{R}{c}, & R \in \tilde{I}(u-1, u) \\ (1+u)\Delta t - \frac{R}{c}, & R \in \tilde{I}(u, u+1) \\ 0, & \text{otherwise,} \end{cases} \quad (3.51)$$

$$I_2^0(R, u) = \begin{cases} -1, & R \in \tilde{I}(u-1, u) \\ 1, & R \in \tilde{I}(u, u+1) \\ 0, & \text{otherwise,} \end{cases} \quad (3.52)$$

$$I_3^0(R, u) = \begin{cases} \Delta t^2, & R \in \tilde{I}(0, u-1) \\ \left(\frac{1}{2} + u - \frac{u^2}{2}\right) \Delta t^2 + (u-1)\frac{R\Delta t}{c} - \frac{R^2}{2c^2}, & R \in \tilde{I}(u-1, u) \\ \left(\frac{1}{2} + u + \frac{u^2}{2}\right) \Delta t^2 - (u+1)\frac{R\Delta t}{c} + \frac{R^2}{2c^2}, & R \in \tilde{I}(u, u+1) \\ 0, & \text{otherwise,} \end{cases} \quad (3.53)$$

where \tilde{I} is defined in (3.47).

The integrations over time produces strips in space with a radius that depends on the difference in basis functions indices in time. Introduce δ such that

$$R = (u + \delta)c\Delta t. \quad (3.54)$$

The integrals I_p^ω are functions of δ (up to a factor in Δt and ω). In figure 3.1, the integrals I_p^ω are presented as a function of δ . The functions I_p has been normalized to have the maximum height 1. (For the case when $\omega = 0$, this corresponds to $\Delta t = 1$). Observe that I_3^ω is nonzero for all negative δ . This corresponds to an integration over all earlier potentials. It is interesting to see that for $\omega = 0$, the mass (or area) of I_1^0 and I_2^0 is symmetric and antisymmetric, respectively at $\delta = 0$. When ω is increased, the mass center moves to the left. This can be interpreted as the method is becoming less implicit.

3.7 Dirichlet discretization

After discretizing the outer integral of variational problem 3 and introducing the integrals I_p^ω , the Dirichlet integral equation becomes

Variational formulation 7 (Dirichlet problem). Find the coefficients J_{ml} of $J \in V_h^1 \times W_{\Delta t}^0$ in (3.20) such that

$$\begin{aligned} & \frac{1}{4\pi} \sum_{m,l,p} J_{ml} w_p \Phi_j(\mathbf{r}_p) \int \frac{\Phi_m(\mathbf{r}')}{R} I_2^\omega(R, u) d\Gamma' \\ &= - \iint e^{-\omega t} \frac{\partial}{\partial t} u^{inc}(t + k\Delta t, \mathbf{r}) \Phi_j(\mathbf{r}) \Psi(t) dt d\Gamma, \\ & \forall \Phi_j(\mathbf{r}) \Psi_k(t) \in V_h^1 \times W_{\Delta t}^0. \end{aligned} \quad (3.55)$$

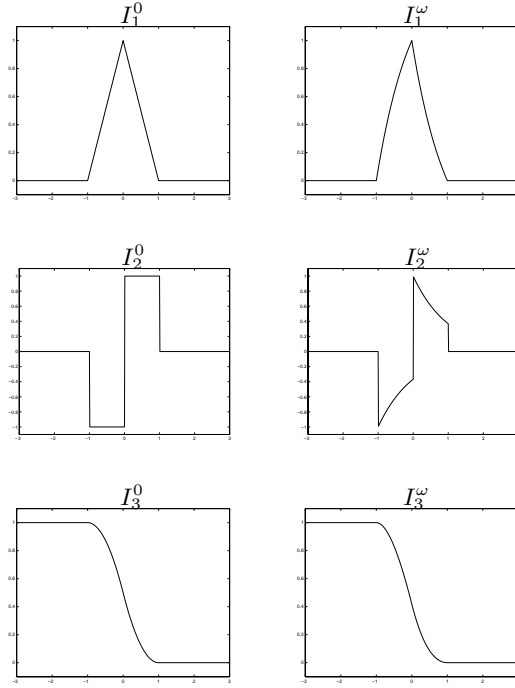


Figure 3.1. Time integral contribution

where $R = |\mathbf{r}' - \mathbf{r}_p|$. In the assembly process, we need to evaluate the integral

$$J_2^\omega = \int \frac{\Phi_m(\mathbf{r}')}{R} I_2^\omega(R, u) dS, \quad (3.56)$$

where S is a triangle, circle sector, circle segment or a circle, lying on the triangle $K' \subset \Gamma'$.

3.8 Neumann discretization

To obtain the discretized Neumann formulation, the following lemmas are needed in order to write a useful discretization.

Lemma 3 (Gradient chain rule). *Suppose that $R = |\mathbf{r}' - \mathbf{r}|$. Then*

$$\nabla' (\Phi(\mathbf{r}') \Psi(\tau - R/c)) = \nabla' (\Phi(\mathbf{r}')) \Psi(\tau - R/c) + \frac{\partial}{\partial \tau} \Psi(\tau - R/c) \frac{\mathbf{r} - \mathbf{r}'}{cR} \Phi(\mathbf{r}'). \quad (3.57)$$

Proof. Let $\tau^* = \tau - R/c$. Now we have the chain rule

$$\nabla'(\Phi(\mathbf{r}')\Psi(\tau^*)) = \nabla'(\Phi(\mathbf{r}'))\Psi(\tau^*) + \Phi(\mathbf{r}')\nabla'(\Psi(\tau^*)), \quad (3.58)$$

where

$$\begin{aligned} \nabla'(\Psi(\tau^*)) &= \frac{\partial\Psi(\tau^*)}{\partial\tau} \frac{\partial\tau}{\partial\tau^*} \nabla'\tau^* \\ &= \frac{\partial\Psi(\tau^*)}{\partial\tau} \cdot 1 \cdot \frac{\mathbf{r} - \mathbf{r}'}{cR}. \end{aligned} \quad (3.59)$$

Inserting (3.59) in (3.58) yields the lemma. \square

Lemma 4 (Derivative of integral). *Suppose that $\Psi(t) = 0$ for $t \leq 0$. Then*

$$\frac{\partial}{\partial t} \int_{-\infty}^t \Psi(\tau - R/c) d\tau = \Psi(t - R/c). \quad (3.60)$$

Lemma 5 (Cross product simplification). *Suppose that \mathbf{n}' is a normal to the K' -plane and that $P\mathbf{r}$ is the projection of \mathbf{r} onto the K' -plane. Let $\mathbf{r}' \in K'$ -plane. Then the following holds*

$$\mathbf{n}' \times (\mathbf{r} - \mathbf{r}') = \mathbf{n}' \times (P\mathbf{r} - \mathbf{r}'). \quad (3.61)$$

Proof. Since \mathbf{n}' and $\mathbf{r} - P\mathbf{r}$ are parallel it is true that

$$\mathbf{n}' \times (\mathbf{r} - \mathbf{r}') = \mathbf{n}' \times (\mathbf{r} - P\mathbf{r} + P\mathbf{r} - \mathbf{r}') = 0 + \mathbf{n}' \times (P\mathbf{r} - \mathbf{r}').$$

\square

Lemma 6 (Combination of lemmas).

$$\begin{aligned} \mathbf{n}' \times \nabla' \left(\Phi(\mathbf{r}') \int_{-\infty}^t \Psi(\tau - R/c) d\tau \right) &= \mathbf{n}' \times \nabla'(\Phi(\mathbf{r}')) \int_{-\infty}^t \Psi(\tau - R/c) d\tau \\ &\quad + \mathbf{n}' \times (P\mathbf{r} - \mathbf{r}') \frac{\Phi(\mathbf{r}')\Psi(t - R/c)}{cR}. \end{aligned} \quad (3.62)$$

Using the lemmas and discretizing the outer integral, we get the integral equation for the Neumann integral equation

Variational formulation 8 (Neumann problem). *Find the coefficients J_{ml} of $J \in V_h^1 \times W_{\Delta t}^1$ in (3.24) such that*

$$\begin{aligned} &\frac{1}{4\pi} \sum_{m,l,p} J_{ml} \omega_p \left((\mathbf{n} \cdot \mathbf{n}') \Phi_j(\mathbf{r}_p) \int \frac{\Phi_m(\mathbf{r}')}{R} I_2^\omega(R, k-l) d\Gamma' \right. \\ &\quad + (\mathbf{n} \times \nabla \Phi_j(\mathbf{r}_p)) \cdot (\mathbf{n}' \times \nabla' \Phi_m(\mathbf{r}')) \int \frac{1}{R} I_3^\omega(R, k-l) d\Gamma' \\ &\quad \left. + (\mathbf{n} \times \nabla \Phi_j(\mathbf{r}_p)) \cdot \int \frac{(\mathbf{n}' \times (P\mathbf{r} - \mathbf{r}'))}{cR^2} \Phi_m(\mathbf{r}') I_1^\omega(R, k-l) d\Gamma' \right) \\ &= - \iint \frac{\partial}{\partial n} u^{inc}(t, \mathbf{r}) \Phi_j(\mathbf{r}) \Psi_k(t) dt d\Gamma, \\ &\quad \forall \Phi_j(\mathbf{r}) \int_{-\infty}^t \Psi_k(\tau) \in V_h^1 \times W_{\Delta t}^1. \end{aligned} \quad (3.63)$$

where $R = |\mathbf{r}' - \mathbf{r}_p|$. Observe that $\mathbf{n}' \times \nabla' \Phi_m(\mathbf{r}')$ can be moved outside the integral over Γ' , since Φ_m is linear.

In the assembly process, the following integrals

$$J_1^\omega = \int \frac{(\mathbf{n}' \times (P\mathbf{r} - \mathbf{r}')) \Phi_m(\mathbf{r}')}{cR^2} I_1^\omega(R, u) dS, \quad (3.64)$$

$$J_2^\omega = \int \frac{\Phi_m(\mathbf{r}')}{R} I_2^\omega(R, u) dS, \quad (3.65)$$

$$J_3^\omega = \int \frac{1}{R} I_3^\omega(R, u) dS, \quad (3.66)$$

has to be evaluated where S is either a triangle, circle sector, circle segment or a circle, lying on the triangle $K' \subset \Gamma'$.

3.9 Integrals J_p^ω

After discretizing the integrals over K and by using analytical evaluation of the time integrals, we are left with the integrals J_p^ω over K' . In order to simplify the integrals, we define points of integration

$$\mathbf{r} = P\mathbf{r} + (0, 0, ((\mathbf{r} - P\mathbf{r}) \cdot \mathbf{e}_3^{K'}))_{K'}, \quad (3.67)$$

$$\mathbf{r}' = P\mathbf{r} + (r'_1, r'_2, 0)_{K'}, \quad (3.68)$$

where $P\mathbf{r}$ is the projection of \mathbf{r} onto the K' -plane and

$$\mathbf{n}' \times (P\mathbf{r} - \mathbf{r}') = (r'_2, -r'_1, 0)_{K'}, \quad (3.69)$$

$$R = \sqrt{|\mathbf{r} - P\mathbf{r}|^2 + |(r'_1, r'_2, 0)_{K'}|^2} \quad (3.70)$$

can now be computed.

3.9.1 Case when $\omega = 0$

In the case when $\omega = 0$, we obtain

$$J_1^0 = d_0 \int \frac{(r'_2, -r'_1, 0)_{K'}}{cR^2} \Phi_m(\mathbf{r}') dS + d_1 \int \frac{(r'_2, -r'_1, 0)_{K'}}{cR} \Phi_m(\mathbf{r}') dS, \quad (3.71)$$

$$J_2^0 = d_0 \int \frac{1}{R} \Phi_m(\mathbf{r}') dS, \quad (3.72)$$

$$J_3^0 = d_0 \int \frac{1}{R} dS + d_1 \int dS + d_2 \int R dS, \quad (3.73)$$

where d_j , $j = 0, 1, 2$ matches the coefficients in I_p^0 , $p = 1, 2, 3$. Since there are three different basis functions Φ_m on each triangle, this is 18 different scalar integral evaluations. (Twelve for J_1^0 and three for J_2^0 and J_3^0 , respectively.) In the Dirichlet case, only three different scalar integrals has to be evaluated. Most parts of these integrals are computed analytically. Some parts of the integrals are computed numerically. A detailed description of the integration is given in chapter 4.

3.9.2 Case when $\omega > 0$

When $\omega > 0$, the following integrals are obtained:

$$J_1^\omega = d_0 \int \frac{(r'_2, -r'_1, 0)_{K'}}{cR^2} \Phi_m(\mathbf{r}') dS + d_2 \int \frac{e^{-\frac{\omega}{c}R} (r'_2, -r'_1, 0)_{K'}}{cR^2} \Phi_m(\mathbf{r}') dS, \quad (3.74)$$

$$J_2^\omega = d_0 \int \frac{e^{-\frac{\omega}{c}R}}{R} \Phi_m(\mathbf{r}') dS, \quad (3.75)$$

$$J_3^\omega = d_0 \int \frac{1}{R} dS + d_1 \int dS + d_2 \int \frac{e^{-\frac{\omega}{c}R}}{R} dS, \quad (3.76)$$

where d_j , $j = 0, 1, 2$ matches the coefficients in I_p^ω , $p = 1, 2, 3$. There are the same number of scalar integral evaluations as in the case $\omega = 0$. The terms containing $e^{-\frac{\omega}{c}R}$ are evaluated numerically except for some special cases, which are explained in chapter 4. The other terms appears also in the case when $\omega = 0$.

Chapter 4

Quadrature

4.1 Background

In chapter 3, we use the variational formulations proposed by Bamberger and Ha Doung in [1], [2] for a Dirichlet and a Neumann scatterer. Those variational formulations resulted in integrals J_p^ω , $p = 1, \dots, 3$, see (3.64)- (3.66) after discretizing the integral over the triangles K and integrating in time analytically. These integrals also applies to the Kirchhoff variational formulation 1 of the Dirichlet problem. In this chapter, we will show how the remaining integrals are evaluated over triangles, circle sectors, circles and circle segments, lying in the K' -plane.

4.2 Integration of a triangle

In section 4.2.1 the parameterization of a triangle K'' is given in local coordinates, as well as the representation of the spatial basis function. The rest of section 4.2 treats the computation of the integrals J_p , in the two cases $\omega = 0$ and $\omega > 0$, respectively. The integration is done in three steps. The first step is to compute integrals analytically and in some cases also numerically. Some of the integrals become infinite for certain locations of origo relative to the triangle. These locations can be avoided by reordering the nodes in the triangle. In the second step the computed integrals are combined to evaluate (4.35)-(4.37) when $\omega = 0$. In the third step, the integrals obtained in the second step is finally combined to get the integrals J_p^0 . The case $\omega > 0$ are also treated, in a similar manner.

4.2.1 Local coordinates on a triangle

Consider a triangle K'' with corners \mathbf{r}_4 , \mathbf{r}_5 and \mathbf{r}_6 , where \mathbf{r}_4 is closest to the point $P\mathbf{r}$ in the triangle plane of K' . K'' lye in the same plane as the triangle K' with corners

$\mathbf{r}_1, \mathbf{r}_2$ and \mathbf{r}_3 . Denote $\mathbf{r}_{ij} = \mathbf{r}_i - \mathbf{r}_j$. The points \mathbf{r}'' on K'' are then parameterized on both K' and K'' by

$$\mathbf{r}'' = \mathbf{r}_4 + \alpha \mathbf{r}_{54} + \beta \mathbf{r}_{64}, \quad \alpha, \beta \geq 0, \quad \alpha + \beta \leq 1, \quad (4.1)$$

$$\mathbf{r}'' = \mathbf{r}_1 + x \mathbf{r}_{21} + y \mathbf{r}_{31}, \quad (4.2)$$

where x and y depends on α and β . In the local variables α and β , a general integral can be written as

$$\int f(\mathbf{r}'') dK'' = 2|K''| \int_0^1 \int_0^{1-\alpha} f(\mathbf{r}''(\alpha, \beta)) d\beta d\alpha. \quad (4.3)$$

In the calculation of the spatial basis function, the parameters x and y needs to be expressed in α and β . This produces the system

$$\begin{pmatrix} \mathbf{r}_{21}^T \mathbf{r}_{21} & \mathbf{r}_{31}^T \mathbf{r}_{21} \\ \mathbf{r}_{21}^T \mathbf{r}_{31} & \mathbf{r}_{31}^T \mathbf{r}_{31} \end{pmatrix} \begin{pmatrix} x \\ y \end{pmatrix} = \begin{pmatrix} \mathbf{r}_{41}^T \mathbf{r}_{21} \\ \mathbf{r}_{41}^T \mathbf{r}_{31} \end{pmatrix} + \alpha \begin{pmatrix} \mathbf{r}_{54}^T \mathbf{r}_{21} \\ \mathbf{r}_{54}^T \mathbf{r}_{31} \end{pmatrix} + \beta \begin{pmatrix} \mathbf{r}_{64}^T \mathbf{r}_{21} \\ \mathbf{r}_{64}^T \mathbf{r}_{31} \end{pmatrix}. \quad (4.4)$$

Solving this system yields the local spatial basis functions

$$\Phi_j^{K''}(\mathbf{r}''(\alpha, \beta)) = a_0 + a_1 \alpha + a_2 \beta. \quad (4.5)$$

Observe that the a 's differ for the different j 's. The matrix inverse depends only on the coordinates of triangle K and can be precalculated before the assembly process.

4.2.2 Case $\omega = 0$

The goal is to evaluate the integrals J_p^0 , $p = 1, 2, 3$, introduced in (3.71)-(3.73). To do this, we first need to compute some integrals analytically but also some numerically, which are combined to obtain middle-step integrals. These middle-step integrals are then combined to evaluate J_p^0 , $p = 1, 2, 3$.

Analytically evaluated integrals

We want to evaluate the integrals $I_{R40}, I_{R41}, I_{R60}, I_{R61}, I_{R10}$ and I_{R11} , defined as

$$I_{R4j} = \int_0^1 \alpha^j \sqrt{|\mathbf{r} - P\mathbf{r}|^2 + |\mathbf{r}_4 + \alpha \mathbf{r}_{54}|^2} d\alpha, \quad (4.6)$$

$$I_{R6j} = \int_0^1 \alpha^j \sqrt{|\mathbf{r} - P\mathbf{r}|^2 + |\mathbf{r}_6 + \alpha \mathbf{r}_{56}|^2} d\alpha, \quad (4.7)$$

$$I_{R1j} = \int_0^1 \alpha^j R_1(\alpha) d\alpha, \quad (4.8)$$

where

$$R_1(\alpha) = \sqrt{(|\mathbf{r} - P\mathbf{r}|^2 + |\mathbf{r}_4 + \alpha \mathbf{r}_{54}|^2) |\mathbf{r}_{64}|^2 - ((\mathbf{r}_4 + \alpha \mathbf{r}_{54})^T \mathbf{r}_{64})^2}. \quad (4.9)$$

To do this, the integrals

$$I_R(\mathbf{b}_0, \mathbf{b}_1, n) = \int_0^1 \alpha^n |\mathbf{b}_0 + \alpha \mathbf{b}_1| d\alpha, \quad (4.10)$$

are required. In the case $n = 0, 1$, an analytical solution can be computed,

$$I_R(\mathbf{b}_0, \mathbf{b}_1, 0) = A_1 + A_2 \log A_3, \quad (4.11)$$

$$I_R(\mathbf{b}_0, \mathbf{b}_1, 1) = B_1 + B_2 \log B_3, \quad (4.12)$$

$$A_1 = \frac{|\mathbf{b}_0 + \mathbf{b}_1| |\mathbf{b}_1|^2 + \mathbf{b}_0^T \mathbf{b}_1 |\mathbf{b}_0 + \mathbf{b}_1| - \mathbf{b}_0^T \mathbf{b}_1 |\mathbf{b}_0|}{2|\mathbf{b}_1|^2}, \quad (4.13)$$

$$A_2 = \frac{|\mathbf{b}_0|^2 |\mathbf{b}_1|^2 - (\mathbf{b}_0^T \mathbf{b}_1)^2}{2|\mathbf{b}_1|^3}, \quad (4.14)$$

$$A_3 = \frac{(\mathbf{b}_0 + \mathbf{b}_1)^T \mathbf{b}_1 + |\mathbf{b}_0 + \mathbf{b}_1| |\mathbf{b}_1|}{\mathbf{b}_0^T \mathbf{b}_1 + |\mathbf{b}_0| |\mathbf{b}_1|}, \quad (4.15)$$

$$B_1 = \frac{|\mathbf{b}_0 + \mathbf{b}_1|^3 - |\mathbf{b}_0|^3}{3|\mathbf{b}_1|^2} - \frac{\mathbf{b}_0^T \mathbf{b}_1}{|\mathbf{b}_1|^2} A_1, \quad (4.16)$$

$$B_2 = -\frac{\mathbf{b}_0^T \mathbf{b}_1}{|\mathbf{b}_1|^2} A_2, \quad (4.17)$$

$$B_3 = A_3, \quad (4.18)$$

and

$$I_{R10} = \frac{t_3}{2} + \frac{t_5(t_3 - t_2)}{2t_1^2} + \frac{(t_1^2(|\mathbf{r} - P\mathbf{r}|^2 + |\mathbf{r}_4|^2) + t_4 \mathbf{r}_4^T \mathbf{r}_{64} - t_5 \mathbf{r}_4^T \mathbf{r}_{54}) t_6 |\mathbf{r}_{64}|^2}{2t_1^3}, \quad (4.19)$$

$$I_{R11} = \frac{t_3^3 - t_2^3}{3t_1^2} - \frac{t_5}{2t_1^5} \cdot \left(t_1^3 t_3 + t_1 t_5 (t_3 - t_2) + t_6 |\mathbf{r}_{64}|^2 (|\mathbf{r} - P\mathbf{r}|^2 + |\mathbf{r}_4|^2) t_1^2 + \mathbf{r}_4^T \mathbf{r}_{64} t_4 - \mathbf{r}_4^T \mathbf{r}_{54} t_5 \right) \quad (4.20)$$

where the constants t_j are defined as

$$t_1 = \sqrt{|\mathbf{r}_{54}|^2 |\mathbf{r}_{64}|^2 - (\mathbf{r}_{54}^T \mathbf{r}_{64})^2}, \quad (4.21)$$

$$t_2 = \sqrt{(|\mathbf{r} - P\mathbf{r}|^2 + |\mathbf{r}_4|^2) |\mathbf{r}_{64}|^2 - (\mathbf{r}_4^T \mathbf{r}_{64})^2}, \quad (4.22)$$

$$t_3 = \sqrt{(|\mathbf{r} - P\mathbf{r}|^2 + |\mathbf{r}_5|^2) |\mathbf{r}_{64}|^2 - (\mathbf{r}_5^T \mathbf{r}_{64})^2}, \quad (4.23)$$

$$t_4 = \mathbf{r}_4^T \mathbf{r}_{54} \cdot \mathbf{r}_{54}^T \mathbf{r}_{64} - \mathbf{r}_4^T \mathbf{r}_{64} \cdot |\mathbf{r}_{54}|^2, \quad (4.24)$$

$$t_5 = \mathbf{r}_4^T \mathbf{r}_{54} \cdot |\mathbf{r}_{64}|^2 - \mathbf{r}_4^T \mathbf{r}_{64} \cdot \mathbf{r}_{54}^T \mathbf{r}_{64}, \quad (4.25)$$

$$t_6 = \log \frac{(\mathbf{r}_5^T \mathbf{r}_{54} \cdot |\mathbf{r}_{64}|^2 - \mathbf{r}_5^T \mathbf{r}_{64} \cdot \mathbf{r}_{54}^T \mathbf{r}_{64}) + t_1 t_3}{t_1 t_2 + t_5}. \quad (4.26)$$

Next, define

$$I_R^*(|\mathbf{b}_0|, |\mathbf{b}_1|, |\mathbf{b}_0 + \mathbf{b}_1|, \mathbf{b}_0^T \mathbf{b}_1, (\mathbf{b}_0 + \mathbf{b}_1)^T \mathbf{b}_1, n) = I_R(\mathbf{b}_0, \mathbf{b}_1, n), \quad (4.27)$$

and evaluate

$$I_{R40} = I_R^*(\sqrt{|\mathbf{r} - P\mathbf{r}|^2 + |\mathbf{r}_4|^2}, |\mathbf{r}_{54}|, \sqrt{|\mathbf{r} - P\mathbf{r}|^2 + |\mathbf{r}_5|^2}, \mathbf{r}_4^T \mathbf{r}_{54}, \mathbf{r}_5^T \mathbf{r}_{54}, 0), \quad (4.28)$$

$$I_{R41} = I_R^*(\sqrt{|\mathbf{r} - P\mathbf{r}|^2 + |\mathbf{r}_4|^2}, |\mathbf{r}_{54}|, \sqrt{|\mathbf{r} - P\mathbf{r}|^2 + |\mathbf{r}_5|^2}, \mathbf{r}_4^T \mathbf{r}_{54}, \mathbf{r}_5^T \mathbf{r}_{54}, 1), \quad (4.29)$$

$$I_{R60} = I_R^*(\sqrt{|\mathbf{r} - P\mathbf{r}|^2 + |\mathbf{r}_6|^2}, |\mathbf{r}_{56}|, \sqrt{|\mathbf{r} - P\mathbf{r}|^2 + |\mathbf{r}_5|^2}, \mathbf{r}_6^T \mathbf{r}_{56}, \mathbf{r}_5^T \mathbf{r}_{56}, 0), \quad (4.30)$$

$$I_{R61} = I_R^*(\sqrt{|\mathbf{r} - P\mathbf{r}|^2 + |\mathbf{r}_6|^2}, |\mathbf{r}_{56}|, \sqrt{|\mathbf{r} - P\mathbf{r}|^2 + |\mathbf{r}_5|^2}, \mathbf{r}_6^T \mathbf{r}_{56}, \mathbf{r}_5^T \mathbf{r}_{56}, 1). \quad (4.31)$$

Numerical integrals

The integrals to be evaluated numerically are $I_{\log 1,j}$, $j = 0, 1, 2$, $I_{\log 2,j}$, $j = 0, 1$, $I_{at,j}$, $j = 0, 1, 2$ defined as

$$I_{\log 1,j} = \frac{1}{|\mathbf{r}_{64}|^2} \int_0^1 \alpha^j \log \left(\frac{(\mathbf{r}_6 + \alpha \mathbf{r}_{56})^T \mathbf{r}_{64} + |\mathbf{r}_6 + \alpha \mathbf{r}_{56}| |\mathbf{r}_{64}|}{(\mathbf{r}_4 + \alpha \mathbf{r}_{54})^T \mathbf{r}_{64} + |\mathbf{r}_4 + \alpha \mathbf{r}_{54}| |\mathbf{r}_{64}|} \right) d\alpha, \quad (4.32)$$

$$I_{\log 2,j} = \int_0^1 \alpha^j \log \frac{|\mathbf{r}_6 + \alpha \mathbf{r}_{56}|^2}{|\mathbf{r}_4 + \alpha \mathbf{r}_{54}|^2} d\alpha, \quad (4.33)$$

$$I_{at,j} = \int_0^1 \alpha^j \frac{\arctan \frac{(\mathbf{r}_6 + \alpha \mathbf{r}_{56})^T \mathbf{r}_{64}}{R_1(\alpha)} - \arctan \frac{(\mathbf{r}_4 + \alpha \mathbf{r}_{54})^T \mathbf{r}_{64}}{R_1(\alpha)}}{R_1(\alpha)} d\alpha. \quad (4.34)$$

These integrals are evaluated using numerical integration, where an adaptive Romberg method is used. The integration method is described in algorithm 5, in the appendix.

Forbidden domains and node reordering

Some of the integrals becomes infinite when origo of the triangle plane is in the wrong place. When $|\mathbf{r} - P\mathbf{r}| = 0$, the integral I_{R4j} becomes infinite if $\mathbf{r}_4 + \theta \mathbf{r}_{54} = 0$, for $\theta \geq 0$. The same happens for I_{R6j} when $\mathbf{r}_6 + \theta \mathbf{r}_{56} = 0$, for $\theta \geq 0$. The integral $I_{at,j}$ is infinite whenever $R_1(\alpha) = 0$. This yields the forbidden strip $\mathbf{r}_4 + \alpha \mathbf{r}_{54} + \theta \mathbf{r}_{64} = 0$, $\alpha \in [0, 1]$ and $\theta \in \mathbb{R}$. All other forbidden points are covered by those three cases. The forbidden strip and the two forbidden lines are indicated in figure 4.1.

In order to avoid the forbidden domains, the nodes in the triangle are reordered. The goal is to order the nodes such that origo is to the left of the shaded strip in figure 4.1. To find out how to order the nodes, we compute cross products s_j , that gives information about the angles between $-\mathbf{r}_m$ and $\mathbf{r}_j - \mathbf{r}_m$, for $j = 1, 2, 3$. If two angles ϕ_{j_1} and ϕ_{j_2} (or equivalently s_{j_1} and s_{j_2}) have different signs, then we know that we are on one out of two domains restricted by two lines $\mathbf{r}_{j_1} - \mathbf{r}_m$ and $\mathbf{r}_{j_2} - \mathbf{r}_m$. To exclude the wrong domain, we take one more cross product, to see on which side of $\mathbf{r}_{j_2} - \mathbf{r}_{j_1}$, the origo is. The last check depends on the node orientation, which also is computed. A pseudo code is listed in algorithm 1.

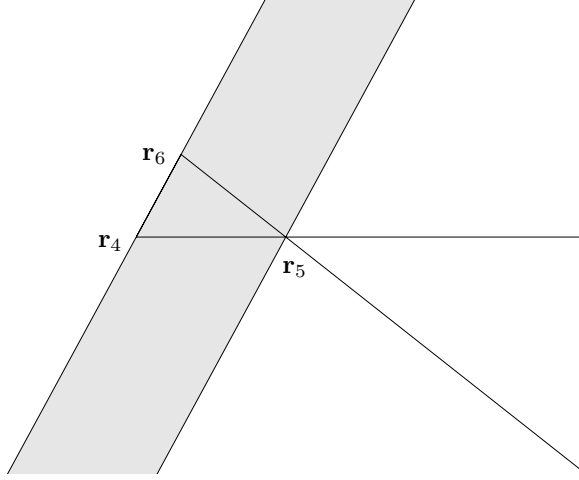


Figure 4.1. Forbidden domain for a triangle.

Algorithm 1 Triangle node reordering

-
- 1: Compute $\mathbf{r}_m = (\mathbf{r}_4 + \mathbf{r}_5 + \mathbf{r}_6)/3$
 - 2: Compute $\text{orient} = \mathbf{r}_{54} \times \mathbf{r}_{64}$
 - 3: Compute $s_4 = (-\mathbf{r}_m) \times (\mathbf{r}_4 - \mathbf{r}_m)$
 - 4: Compute $s_5 = (-\mathbf{r}_m) \times (\mathbf{r}_5 - \mathbf{r}_m)$
 - 5: Compute $s_6 = (-\mathbf{r}_m) \times (\mathbf{r}_6 - \mathbf{r}_m)$
 - 6: **if** $s_4 s_5 < 0$ and $\text{orient} \cdot (-\mathbf{r}_m) \times (\mathbf{r}_{45}) < 0$ **then**
 - 7: $\text{swap}(\mathbf{r}_5, \mathbf{r}_6)$
 - 8: **else if** $s_5 s_6 < 0$ and $\text{orient} \cdot (-\mathbf{r}_m) \times (\mathbf{r}_{56}) < 0$ **then**
 - 9: $\text{swap}(\mathbf{r}_4, \mathbf{r}_5)$
 - 10: **end if**
-

Middle step of integration, nonsingular case

Here we evaluate the integrals

$$Int_1(n, m) = \int_0^1 \int_0^{1-\alpha} \frac{\alpha^n \beta^m}{R} d\beta d\alpha, \quad (4.35)$$

$$Int_2(n, m) = \int_0^1 \int_0^{1-\alpha} \frac{\alpha^n \beta^m}{R^2} d\beta d\alpha, \quad (4.36)$$

$$Int_R = \int_0^1 \int_0^{1-\alpha} R d\beta d\alpha. \quad (4.37)$$

The interesting tuples (n, m) are $(0, 0), (1, 0), (0, 1), (1, 1), (2, 0)$ and $(0, 2)$. These integrals can be computed using the analytical and numerical integrals evaluated

previously.

$$Int_1(0,0) = I_{\log 1,0}, \quad (4.38)$$

$$Int_1(1,0) = I_{\log 1,1}, \quad (4.39)$$

$$Int_1(0,1) = \frac{I_{R60} - I_{R40} - \mathbf{r}_4^T \mathbf{r}_{64} I_{\log 1,0} - \mathbf{r}_{54}^T \mathbf{r}_{64} I_{\log 1,1}}{|\mathbf{r}_{64}|^2}, \quad (4.40)$$

$$Int_1(1,1) = \frac{I_{R61} - I_{R41} - \mathbf{r}_4^T \mathbf{r}_{64} I_{\log 1,1} - \mathbf{r}_{54}^T \mathbf{r}_{64} I_{\log 1,2}}{|\mathbf{r}_{64}|^2}, \quad (4.41)$$

$$Int_1(2,0) = I_{\log 1,2}, \quad (4.42)$$

$$\begin{aligned} Int_1(0,2) = & \frac{1}{2|\mathbf{r}_{64}|^4} \left((3(\mathbf{r}_{54}^T \mathbf{r}_{64})^2 - |\mathbf{r}_{54}|^2 |\mathbf{r}_{64}|^2) \cdot I_{\log 1,2} \right. \\ & + (6(\mathbf{r}_4^T \mathbf{r}_{64})(\mathbf{r}_{54}^T \mathbf{r}_{64}) - 2\mathbf{r}_4^T \mathbf{r}_{54} |\mathbf{r}_{64}|^2) \cdot I_{\log 1,1} \\ & + (3(\mathbf{r}_4^T \mathbf{r}_{64})^2 - (|\mathbf{r} - P\mathbf{r}|^2 + |\mathbf{r}_4|^2) |\mathbf{r}_{64}|^2) \cdot I_{\log 1,0} \\ & + (\mathbf{r}_6^T \mathbf{r}_{64} - 4\mathbf{r}_4^T \mathbf{r}_{64}) \cdot I_{R60} + 3\mathbf{r}_4^T \mathbf{r}_{64} \cdot I_{R40} \\ & \left. + (\mathbf{r}_{56}^T \mathbf{r}_{64} - 4\mathbf{r}_{54}^T \mathbf{r}_{64}) \cdot I_{R61} + 3\mathbf{r}_{54}^T \mathbf{r}_{64} \cdot I_{R41} \right), \quad (4.43) \end{aligned}$$

$$Int_2(0,0) = I_{at,0}, \quad (4.44)$$

$$Int_2(1,0) = I_{at,0}, \quad (4.45)$$

$$Int_2(0,1) = \frac{\frac{1}{2} I_{\log 2,0} - \mathbf{r}_4^T \mathbf{r}_{64} \cdot I_{at,0} - \mathbf{r}_{54}^T \mathbf{r}_{64} \cdot I_{at,1}}{|\mathbf{r}_{64}|^2}, \quad (4.46)$$

$$Int_2(1,1) = \frac{\frac{1}{2} I_{\log 2,1} - \mathbf{r}_4^T \mathbf{r}_{64} \cdot I_{at,1} - \mathbf{r}_{54}^T \mathbf{r}_{64} \cdot I_{at,2}}{|\mathbf{r}_{64}|^2}, \quad (4.47)$$

$$Int_2(2,0) = I_{at,0}, \quad (4.48)$$

$$\begin{aligned} Int_2(0,2) = & \frac{1}{|\mathbf{r}_{64}|^4} \cdot \left(\frac{1}{2} |\mathbf{r}_{64}|^2 - \mathbf{r}_4^T \mathbf{r}_{64} \cdot I_{\log 2,0} - \mathbf{r}_{54}^T \mathbf{r}_{64} \cdot I_{\log 2,1} \right. \\ & - ((|\mathbf{r} - P\mathbf{r}|^2 + |\mathbf{r}_4|^2) |\mathbf{r}_{64}|^2 - 2(\mathbf{r}_4^T \mathbf{r}_{64})^2) \cdot I_{at,0} \\ & - (2\mathbf{r}_4^T \mathbf{r}_{54} |\mathbf{r}_{64}|^2 - 4\mathbf{r}_4^T \mathbf{r}_{64} \mathbf{r}_{54}^T \mathbf{r}_{64}) \cdot I_{at,1} \\ & \left. - (|\mathbf{r}_{54}|^2 |\mathbf{r}_{64}|^2 - 2(\mathbf{r}_{54}^T \mathbf{r}_{64})^2) \cdot I_{at,2} \right), \quad (4.49) \end{aligned}$$

$$\begin{aligned} Int_R = & \frac{1}{2|\mathbf{r}_{64}|^2} \cdot \left(\mathbf{r}_6^T \mathbf{r}_{64} \cdot I_{R60} + \mathbf{r}_{56}^T \mathbf{r}_{64} \cdot I_{R61} \right. \\ & - \mathbf{r}_4^T \mathbf{r}_{64} \cdot I_{R40} - \mathbf{r}_{54}^T \mathbf{r}_{64} \cdot I_{R41} \\ & \left. + t_2^2 \cdot I_{ln10} + 2t_5 \cdot I_{ln11} + t_1^2 \cdot I_{ln12} \right) \quad (4.50) \end{aligned}$$

The constants t_j have been defined in (4.21)-(4.26).

Middle step of integration, singular case

In the singular case, $|\mathbf{r} - P\mathbf{r}|^2 + |\mathbf{r}_4|^2 = 0$. Also here we evaluate the integrals

$$Int_1(n, m) = \int_0^1 \int_0^{1-\alpha} \frac{\alpha^n \beta^m}{R} d\beta d\alpha, \quad (4.51)$$

$$Int_2(n, m) = \int_0^1 \int_0^{1-\alpha} \frac{\alpha^n \beta^m}{R^2} d\beta d\alpha, \quad (4.52)$$

$$Int_R = \int_0^1 \int_0^{1-\alpha} R d\beta d\alpha, \quad (4.53)$$

where $R = |\alpha \mathbf{r}_{54} + \beta \mathbf{r}_{64}|$. The integrands (4.51) and (4.52) become singular as $\alpha, \beta \rightarrow 0$. The interesting tuples (n, m) are $(0, 0), (1, 0), (0, 1), (1, 1), (2, 0)$ and $(0, 2)$. To get rid of the singularity, we perform a Duffy transform, $\alpha = \xi_1 \xi_2$ and $\beta = \xi_1(1 - \xi_2)$. The Jacobian contribution is ξ_1 . Define R_s and we get

$$R_s(\xi_2) = |\mathbf{r}_{64} + \xi_2 \mathbf{r}_{56}|, \quad (4.54)$$

$$R(\alpha, \beta) = \xi_1 R_s(\xi_2), \quad (4.55)$$

$$R_{1s} = \sqrt{|\mathbf{r}_6|^2 |\mathbf{r}_{56}|^2 - (\mathbf{r}_6^T \mathbf{r}_{56})^2}. \quad (4.56)$$

Consider

$$\begin{aligned} Int_p(n, m) &= \int_0^1 \int_0^{1-\alpha} \frac{\alpha^n \beta^m}{R^p} d\beta d\alpha \\ &= \int_0^1 \xi_1^{1+n+m-p} d\xi_1 \cdot \int_0^1 \frac{\xi_2^n (1-\xi_2)^m}{R_s^p(\xi_2)} d\xi_2 \\ &= \frac{1}{2+n+m-p} \int_0^1 \frac{\xi_2^n (1-\xi_2)^m}{R_s^p(\xi_2)} d\xi_2. \end{aligned} \quad (4.57)$$

This is valid in the case $2+n+m > p$. Otherwise integral is improper. Hence, $Int_2(0, 0)$ is an improper integral. This integral is not needed, as we will see in the last step of integration. Define

$$Int_p^s(n) = \int_0^1 \frac{\xi_2^n}{R_s^p(\xi_2)} d\xi_2, \quad (4.58)$$

which can be evaluated analytically,

$$Int_1^s(0) = \frac{1}{|\mathbf{r}_{56}|} \log \left(\frac{\mathbf{r}_5^T \mathbf{r}_{56} + |\mathbf{r}_5| |\mathbf{r}_{56}|}{\mathbf{r}_6^T \mathbf{r}_{56} + |\mathbf{r}_6| |\mathbf{r}_{56}|} \right), \quad (4.59)$$

$$Int_1^s(1) = \frac{|\mathbf{r}_5| - |\mathbf{r}_6|}{|\mathbf{r}_{56}|^2} - \frac{\mathbf{r}_6^T \mathbf{r}_{56}}{|\mathbf{r}_{56}|^2} Int_1^s(0), \quad (4.60)$$

$$Int_1^s(2) = \frac{1}{2|\mathbf{r}_{56}|^4} \left((|\mathbf{r}_{56}|^2 - 3\mathbf{r}_6^T \mathbf{r}_{56}) |\mathbf{r}_5| + 3\mathbf{r}_6^T \mathbf{r}_{56} |\mathbf{r}_6| \right. \\ \left. + (3(\mathbf{r}_6^T \mathbf{r}_{56})^2 - |\mathbf{r}_6|^2 |\mathbf{r}_{56}|^2) Int_1^s(0) \right), \quad (4.61)$$

$$Int_2^s(0) = \frac{\arctan \left(\frac{\mathbf{r}_5^T \mathbf{r}_{56}}{R_{1s}} \right) - \arctan \left(\frac{\mathbf{r}_6^T \mathbf{r}_{56}}{R_{1s}} \right)}{R_{1s}}, \quad (4.62)$$

$$Int_2^s(1) = \frac{\log (|\mathbf{r}_5|/|\mathbf{r}_6|) - \mathbf{r}_6^T \mathbf{r}_{56} \cdot Int_2^s(0)}{|\mathbf{r}_{56}|^2}, \quad (4.63)$$

$$Int_2^s(2) = \frac{1}{|\mathbf{r}_{56}|^4} \left(|\mathbf{r}_{56}|^2 - 2\mathbf{r}_6^T \mathbf{r}_{56} \log (|\mathbf{r}_5|/|\mathbf{r}_6|) \right. \\ \left. + (2(\mathbf{r}_6^T \mathbf{r}_{56})^2 - |\mathbf{r}_6|^2 |\mathbf{r}_{56}|^2) Int_2^s(0) \right). \quad (4.64)$$

The required integrals can be evaluated

$$Int_1(0,0) = Int_1^s(0), \quad (4.65)$$

$$Int_1(1,0) = \frac{1}{2} Int_1^s(0), \quad (4.66)$$

$$Int_1(0,1) = \frac{1}{2} (Int_1^s(0) - Int_1^s(1)), \quad (4.67)$$

$$Int_1(1,1) = \frac{1}{3} (Int_1^s(1) - Int_1^s(2)), \quad (4.68)$$

$$Int_1(2,0) = \frac{1}{3} Int_1^s(0), \quad (4.69)$$

$$Int_1(0,2) = \frac{1}{3} (Int_1^s(0) - 2Int_1^s(1) + Int_1^s(2)), \quad (4.70)$$

$$Int_2(0,0) = [\text{Improper}], \quad (4.71)$$

$$Int_2(1,0) = Int_2^s(1), \quad (4.72)$$

$$Int_2(0,1) = Int_2^s(0) - Int_2^s(1), \quad (4.73)$$

$$Int_2(1,1) = \frac{1}{2} (Int_2^s(1) - Int_2^s(2)), \quad (4.74)$$

$$Int_2(2,0) = \frac{1}{2} Int_2^s(2), \quad (4.75)$$

$$Int_2(0,2) = \frac{1}{2} (Int_2^s(0) - 2Int_2^s(1) + Int_2^s(2)). \quad (4.76)$$

The integral Int_R is evaluated from

$$Int_R = I_R(\mathbf{r}_{64}, \mathbf{r}_{56}, 0), \quad (4.77)$$

with I_R defined in the nonsingular case.

Last step of integration

The last step is to combine the integrals (4.35)-(4.37) in the middle step, in order to evaluate the integrals J_p^0 . At this point, it does not matter if the integrand was singular in the middle step of integration. When computing J_1^0 we evaluate

$$J_1^0(p, j) = \int \frac{r'_j}{cR^p} \Phi_m(\mathbf{r}') dS, \quad j = 1, 2, \quad p = 1, 2, \quad (4.78)$$

where

$$r'_j = r_{4,j} + \alpha r_{54,j} + \beta r_{64,j}, \quad (4.79)$$

$$\Phi_m(\mathbf{r}') = a_0 + a_1 \alpha + a_2 \beta. \quad (4.80)$$

The integrals $J_1^0(p, j)$ and $J_2^0(p, j)$ are linear combinations of the integrals $Int_p(n, m)$ computed for both the nonsingular and singular cases. It should be noted that in the singular case $r_{4,j} = 0$, and we get no contribution from $Int_p(0, 0)$, which is an improper integral. The integral J_3^0 is a linear combination of $Int_p(n, m)$ and Int_R .

4.2.3 Case $\omega > 0$

Our goal is to evaluate the integrals J_p^ω , $p = 1, 2, 3$, introduced earlier in (3.74)-(3.76). We focus on

$$\int \frac{r'_j}{cR^2} e^{-\frac{\omega}{c}R} \Phi_m(\mathbf{r}') dS, \quad \int \frac{1}{R} e^{-\frac{\omega}{c}R} \Phi_m(\mathbf{r}') dS$$

since the other integrals are either special cases of those above or evaluated in the case when $\omega = 0$. We have not found any analytical expressions for these integrals, and numerical quadrature is used. As a first step we evaluate the integrals

$$\int_0^1 \int_0^{1-\alpha} \frac{\{1, \alpha, \beta, \alpha\beta, \alpha^2, \beta^2\}}{R^2} e^{-\frac{\omega}{c}R} d\beta d\alpha, \quad \int_0^1 \int_0^{1-\alpha} \frac{\{1, \alpha, \beta\}}{R} e^{-\frac{\omega}{c}R} d\beta d\alpha,$$

numerically, using an algorithm 6 in the appendix A.1.2. Those integrals are then combined to get the required integrals, for different r'_j and $\Phi_m(\mathbf{r}')$. In the singular case, we perform the Duffy transform, $\alpha = \xi_1 \xi_2$ and $\beta = \xi_1(1 - \xi_2)$. When $\omega > 0$, the integrals does not decouple, which leads to numerical integration over a square, in appendix A.1.3. This is done by integrating over two triangles with the same algorithm as in the nonsingular case.

4.3 Integration of a circle sector

4.3.1 Local coordinates on a circle sector

We want to integrate over a circle sector in the K' triangle plane with center in $P\mathbf{r}$. The circle sector has radius v_2 and angles between ϕ_1 and ϕ_2 in the K' triangle plane. We have the parameterization

$$\mathbf{r}'(v, \phi) = P\mathbf{r} + v \cos \phi \mathbf{e}_1^{K'} + v \sin \phi \mathbf{e}_2^{K'} \quad (4.81)$$

where

$$v \in [0, v_2], \quad \phi \in [\phi_1, \phi_2], \quad (4.82)$$

and $e_j^{K'}$ are the basis functions for the K' triangle plane. The integral to be computed is

$$\int f(\mathbf{r}') d\mathbf{r}' = \int_0^{v_2} \int_{\phi_1}^{\phi_2} v f(\mathbf{r}'(v, \phi)) d\phi dv. \quad (4.83)$$

We need to express x and y that appears in $\Phi_j^{K'}$ in α and β , by solving the system (3.11), with $\mathbf{r} = \mathbf{r}'(v, \phi)$. The spatial basis function can then be computed

$$\Phi_j^{K'}(\mathbf{r}'(v, \phi)) = a_0 + a_1 v \cos \phi + a_2 v \sin \phi, \quad (4.84)$$

following the same procedure as in the triangle case.

4.3.2 Elimination of ϕ

It should be observed that $R = \sqrt{|\mathbf{r} - P\mathbf{r}|^2 + v^2}$ is independent of ϕ . This means that ϕ only appears in r'_j and $\Phi_m(\mathbf{r}')$, when computing the integrals J_p^ω . Let $f(R)$ be the part of J_p^ω that is independent of ϕ and consider the integrals

$$\iint v \Phi_m(\mathbf{r}') f(R) d\phi dv = \int \left(\int v \Phi_m(\mathbf{r}') d\phi \right) f(R) dv, \quad (4.85)$$

$$\iint v r'_j \Phi_m(\mathbf{r}') f(R) d\phi dv = \int \left(\int v r'_j \Phi_m(\mathbf{r}') d\phi \right) f(R) dv. \quad (4.86)$$

From (4.85) we obtain the integral

$$\int v \Phi_m(\mathbf{r}') d\phi = b_0 v + b_1 v^2, \quad (4.87)$$

where

$$b_0 = (\phi_2 - \phi_1) a_0, \quad (4.88)$$

$$b_1 = (\sin \phi_2 - \sin \phi_1) a_1 - (\cos \phi_2 - \cos \phi_1) a_2. \quad (4.89)$$

Since $r'_1 = v \cos \phi$ and $r'_2 = v \sin \phi$, we obtain the integrals

$$\int vr'_1 \Phi_m(\mathbf{r}') d\phi = b_{01}v^2 + b_{11}v^3, \quad (4.90)$$

$$\int vr'_2 \Phi_m(\mathbf{r}') d\phi = b_{02}v^2 + b_{12}v^3, \quad (4.91)$$

from (4.86) where

$$b_{01} = (\sin \phi_2 - \sin \phi_1)a_0, \quad (4.92)$$

$$b_{11} = (t_1 + t_2)a_1 + t_3a_2, \quad (4.93)$$

$$b_{02} = -(\cos \phi_2 - \cos \phi_1)a_0, \quad (4.94)$$

$$b_{12} = t_3a_1 + (t_1 - t_2)a_2, \quad (4.95)$$

$$t_1 = \frac{1}{2}(\phi_2 - \phi_1), \quad (4.96)$$

$$t_2 = \frac{1}{2}(\cos \phi_2 \sin \phi_2 - \cos \phi_1 \sin \phi_1), \quad (4.97)$$

$$t_3 = -\frac{1}{2}(\cos^2 \phi_2 - \cos^2 \phi_1). \quad (4.98)$$

4.3.3 Case $\omega = 0$

When the integral over ϕ has been eliminated, the integrals J_p^0 can be reduced to the cases

$$Int_1(p) = \int_0^{v_2} \frac{v^p}{\sqrt{|\mathbf{r}-P\mathbf{r}|^2 + v^2}} dv, \quad p = 1, 2, 3, \quad (4.99)$$

$$Int_2(p) = \int_0^{v_2} \frac{v^p}{|\mathbf{r}-P\mathbf{r}|^2 + v^2} dv, \quad p = 2, 3, \quad (4.100)$$

$$Int_R = \int_0^{v_2} v \sqrt{|\mathbf{r}-P\mathbf{r}|^2 + v^2} dv, \quad (4.101)$$

$$Int_0 = \int_0^{v_2} v dv. \quad (4.102)$$

These can be computed analytically and we obtain

$$Int_1(1) = \frac{v_2^2}{\sqrt{|\mathbf{r}-P\mathbf{r}|^2 + v_2^2} + \sqrt{|\mathbf{r}-P\mathbf{r}|^2}}, \quad (4.103)$$

$$Int_1(2) = \frac{v_2}{2} \sqrt{|\mathbf{r}-P\mathbf{r}|^2 + v_2^2} - \frac{|\mathbf{r}-P\mathbf{r}|^2}{2} \log \left(\frac{v_2 + \sqrt{|\mathbf{r}-P\mathbf{r}|^2 + v_2^2}}{|\mathbf{r}-P\mathbf{r}|} \right), \quad (4.104)$$

$$Int_1(3) = \frac{v_2^2}{3} \left(\sqrt{|\mathbf{r}-P\mathbf{r}|^2 + v_2^2} - \frac{2|\mathbf{r}-P\mathbf{r}|^2}{(\sqrt{|\mathbf{r}-P\mathbf{r}|^2 + v_2^2} + |\mathbf{r}-P\mathbf{r}|)} \right), \quad (4.105)$$

$$Int_2(2) = v_2 - |\mathbf{r}-P\mathbf{r}| \arctan \left(\frac{v_2}{d_2} \right), \quad (4.106)$$

$$Int_2(3) = \frac{v_2^2}{2} - |\mathbf{r}-P\mathbf{r}|^2 \log \left(\frac{\sqrt{|\mathbf{r}-P\mathbf{r}|^2 + v_2^2}}{|\mathbf{r}-P\mathbf{r}|} \right), \quad (4.107)$$

$$Int_R = \frac{(\sqrt{|\mathbf{r}-P\mathbf{r}|^2 + v_2^2})^3 - |\mathbf{r}-P\mathbf{r}|^3}{3}, \quad (4.108)$$

$$Int_0 = \frac{v_2^2}{2}. \quad (4.109)$$

In the singular case, when $|\mathbf{r}-P\mathbf{r}| = 0$, the integrals are

$$Int_1(1) = v_2, \quad (4.110)$$

$$Int_1(2) = \frac{v_2^2}{2}, \quad (4.111)$$

$$Int_1(3) = \frac{v_2^3}{3}, \quad (4.112)$$

$$Int_2(2) = v_2, \quad (4.113)$$

$$Int_2(3) = \frac{v_2^2}{2}, \quad (4.114)$$

$$Int_R = \frac{v_2^3}{3}, \quad (4.115)$$

$$Int_0 = \frac{v_2^2}{2}. \quad (4.116)$$

The integrals J_p^0 are linear combinations of the integrals above.

4.3.4 Case $\omega > 0$

After eliminating the integral over ϕ , we focus on the integrals

$$Int_1(p) = \int_0^{v_2} \frac{v^p e^{-\frac{\omega}{c}R}}{R} dv, \quad p = 1, 2, \quad (4.117)$$

$$Int_2(p) = \int_0^{v_2} \frac{v^p e^{-\frac{\omega}{c}R}}{R^2} dv, \quad p = 2, 3. \quad (4.118)$$

All other integrals are evaluated for the case $\omega = 0$. We can compute

$$Int_1(1) = -\frac{c}{\omega} \left(e^{-\frac{\omega}{c} \sqrt{|\mathbf{r}-P\mathbf{r}|^2+v_2^2}} - e^{-\frac{\omega}{c} |\mathbf{r}-P\mathbf{r}|} \right) \quad (4.119)$$

analytically. The other integrals are computed numerically, using an adaptive Romberg method, described in algorithm 5 in appendix A.1.1.

4.4 Integration of a circle

This is a special case of the circle sector case with $\phi_1 = 0$ and $\phi_2 = 2\pi$. In the elimination of the integral over ϕ , we get

$$b_0 = 2\pi a_0, \quad b_{11} = \pi a_1, \quad b_{12} = \pi a_2, \quad b_1 = b_{01} = b_{02} = 0.$$

Some of the integrals over the circle sector can therefore be omitted.

4.5 Integration of a circle segment

When the domain is a circle segment, we have two alternatives in evaluating the integral. The first is to integrate the corresponding circle sector and subtract the corresponding triangle. The other alternative is to evaluate the integrals numerically, using Gaussian quadrature. The second approach is good for small angles. If the angle increases, then R is not approximately constant and the Gaussian quadrature is no longer usable. Then we use the first approach.

If Gaussian quadrature is to be used, the integrand has to behave like a polynomial, i.e. the distance term has to be close to constant. The worst case when $|\mathbf{r}-P\mathbf{r}| = 0$. If R is allowed to vary

$$|\mathbf{r}' - P\mathbf{r}| \in [(1 - \varepsilon)v, v],$$

the maximum angle can be computed as

$$\Delta\phi = 2 \arccos(1 - \varepsilon).$$

For small ε , $1/|\mathbf{r}' - P\mathbf{r}|$ can be considered to be constant. For instance, if $\varepsilon = 0.1$, angles up to 51.7° are allowed. Numerical experiments show that it is sufficient to use 10 gauss points for α and 4 gauss points for β to evaluate the integrals to machine precision, in the case when $|\mathbf{r}-P\mathbf{r}| = 0$ and $\Delta\phi = 45^\circ$. When $\Delta\phi = 22.5^\circ$, it suffices with 6 gauss points for α and 2 gauss points for β to get at least 14 digits accuracy. The rest of the chapter will treat the evaluation of the integral numerically.

4.5.1 Local coordinates on a circle segment

We want to integrate over a circle segment in the K' triangle plane with center in $P\mathbf{r}$ and radius v . Let $\mathbf{r}'_c(\alpha)$ denote a point on the circle between the angles ϕ_1 and ϕ_2 and $\mathbf{r}'_l(\alpha)$ denote a point on the line between the same angles. Introducing the notation

$$c(\alpha) = (1 - \alpha) \cos \phi_1 + \alpha \cos \phi_2, \quad (4.120)$$

$$s(\alpha) = (1 - \alpha) \sin \phi_1 + \alpha \sin \phi_2, \quad (4.121)$$

$$\phi(\alpha) = (1 - \alpha)\phi_1 + \alpha\phi_2, \quad (4.122)$$

yields the parameterization

$$\mathbf{r}'_c(\alpha) = P\mathbf{r} + v \cos \phi(\alpha) \mathbf{e}_1^{K'} + v \sin \phi(\alpha) \mathbf{e}_2^{K'}, \quad (4.123)$$

$$\mathbf{r}'_l(\alpha) = P\mathbf{r} + vc(\alpha) \mathbf{e}_1^{K'} + vs(\alpha) \mathbf{e}_2^{K'} \quad (4.124)$$

where v is the radius of the circle. The points on the circle segment can be parameterized

$$\mathbf{r}'(\alpha, \beta) = (1 - \beta) \mathbf{r}'_c(\alpha) + \beta \mathbf{r}'_l(\alpha). \quad (4.125)$$

The integral to be computed is

$$\int f(\mathbf{r}') d\mathbf{r}' = \int_0^1 \int_0^1 f(\mathbf{r}'(\alpha, \beta)) \left| \frac{d\mathbf{r}'(\alpha, \beta)}{d(\alpha, \beta)} \right| d\alpha d\beta. \quad (4.126)$$

Integration over α and β yields a Jacobian contribution

$$\begin{aligned} \frac{d\mathbf{r}'}{d(\alpha, \beta)} &= v^2(1 - \beta)(\phi_2 - \phi_1)[1 - c(\alpha) \cos \phi(\alpha) - s(\alpha) \sin \phi(\alpha)] + \\ &+ v^2\beta[(s_2 - s_1)(\cos \phi(\alpha) - c(\alpha)) - (c_2 - c_1)(\sin \phi(\alpha) - s(\alpha))], \end{aligned} \quad (4.127)$$

where $c_j = \cos(\phi_j)$ and $s_j = \sin(\phi_j)$.

For the case of a circle segment, the basis function can be written

$$\Phi_j^{K'} = a_0 + a_1\beta + a_2\alpha\beta + a_3 \cos \phi + a_4 \sin \phi + a_5\beta \cos \phi + a_6\beta \sin \phi, \quad (4.128)$$

where $\Phi_j^{K'} = \Phi_j^{K'}(\mathbf{r}'(\alpha, \beta))$ and $\phi = \phi(\alpha)$. Using the two representations of \mathbf{r}' , we derive a matrix system, as in (3.11), where the solution are the parameters x and y . The system is

$$\begin{pmatrix} \mathbf{r}_{21} \cdot \mathbf{r}_{21} & \mathbf{r}_{31} \cdot \mathbf{r}_{21} \\ \mathbf{r}_{21} \cdot \mathbf{r}_{31} & \mathbf{r}_{31} \cdot \mathbf{r}_{31} \end{pmatrix} \begin{pmatrix} x \\ y \end{pmatrix} = \begin{pmatrix} b_2 \\ b_3 \end{pmatrix}, \quad (4.129)$$

where

$$c_0^j = (-\mathbf{r}_1, \mathbf{r}_{j1}), \quad (4.130)$$

$$c_1^j = (\mathbf{e}_1, \mathbf{r}_{j1}), \quad (4.131)$$

$$c_2^j = (\mathbf{e}_2, \mathbf{r}_{j1}), \quad (4.132)$$

$$\begin{aligned} b_j = & c_0^j + v[c_1^j \cos(\phi_1) + c_2^j \sin(\phi_1)]\beta \\ & + v[c_1^j (\cos(\phi_2) - \cos(\phi_1)) + c_2^j (\sin(\phi_2) - \sin(\phi_1))]\alpha\beta \\ & + vc_1^j \cos \phi(\alpha) + vc_2^j \sin \phi(\alpha) - vc_1^j \beta \cos \phi(\alpha) - vc_2^j \beta \sin \phi(\alpha). \end{aligned} \quad (4.133)$$

Solving this system of equation for a_p with seven different right hand sides, yields the constants a_p , $p = 0, 1, \dots, 6$, for the different spatial basis functions. The computation of J_p^0 and J_p^ω is now direct, using Gaussian quadrature.

Chapter 5

Stabilization

5.1 Background

Our Marching On in Time method described in chapter 6 is on the form

$$\mathbf{A}_0 \mathbf{J}_n + \mathbf{A}_1 \mathbf{J}_{n-1} + \dots + \mathbf{A}_k \mathbf{J}_{n-k} = \mathbf{b}_n, \quad (5.1)$$

$$\mathbf{J}_p = \mathbf{0}, \quad p \leq 0. \quad (5.2)$$

where $\mathbf{A}_p \in \mathbb{R}^{N \times N}$, $\mathbf{J}_p, \mathbf{b}_n \in \mathbb{R}^N$ and N is the number of nodes on the scatterer surface. Moreover we require $\mathbf{b}_p = \mathbf{0}$, for $p \leq 0$. It is assumed that \mathbf{A}_0 is non-singular, otherwise the solution does not exist or is non-unique. When we solve the Dirichlet problem with the variational formulation 1 coming from the Kirchhoff formula, we have some eigenvalues close to -1 . If those eigenvalues leaves the unit circle due to numerical errors, the time marching scheme becomes unstable. In [6], P.J. Davies and D.B. Duncan uses a time averaging scheme, with a filter $\mathbf{J}_n \rightarrow \frac{1}{4}(\mathbf{J}_{n+1} + 2\mathbf{J}_n + \mathbf{J}_{n-1})$. The scheme is listed in algorithm 2.

Algorithm 2 Averaging scheme of Davies and Duncan

- 1: $\sigma_n = \mathbf{b}_n - \sum_{p=2}^k \mathbf{A}_p \mathbf{J}_{n-p}$
 - 2: $\mathbf{J}_n^* = \mathbf{A}_0^{-1} (\sigma_n - \mathbf{A}_1 \mathbf{J}_{n-1}^{**})$
 - 3: $\mathbf{J}_{n-1} = \frac{1}{4} (\mathbf{J}_n^* + 2\mathbf{J}_{n-1}^{**} + \mathbf{J}_{n-2})$
 - 4: $\mathbf{J}_n^{**} = \mathbf{A}_0^{-1} (\sigma_n - \mathbf{A}_1 \mathbf{J}_{n-1})$
-

In algorithm 2, \mathbf{J}_n^* and \mathbf{J}_n^{**} are stored only temporarily. We will see that this averaging scheme is a natural choice. To do this we define what we mean with stability.

Definition 4. The algorithm (5.1) is stable iff

$$\|\mathbf{J}_n\| \leq C_1 \sum_{p=0}^n \|\mathbf{b}_p\|, \quad (5.3)$$

where the constant C_1 does not depend on n .

Two different problem types can be distinguished:

- Finite object, with fixed number of matrix blocks k (for given Δt).
- Infinite object, with increasing matrix blocks k (for given Δt).

Here we only consider the case of a finite object.

5.2 Stability analysis for a finite object

By writing (5.1) as a one step method, we can examine the stability.

$$\tilde{\mathbf{J}}_n = \tilde{\mathbf{A}}_k \tilde{\mathbf{J}}_{n-1} + \tilde{\mathbf{b}}_n, \quad \tilde{\mathbf{J}}_0 = \mathbf{0}, \quad (5.4)$$

$$\tilde{\mathbf{A}}_k = \begin{pmatrix} -\mathbf{A}_0^{-1} \mathbf{A}_1 & \dots & -\mathbf{A}_0^{-1} \mathbf{A}_{k-1} & -\mathbf{A}_0^{-1} \mathbf{A}_k \\ \mathbf{I} & & & \\ & \ddots & & \\ & & & \mathbf{I} \end{pmatrix}, \quad (5.5)$$

$$\tilde{\mathbf{J}}_n^T = (\mathbf{J}_n, \dots, \mathbf{J}_{n-k}), \quad (5.6)$$

$$\tilde{\mathbf{b}}_n^T = \left((\mathbf{A}_0^{-1} \mathbf{b}_n)^T, 0, \dots, 0 \right). \quad (5.7)$$

Lemma 7. If the eigenvalues of $\tilde{\mathbf{A}}_k$ are strictly inside the unit circle, then the algorithm (5.1) is stable.

Proof. Since $\tilde{\mathbf{J}}_0 = \mathbf{0}$, we have

$$\begin{aligned} \tilde{\mathbf{J}}_n &= \sum_{p=0}^n \tilde{\mathbf{A}}_k^p \tilde{\mathbf{b}}_{n-p} \\ &= [\text{Jordan decomposition } \tilde{\mathbf{A}}_k = \tilde{\mathbf{S}} \tilde{\mathbf{K}} \tilde{\mathbf{S}}^{-1}] \\ &= \sum_{p=0}^n \tilde{\mathbf{S}} \tilde{\mathbf{K}}^p \tilde{\mathbf{S}}^{-1} \tilde{\mathbf{b}}_{n-p} \end{aligned} \quad (5.8)$$

If all eigenvalues of $\tilde{\mathbf{A}}_k$ are strictly inside the unit circle, then $\|\tilde{\mathbf{S}} \tilde{\mathbf{K}}^p \tilde{\mathbf{S}}^{-1}\| \leq C$ and $\tilde{\mathbf{J}}_n$ is bounded by

$$\|\tilde{\mathbf{J}}_n\| \leq C \sum_{p=0}^n \|\tilde{\mathbf{b}}_{n-p}\|. \quad (5.9)$$

The constant C depends on the largest eigenvalue and the size of the largest Jordan block, which both are independent of n . For the original problem, this yields

$$\|\mathbf{J}_n\| \leq C_1 \sum_{p=0}^n \|\mathbf{b}_p\|, \quad C_1 = \|A_0^{-1}\|C, \quad (5.10)$$

i.e. the constant C_1 does not depend on n . \square

A stabilizing filter should have at least two properties

- Sufficiently high order in time, not to destroy the time order
- Increase the stability region of the scheme

Such a filter is

$$\tilde{\mathbf{J}}_n \rightarrow \frac{1}{4} \left(\tilde{\mathbf{J}}_{n+1} + 2\tilde{\mathbf{J}}_n + \tilde{\mathbf{J}}_{n-1} \right). \quad (5.11)$$

We can show the following

Lemma 1. *The filter (5.11) applied on the scalar scheme $y_n = \lambda y_{n-1}$ is second order accurate in time and is stable for λ such that $|\lambda + 1| < 2$.*

Proof. The second order accuracy is shown by Taylor expansion of $y_{n\pm 1}$. Applying the filter, yields

$$y_n \rightarrow \frac{1}{4} (y_{n+1} + 2y_n + y_{n-1}) = \left(\frac{\lambda + 1}{2} \right)^2 y_{n-1}. \quad (5.12)$$

This shows that the stability region is λ such that $|\lambda + 1| < 2$. \square

Using the filter yields produces the following modified algorithm

$$\tilde{\mathbf{J}}_n = \left(\frac{\tilde{\mathbf{A}}_k + \mathbf{I}}{2} \right)^2 \tilde{\mathbf{J}}_{n-1} + \frac{1}{4} \left(\tilde{\mathbf{A}}_k \tilde{\mathbf{b}}_n + 2\tilde{\mathbf{b}}_n + \tilde{\mathbf{b}}_{n+1} \right), \quad \tilde{\mathbf{J}}_{-1} = \mathbf{0}. \quad (5.13)$$

If we require $\tilde{\mathbf{b}}_1 = \mathbf{0}$, then we can have the same initial condition as in the non-stabilized algorithm, i.e. $\tilde{\mathbf{J}}_0 = \mathbf{0}$. In the case of solving the wave equation, we can delay the incident transient by Δt , to force $\tilde{\mathbf{b}}_1 = \mathbf{0}$. Writing the filter on the k -step form yields algorithm 3.

Algorithm 3 New averaging scheme

- 1: $\sigma_{n+1} = \mathbf{b}_{n+1} - \sum_{p=2}^k \mathbf{A}_p \mathbf{J}_{n+1-p}$,
 - 2: $\mathbf{J}_{n+1}^* = \mathbf{A}_0^{-1} (\sigma_{n+1} - \mathbf{A}_1 \mathbf{J}_n^{**})$,
 - 3: $\mathbf{J}_n = \frac{1}{4} (\mathbf{J}_{n+1}^* + \mathbf{J}_n^{**} + \mathbf{J}_{n-1})$,
 - 4: $\mathbf{J}_{n-1} = \frac{1}{4} (\mathbf{J}_n^{**} + 2\mathbf{J}_{n-1} + \mathbf{J}_{n-2})$,
 - 5: $\mathbf{J}_{n-p} = \frac{1}{4} (\mathbf{J}_{n-p+1} + 2\mathbf{J}_{n-p} + \mathbf{J}_{n-p-1})$, $p = 2, \dots, k-1$,
 - 6: $\mathbf{J}_{n+1}^{**} = \mathbf{A}_0^{-1} (\sigma_{n+1} - \mathbf{A}_1 \mathbf{J}_n)$.
-

The algorithm updates the last k time-steps of \mathbf{J} in each iteration. This means that \mathbf{J}_{n-k} has an $k\Delta t^2$ error. In case of a wave propagation algorithm, k depends on the size of the scatterer as $k \sim (\text{Size of scatterer})/c\Delta t$. The error of the filter increases with the object size. If we ignore all but the first smoothing step, then this scheme becomes identical to the scheme proposed by Davies and Duncan. This will actually be the most stable choice. In the numerical experiments we will only use one smoothing step.

Chapter 6

Marching On in Time method

In this chapter we will discuss how to make an algorithm out of the different variational formulations obtained in the previous chapters. Variational formulations containing retarded potentials has a coupling in space and time, where the solutions at a time depends on solutions at other times. In the case of constant elements in time, the solution only depends on solutions from the past. We can then step forward in time in an explicit way. If we are using higher order elements, the solution depends also on later time steps, which makes the scheme implicit. We will only consider the case with an explicit scheme.

In section 6.1, the matrix structure in the method is discussed. The method results in a lower triangular block matrix, which can be solved with forward substitution.

In section 6.2, the assembly procedure is explained. The integral over the spatial test functions are evaluated using numerical quadrature. For each quadrature point on each test triangle, a strip is obtained, with a radius depending on the difference in basis function index in time. Those strips cover parts of some triangles, and these triangle parts are detected.

6.1 Matrix structure in MOT

Solving the wave equation using one of the variational formulations discussed in chapter 2 and 3 is done in two steps.

- Assembly of matrix
- Solving the system (or stepping in time)

For test functions $J_{jk}^t(\mathbf{r}, t) = \Phi_j(\mathbf{r})\tilde{\Psi}_k(t)$, defined in section 3.2, we get the system

$$\sum_{m,l} A_{j,m,k-l} J_{ml} = b_{jk}.$$

For the constant time element case, when $k < l$ in our variational formulations, then $A_{j,m,k-l} = 0$. Ordering the vector \mathbf{J}_l , \mathbf{b}_k and the matrix \mathbf{A}_u , with $u = k - l$ s.t.

$$(\mathbf{J}_l)_m = J_{ml}, \quad (\mathbf{b}_k)_j = b_{jk}, \quad (\mathbf{A}_u)_{j,m} = A_{j,m,u},$$

the following block matrix system

$$\begin{pmatrix} \mathbf{A}_0 & & & & & \\ \mathbf{A}_1 & \mathbf{A}_0 & & & & \\ \mathbf{A}_2 & \mathbf{A}_1 & \mathbf{A}_0 & & & \\ \mathbf{A}_3 & \mathbf{A}_2 & \mathbf{A}_1 & \ddots & & \\ \vdots & \mathbf{A}_3 & \mathbf{A}_2 & \ddots & & \\ & \vdots & \mathbf{A}_3 & \ddots & & \\ & & \vdots & \ddots & & \end{pmatrix} \begin{pmatrix} \mathbf{J}_1 \\ \mathbf{J}_2 \\ \mathbf{J}_3 \\ \vdots \end{pmatrix} = \begin{pmatrix} \mathbf{b}_1 \\ \mathbf{b}_2 \\ \mathbf{b}_3 \\ \mathbf{b}_4 \\ \vdots \end{pmatrix} \quad (6.1)$$

is obtained. The system is solved with forward substitution,

$$\mathbf{J}_k = \mathbf{A}_0^{-1} \left(\mathbf{b}_k - \sum_{p=0}^P \mathbf{A}_p \mathbf{J}_{k-p} \right), \quad (6.2)$$

where $\mathbf{J}_q = \mathbf{0}$, if $q \leq 0$. The smallest sphere that includes the whole scatterer has diameter $\lesssim Pc\Delta t$. This diameter determines the number of terms in the sum.

6.2 Assembly of matrix block \mathbf{A}_u

In the assembly process, we have to compute triple integrals, where two of the integrals are over the scatterer and one integral is over time. The time integral is computed analytically. The outer integration is done with a numerical integration method,

$$\iint f(\mathbf{r}, \mathbf{r}') dK' dK = \sum_p w_p \int f(\mathbf{r}_p) dK',$$

where w_p depends on the quadrature formula, e.g. Gaussian quadrature on a triangle. For each triangle K , and for all the integration points \mathbf{r}_p , we get a strip over some of the triangles K' in the inner integral. The integrals over those strips are calculated and assembled into the matrix.

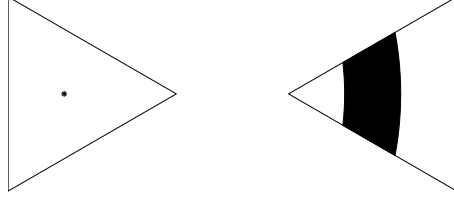


Figure 6.1. Fix a point on triangle K (left) to get a strip over triangle K' (right)

A pseudo code for the assembly process of the matrix blocks \mathbf{A}_u is

Algorithm 4 Assembly process of matrix blocks

```

1: for all triangles  $K$  do
2:   for all quadpoints  $\mathbf{r}$  on triangle  $K$  do
3:     for all triangles  $K'$  do
4:       First selection of admissible time basis differences  $u = k - l$ ,  $p_1 \leq u \leq q_1$ 
5:       for  $u = p_1$  to  $q_1$  do
6:         Find domain  $D \subseteq K'$  that interact with quadpoint  $\mathbf{r}$  with current  $u$ .
7:         if domain  $D \neq \emptyset$  then
8:           Integrate over  $D$ .
9:           Assemble the matrix with the integral value.
10:        end if
11:       end for
12:     end for
13:   end for
14: end for

```

6.2.1 First selection of admissible time differences

Since the basis functions have compact support, for fixed triangles K and K' and time $k\Delta t$, we only get contribution from finite number of time steps at times $l\Delta t$. When using constant time elements, we get a sharp condition for the admissible time basis difference $u = k - l$,

$$\min_{\mathbf{r} \in K, \mathbf{r}' \in K'} \frac{|\mathbf{r} - \mathbf{r}'|}{c\Delta t} - 1 \leq u < \max_{\mathbf{r} \in K, \mathbf{r}' \in K'} \frac{|\mathbf{r} - \mathbf{r}'|}{c\Delta t} + 1,$$

where Ψ_k and Ψ_l are the interacting basis functions in time. Let the midpoint \mathbf{r}_c^K of a triangle K be the mean value of its corners. The triangle radius is defined as

$$\text{rad}(K) = \max_j |\mathbf{r}_j^K - \mathbf{r}_c^K|,$$

where \mathbf{r}_j^K are the nodes of the triangle K . To estimate the bounds on u , we can use the midpoint and radius of the triangles. The first selection of admissible time differences is u in the interval

$$\frac{|\mathbf{r}_c^K - \mathbf{r}_c^{K'}| - \text{rad}(K) - \text{rad}(K')}{c\Delta t} - 1 \leq u < \frac{|\mathbf{r}_c^K - \mathbf{r}_c^{K'}| + \text{rad}(K) + \text{rad}(K')}{c\Delta t} + 1.$$

The radiuses $\text{rad}(K)$ can be precalculated before the assembly process.

6.2.2 Find domain on K'

Let K and $u = k - l$ be given. A point $\mathbf{r} \in K$ interacts with points \mathbf{r}' lying within two spherical shells $v_{\min} \leq |\mathbf{r} - \mathbf{r}'| \leq v_{\text{mid}}$ and $v_{\text{mid}} \leq |\mathbf{r} - \mathbf{r}'| \leq v_{\max}$, s.t.

$$v_{\min} = (u - 1)c\Delta t, \quad (6.3)$$

$$v_{\text{mid}} = uc\Delta t, \quad (6.4)$$

$$v_{\max} = (u + 1)c\Delta t. \quad (6.5)$$

We want to find the domain on triangle K' that intersects with this spherical shell. The triangle plane of K' cuts out a circle from the sphere. The center is the projection $P\mathbf{r}$ of \mathbf{r} onto the K' -plane. The radius Pv of the circle is calculated by

$$Pv = \sqrt{v^2 - |\mathbf{r} - P\mathbf{r}|^2},$$

where $v \in [v_{\min}, v_{\max}]$, see figure 6.2. If $v^2 - |\mathbf{r} - P\mathbf{r}|^2$ is negative, the sphere has not reached the triangle plane. We need the circles corresponding to v_{\min} , v_{mid} and v_{\max} .

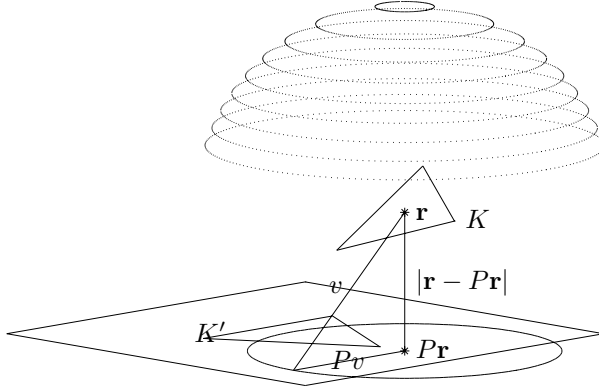


Figure 6.2. Triangle plane cuts out a circle of a sphere

We get the integral of a strip over the triangle by calculating over two domains as indicated in figure 6.3. Each triangle pair (K, K') and each time basis function difference u requires three integrals where the domain is the intersection of a circle and a triangle. Each of the three integral domains are subdivided into triangle, circle, circle sector and circle segment domains, which can be computed, either exact or with numerical integration. The integration is discussed in chapter 4.

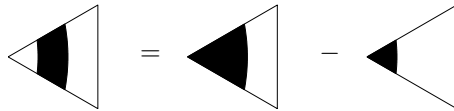


Figure 6.3. Integration of a strip over triangle K'

6.2.3 Circle intersecting a triangle

We want to calculate the intersections between a circle and a triangle. The only time we can get an odd number of intersections is the case when the circle intersect the triangle in a corner and the case when a triangle side is a tangent to the circle. If we treat these as special cases, we can identify the intersected domain with number of intersection points and number of triangle corners inside the circle. There are two different cases, when the projection $P\mathbf{r}$ of the point $\mathbf{r} \in K$ are inside or outside the triangle K' . Each of the cases can be divided in another eight different cases, depending on the number of triangle corners that is inside the circle and the number of intersections between the circle and triangle, see figure 6.4. All of the 16 cases can be constructed from triangles, circles and circle segments. The integrals arising in the different variational formulations in chapters 2 and 3 are treated in chapter 4.

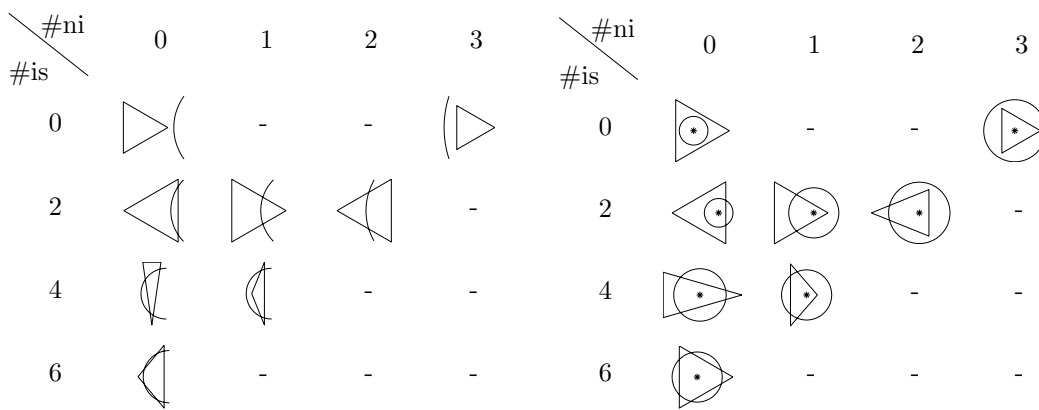


Figure 6.4. *Pr* outside (inside) K' to left (right).
 #ni is the number of triangle nodes inside the circle.
 #is is the number of intersection points.

Chapter 7

Numerical experiments on Kirchhoff integral equation

In this section, we will perform numerical tests on the variational formulation 1 in chapter 2. Two test cases are considered; a point source illuminating a plate and a plane wave illuminating a sphere. Those two cases has an analytical solution.

In the case of a point source illuminating a plate, we use the analytic solution from an infinite plane. In order to determine if the method is stable, we compute eigenvalues of the system matrix in the one-step method (5.4). We conclude that it is necessary to use the stabilization filter in algorithm 2. The stability of the method is related to the number of numerical integration points in the integral over the test functions in space. The method has first order of accuracy in time and approximately second order in space in the computation of the potential on the surface. The computed scattered fields are compared with analytical solutions.

In the case of a plane wave illuminating a sphere, the computed scattered fields are compared with analytical solutions at three different observation points.

7.1 Test case with a plate

Consider a Dirichlet plate $(x, y) \in [-5, 5]^2, z = 0$ as in figure 7.1. We want to compute the potential $\mathbf{J}^{\text{CFL}}(\mathbf{r}, t)$ on the plate for a point source in $\mathbf{r}_s = (0, 0, 2)$, for different CFL -numbers, where $CFL = \frac{c_0 \Delta t}{h}$ and h is the length of the largest edge on the scatterer. The point source produce an incoming wave

$$u^{inc}(\mathbf{r}, t) = \frac{f^\infty((t - |\mathbf{r} - \mathbf{r}_s|/c_0 - t_0)/T)}{|\mathbf{r} - \mathbf{r}_s|} \quad (7.1)$$

$$f^\infty(x) = \begin{cases} e^{1-1/(1-|x|^2)}, & |x| < 1, \\ 0, & |x| \geq 1 \end{cases} \quad (7.2)$$

where t_0 is a time delay and T determines the width of the pulse. The velocity is set to $c_0 = \frac{1}{2}$. The potential can be used to compute the scattered field. In the case of an infinite plate, we can compute the exact scattered field by the method of images [14]. We compare the scattered field of our finite plate with the exact scattered field of the infinite plate. The potential on a 17×17 grid, where $T = 20$ and $t_0 = 30$ is computed with a stabilized scheme and presented in figure 7.2. We see that the effect of the boundary is marginal in the interior of the plate. The scattered field at an observation point in $(0, 0, 0.25)$ is computed with a stabilized scheme and plotted in figure 7.3. From the leftmost subfigures (c) and (f) it is clear that the scheme is stable, since the error rapidly decreases when the incoming pulse has passed the plate.

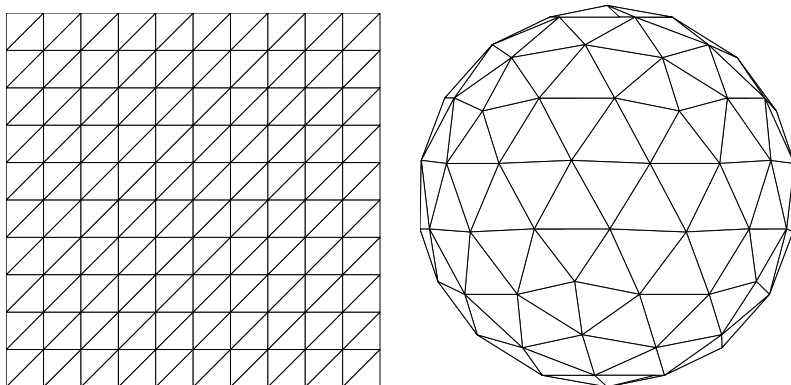


Figure 7.1. Triangulated plate with 11×11 nodes (left) and sphere with 92 nodes (right).

7.2 Stability of Dirichlet plate

In order to determine if a scheme is stable or not, we compute the eigenvalues of the corresponding one-step method given by (5.4). If the largest eigenvalues are outside the unit circle, then the scheme is unstable. We consider a 9×9 grid discretization of the plate. We use a trapezoidal method for the outer integral (over the triangles K), with 6 and 10 points. In table 7.1, we present the largest eigenvalues of the one-step method. The table shows that we get a more stable scheme using 10 quadrature points than using 6 points for the integrals over K . This indicates that the number of required quadrature points increases as the CFL number decreases. When we use the stabilization filter the scheme becomes stable for smaller CFL numbers.

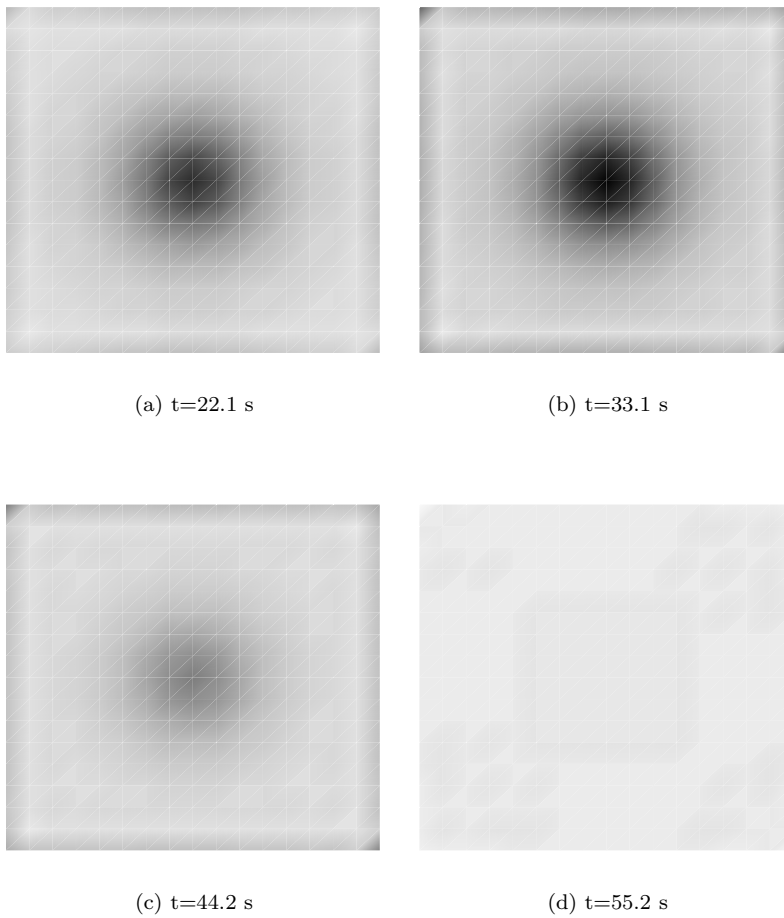


Figure 7.2. Potential at different times for 17×17 plate, with $CFL = 0.5$.

7.3 Order of accuracy in time of Dirichlet plate

In order to get first order of accuracy in time, we need to resolve space sufficiently good. Consider a Dirichlet plate $(x, y) \in [-5, 5], z = 0$. The plate is discretized with 121 and 289 nodes. We compute the potential $\mathbf{J}^{\text{CFL}}(\mathbf{r}, t)$ on the plate for a point source in $\mathbf{r}_s = (0, 0, 2)$, for different CFL-numbers. The point source produces an incoming wave as in (7.1), with $t_0 = 30$ and $T = 20$. We use 10 quadrature points for the integrals over K . The order of accuracy in time can be computed

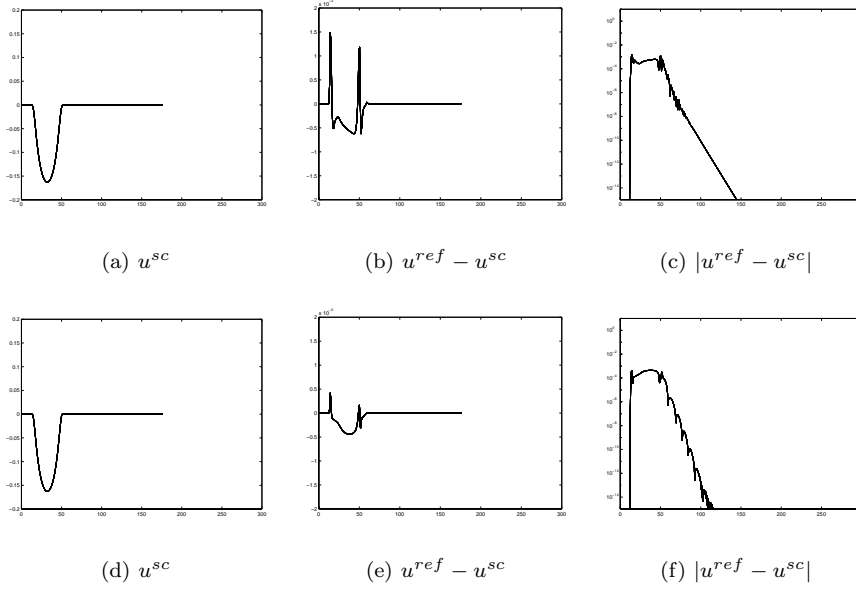


Figure 7.3. Scattered field for a 17×17 plate for $CFL = 1$ (top) and $CFL = 0.5$ (bottom). The scale is different for the first two columns.

numerically by

$$\text{Order of accuracy in time} \approx \log_2 \frac{\|J^{4CFL} - J^{2CFL}\|_{L^2((0, T_{end}), \Gamma)}}{\|J^{2CFL} - J^{CFL}\|_{L^2((0, T_{end}), \Gamma)}}. \quad (7.3)$$

The potential is computed until $t = T_{end} \approx 44.19$. This corresponds to 125 time steps on the 11×11 grid and 200 time steps on the 17×17 grid. The order of accuracy in time is computed and is presented in table 7.2 and we see that this is a first order scheme in time.

CFL	6 pts, no stab.	10 pts, no stab.	6 pts, stab.	10 pts, stab.
1.000	-0.9988	-0.9994	0.6782	0.6752
0.500	-0.9992	-0.9991	0.8212	0.8194
0.250	-1.2189*)	-1.0618*)	0.9062	0.9052
0.125	$-1.4454 \pm 1.6727i^*$)	-2.2671^*)	-1.2997^*)	$0.6597 \pm 0.6885i$

Table 7.1. Eigenvalues of the corresponding one-step method for different CFL-numbers, with and without stabilization filter. *) indicates that the scheme is unstable.

11 × 11 plate			17 × 17 plate		
CFL	$\ J^{2\text{CFL}} - J^{\text{CFL}}\ _{L^2}$	Time order	CFL	$\ J^{2\text{CFL}} - J^{\text{CFL}}\ _{L^2}$	Time order
1.000	0.2754	0.7309	1.000	0.1986	0.8872
0.500	0.1659		0.500	0.1074	
0.250	0.0859	0.9503	0.250	0.0543	0.9841
0.125	0.0431	0.9948	0.125	0.0271	1.0045

Table 7.2. Order of accuracy in time of Dirichlet 11 × 11 plate (left) and a 17 × 17 plate (right).

grid	CFL	$\ J^{2\text{CFL}} - J^{\text{CFL}}\ _{L^2}$	Spatial order
9 × 9	0.81	0.004249	1.5104
13 × 13	0.54		
19 × 19	0.36	0.002303	2.0544
28 × 28	0.24	0.001001	

Table 7.3. Spatial order of Dirichlet plate.

7.4 Order of accuracy in space of Dirichlet plate

We want to do computations to show that the scheme has at least second order of accuracy in space. We have already showed that the scheme is first order in time. The error in the potential is

$$\|J(\Delta t, h) - \tilde{J}\|_{L^2} = C_1 \Delta t + C_2 h^p, \quad (7.4)$$

where \tilde{J} is the exact potential and h is the largest edge of all triangles on the scatterer. In order to get at least second order in space, we compute

$$\text{Spatial order} \geq \log_{\frac{1}{q}} \frac{\|J(\Delta t, h) - J(q^2 \Delta t, qh)\|_{L^2}}{\|J(q^2 \Delta t, qh) - J(q^4 \Delta t, q^2 h)\|_{L^2}}, \quad (7.5)$$

where q is the mesh refinement ratio. Normally $q = \frac{1}{2}$, but this yields a too small CFL-number on the finest grid. In the computation, we use $q = \frac{2}{3}$. The conclusion from the result presented in table 7.3, is that the scheme is second order accurate in space. It would have been good to refine the mesh once more, but then the size of the problem becomes too large.

7.5 Test case with a Dirichlet sphere

As another test, we use a Dirichlet sphere with 92 nodes and 180 triangles, where the incoming field is a plane wave. The speed of sound has been changed to $c_0 = 1$. The incoming field is

$$u^{inc} = \begin{cases} \sin(2\pi\gamma(\mathbf{r}, t))f^\infty\left(\frac{t}{10T} - 1\right), & t < 10T, \\ \sin(2\pi\gamma(\mathbf{r}, t)), & t \geq 10T, \end{cases} \quad (7.6)$$

$$\gamma(\mathbf{r}, t) = \frac{1}{T} \left(t - t_0 - \frac{\hat{k} \cdot \mathbf{r}}{c_0} \right), \quad (7.7)$$

where \hat{k} is the direction of the incoming wave, $T = t_0 = 40$ and $\text{CFL} = \frac{1}{4}$. The solution of this incoming wave is compared to the exact solution of a single frequency, which can be found in [4]. The scattered field is presented in figure 7.4, for three different observation points relative to the direction of the incoming field. The solution matches the analytical solution for all observation points considered.

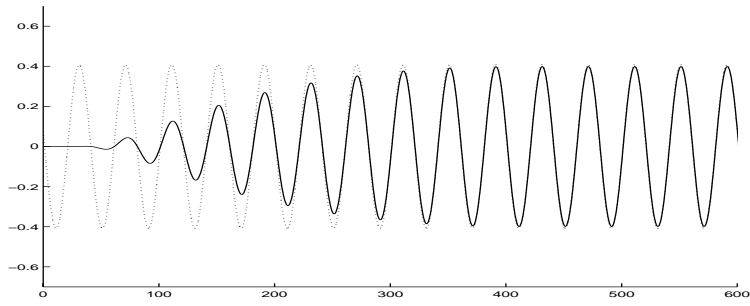
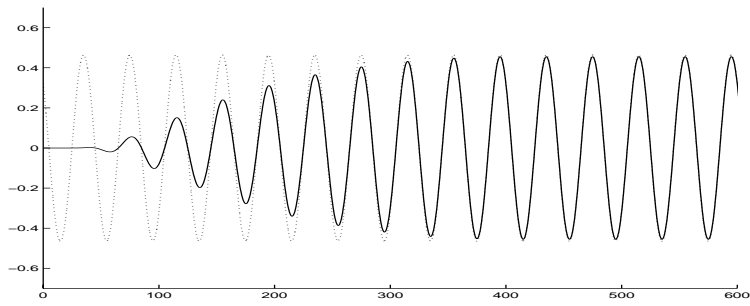
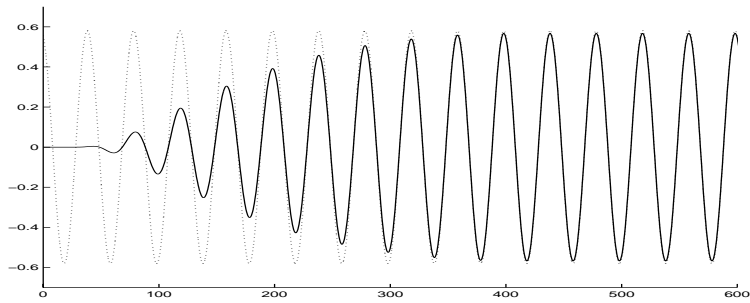
(a) Backscattered field ($\Theta = 0^\circ$).(b) Scattered field perpendicular to incoming field ($\Theta = 90^\circ$).(c) Scattered field behind sphere, relative to incoming field ($\Theta = 180^\circ$).

Figure 7.4. Scattered field for a Dirichlet sphere, with pulse width $T = 40$. The dotted curves are the analytical solutions.

Chapter 8

Numerical experiments on variational formulation from FD

In this section, we will perform numerical tests on the variational formulations 3 and 5 in chapter 3. Two test cases are considered; a point source illuminating a plate and a plane wave illuminating a sphere. Those two cases has an analytical solution.

The variational formulations has a non-negative parameter ω , which depends on the incoming field. Numerical tests are made in the Dirichlet case that indicates that it is sufficient to use $\omega = 0$ in both test cases. The parameter $\omega = 0$ yields a stable scheme for the first 10000 time steps.

In the case of a point source illuminating a Dirichlet plate, the largest eigenvalues are multiple eigenvalues at 1. Long time calculations show no signs of instabilities. The method has first order of accuracy in time in the computation of the potential of the surface, but the spatial order of accuracy seems to be super quadratic.

In the case of a plane wave illuminating a Dirichlet sphere, the computed scattered fields are compared with the analytical solutions at three different observation points.

In the case of a plane wave illuminating a Neumann sphere, the method is unstable. Some comments are made on the possible reasons for the instability.

8.1 Dirichlet plate, with various ω

Consider a 9×9 plate as in section 7.1, with the point source at $\mathbf{r}_s = (0, 0, 2)$ in (7.1). The parameters are $c_0 = 1$, $T = 20$, $t_0 = 30$. The continuous variational formulations discussed in chapter 3 are continuous and coersive whenever a parameter $\omega > 0$, see [1]. In figure 8.1, the errors $u_\omega^{sc} - u_\omega^{ref}$ and $u_\omega^{sc} - u_0^{sc}$ are presented for

different ω . When ω increases, the difference $u_\omega^{sc} - u_0^{sc}$ increases. This indicates that the error increases with ω and the conclusion is that we want to take as small ω as possible. In addition, when $\omega > 0$, many of the integrals are computed numerically. This makes the computer program run much slower than in the case $\omega = 0$, where most integrals has an analytic expression. In practice, the method is only useful for $\omega = 0$. This restricts the incoming field, not to have exponential growth.

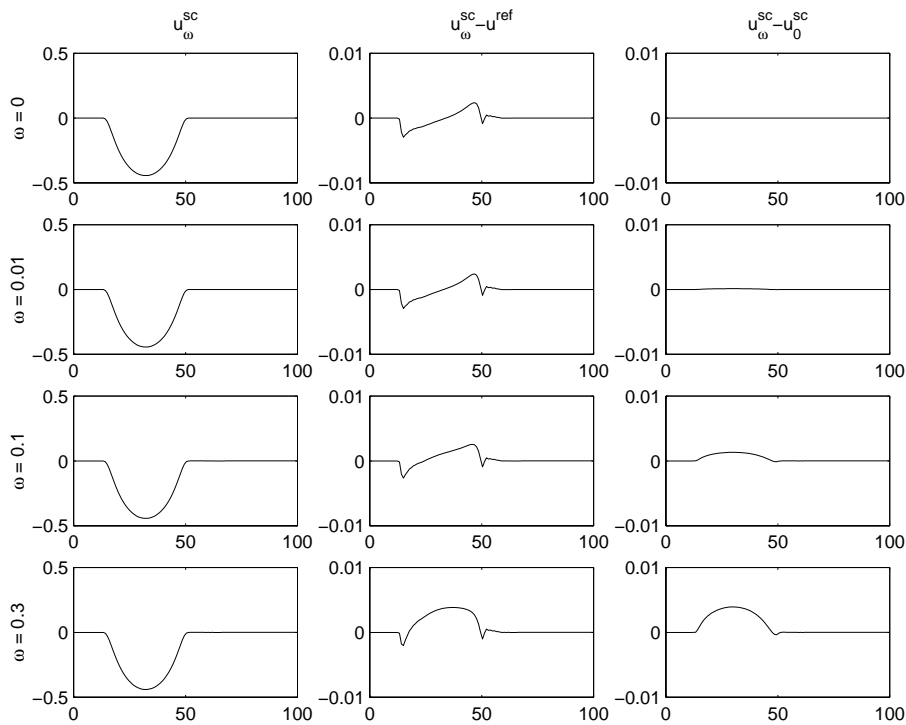


Figure 8.1. Computation on a 9×9 plate, for various ω .

8.2 Stability of Dirichlet plate, with $\omega = 0$

Consider the test case as in (7.1), with a discretized plate with 9×9 nodes. The integral over K is computed with Gaussian quadrature over the triangle, [8]. For adjacent triangle pairs we use 7 Gauss points, for nonadjacent, we use 3 Gauss points. This is not the same quadrature as for the numerical tests of Kirchhoff integral equations. We do computations with CFL-number 1, 0.5, 0.25 and 0.125.

CFL	multiplicity of eigenvalue 1
1.000	≥ 10
0.500	≥ 10
0.250	4
0.125	6

Table 8.1. Multiplicity of eigenvalue 1 on 9×9 plate for different CFL numbers.

The largest eigenvalue is a multiple eigenvalue of 1 (in 14 decimals). The multiplicity of the eigenvalues are listed in table 8.1. The long time behavior, 10000 time steps, of the error with CFL-number 0.5 is illustrated in figure 8.2. This corresponds to a case with an eigenvalue 1 with multiplicity ≥ 10 . There are no visible growth in the error in the first 10000 time steps. The scheme seems to be long time stable.

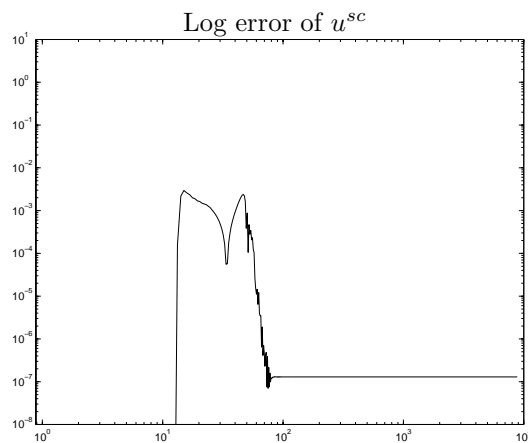


Figure 8.2. Long time error of u^{sc} on test case with a plate with 9×9 nodes and $CFL = 0.5$.

8.3 Stability of Dirichlet sphere, with $\omega = 0$

Consider a Dirichlet sphere with radius 5 and an incidence plane wave as in section 7.5. The parameters are set to $T = t_0 = 20$, $c_0 = 1$ and $\hat{k} = (0, 0, -1)$. Moreover, $CFL = 0.5$. The corresponding one-step method given by (5.4) has a triple eigenvalue at 1. In figure 8.3, we present the computed back scattered field after 10000 time steps. The dotted curve is the analytical solution, in [4]. The computed scattered field match the analytical and there is no indication that the scheme is

unstable. We conclude that for practical computations, $\omega = 0$ is sufficient to get a stable scheme.

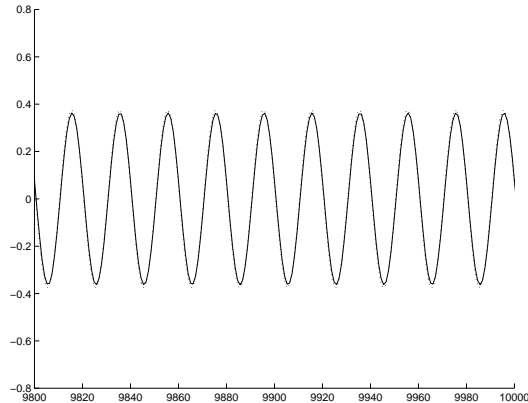


Figure 8.3. Scattered field after 10000 iterations on a test case with a sphere with 92 nodes and $CFL = 0.5$. The dotted curve is the analytical solution.

8.4 Time order of Dirichlet plate, with $\omega = 0$

In order to obtain first order of accuracy in time, we need to resolve the space. Consider a Dirichlet plate $(x, y) \in [-5, 5], z = 0$. The plate is discretized with both 121 and 289 nodes. We want to compute the potential, $\mathbf{J}^{CFL}(\mathbf{r}, t)$, on the plate for a point source at $\mathbf{r}_s = (0, 0, 2)$, using different CFL-numbers. The point source produces an incoming wave as in (7.1), with $t_0 = 30$ and $T = 20$.

I take 125 time steps on the 11×11 plate and 200 time steps on the 17×17 grid. This corresponds to $T_{end} \approx 44.19$. The order of accuracy in time is computed and is presented in table 8.2. This is a first order scheme in time.

8.5 Order of accuracy in space of Dirichlet plate, with $\omega = 0$

In previous section, we concluded that the scheme is first order accurate in time. This is used to determine the order of accuracy in space. We proceed as in section 7.4. Results are presented in table 8.3 and the scheme appears to be more than second order in space.

11 \times 11 plate			17 \times 17 plate		
CFL	$\ J^{2\text{CFL}} - J^{\text{CFL}}\ _{L^2}$	Time order	CFL	$\ J^{2\text{CFL}} - J^{\text{CFL}}\ _{L^2}$	Time order
1.0000	0.8300	0.8951	1.0000	0.4341	0.9131
0.5000	0.4463	0.9477	0.5000	0.2305	0.9564
0.2500	0.2314	0.9736	0.2500	0.1188	0.9761
0.1250	0.1178	0.9919	0.1250	0.0604	0.9912
0.0625	0.0592		0.0625	0.0304	

Table 8.2. Order of accuracy in time of Dirichlet 11 \times 11 plate (left) and a 17 \times 17 plate (right).

grid	CFL	$\ J^{2\text{CFL}} - J^{\text{CFL}}\ _{L^2}$	Spatial order
9 \times 9	0.81	0.010942	
13 \times 13	0.54	0.004400	2.2466
19 \times 19	0.36	0.001721	2.3148
28 \times 28	0.24		

Table 8.3. Order of accuracy in space of Dirichlet plate.

8.6 Dirichlet sphere, with $\omega = 0$

Here we consider a plane wave crossing a Dirichlet sphere with radius 5. The incoming field is a sine wave with a smooth transition at $t = 0$,

$$u^{inc}(\mathbf{r}, t) = \begin{cases} \sin\left(2\pi\frac{t-t_0-\hat{\mathbf{k}}\cdot\mathbf{r}/c_0}{T}\right) f^\infty\left(\frac{t}{10T}\right), & t < 10T, \\ \sin\left(2\pi\frac{t-t_0-\hat{\mathbf{k}}\cdot\mathbf{r}/c_0}{T}\right), & t \geq 10T. \end{cases} \quad (8.1)$$

We compare the computed scattered field with the analytical solution in [4]. In figure 8.4, we compare the back scattered field, the field that is perpendicular to the incoming field and the field behind the sphere relative to the incoming field. We use $CFL = 0.25$ and pulse width $T = 40$. In figure 8.5, we compare the backscattered field for various CFL numbers for pulse width $T = 5$. The energy in the scattered field decreases when CFL is chosen too large.

8.7 Instability of Neumann sphere, with $\omega = 0$

Several test cases have been performed, to get a stable solution to the Neumann sphere. One possible explanation of the instability is that the the spatial basis functions are not sufficiently regular. According to the variational formulation 5 in chapter 3, the basis functions in time should have two continuous derivatives in time. In our implementation, we only use basis functions with one continuous time derivative. This problem can be avoided if we use linear elements in time. However, this results in an implicit scheme.

Another possibility is that we get a problem when we change the order of integration when the integrand contains Dirac δ -functions. This is the case for the integral I_2^ω in section 3.6. However, this integral is also used for the stable Dirichlet variational formulation.

A remark should be made, that if we remove the last term containing I_1^ω in the Neumann variational formulation 8 in chapter 3, then the scheme is stable, but the computed potential does not match the analytical solution.

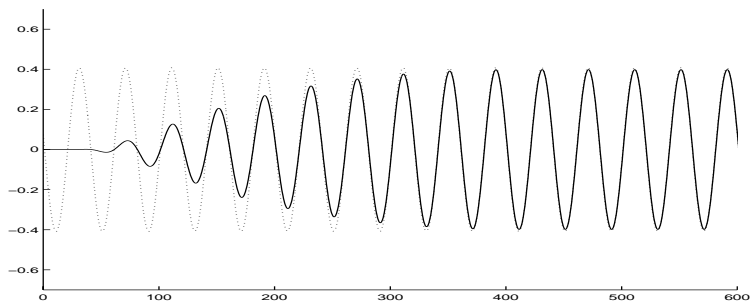
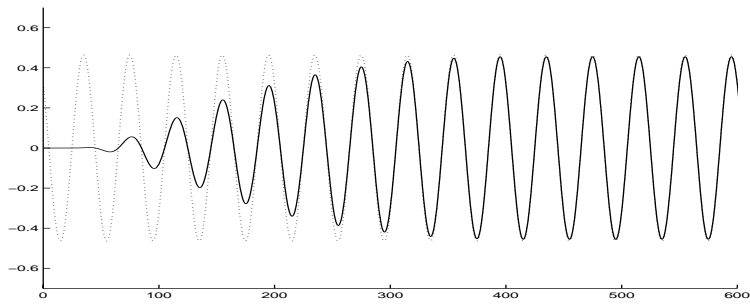
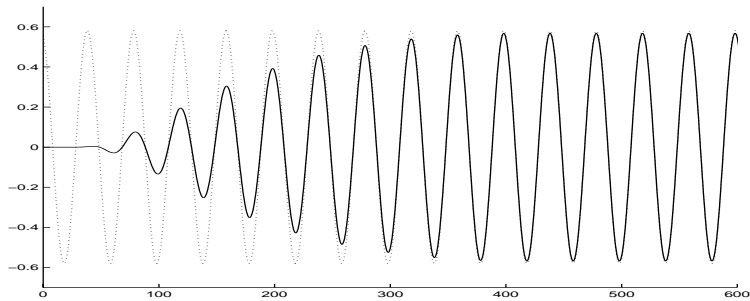
(a) Backscattered field ($\Theta = 0^\circ$).(b) Scattered field perpendicular to incoming field ($\Theta = 90^\circ$).(c) Scattered field behind sphere, relative to incoming field ($\Theta = 180^\circ$).

Figure 8.4. Scattered field for a Dirichlet sphere, with pulse width $T = 40$. The dotted curves are the analytical solutions.

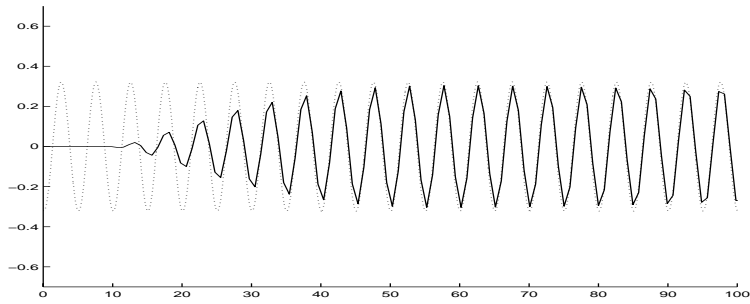
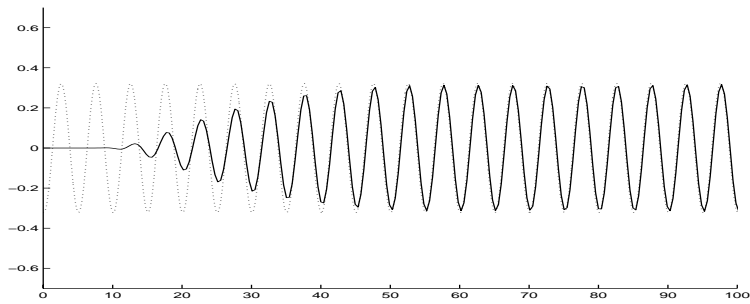
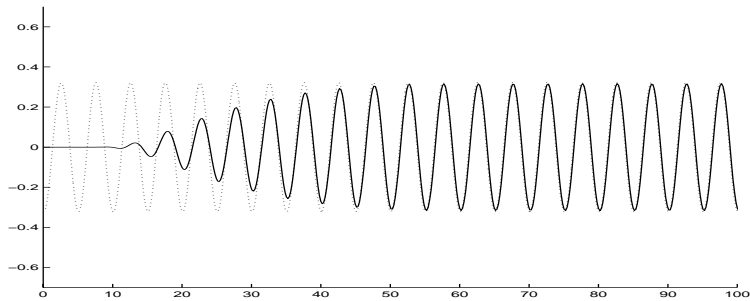
(a) Scattered field ($\Theta = 180^\circ$), when $CFL = 0.4$.(b) Scattered field ($\Theta = 180^\circ$), when $CFL = 0.2$.(c) Scattered field ($\Theta = 180^\circ$), when $CFL = 0.1$.

Figure 8.5. Scattered field for a Dirichlet sphere, with pulse width $T = 5$. The dotted curves are the analytical solutions.

Chapter 9

On Surface Radiation condition

When solving an integral formulation of the wave equation (9.1) with the Marching On in Time method (MOT), described in chapter 6, the computational cost of the k -step marching algorithm increases substantially with the size of the object (or as the frequency increases). In other words, MOT is a low to moderate frequency method. For high frequencies, the method is expensive to use. There are several ways of improving the computational complexity. In frequency domain, we have the fast multipole method. In time domain, Michielssen [10] has developed PWTD, using plane waves to reduce the cost for the matrix-vector multiplications in MOT. Existing high frequency approximations that are used in frequency domain are for instance physical optics (PO), e.g. by Edlund [9] and general theory of diffraction (GTD), by Keller [16]. These methods are only accurate approximations in the limit of high frequencies. We want to develop a high frequency approximation for MOT, by constructing a PDE for the scattered field on the surface of the scatterer. Then we can use the boundary condition to replace the scattered field with the incoming field on the surface. The goal is to express the scattered field as an integral of the incoming field over the surface of the scatterer. This approach is called On Surface Radiation Condition (OSRC). This has been done in frequency domain by G.A. Kriegsmann [18] and D.S. Jones [15].

The OSRC method can be outlined as follows,

- Express scattered field u^{sc} in spherical coordinates and insert the field as a solution in the wave equation.
- We obtain a relation that couples u^{sc} , $\frac{\partial u^{sc}}{\partial t}$ and $\frac{\partial u^{sc}}{\partial n}$.
- Use the boundary condition of the scatterer to eliminate appropriate terms in the relation.

- Insert the relation in Kirchhoff formula for the scattered field, s.t. the scattered field on the surface is eliminated or is easily computed.

The resulting integral formula contains no global coupling over the surface. Instead we at most solve a local problem for each point on the surface.

9.1 On Surface Radiation Condition (OSRC)

We want to solve the scalar wave equation for the scattered field,

$$\nabla^2 u^{sc} - \frac{1}{c^2} \frac{\partial^2}{\partial t^2} u^{sc} = 0, \quad \text{with } u^{sc} = 0, \text{ for } t \leq 0, \quad (9.1)$$

in the exterior of a scatterer. Write the solution in spherical coordinates, [19]

$$u^{sc}(R_0, \theta, \phi, t) = \sum_{i=1}^{\infty} \frac{f_i(t - R_0/c, \theta, \phi)}{R_0^i}, \quad (9.2)$$

where R_0 is the distance to the center of the scatterer. By inserting the expansion in the wave equation (9.1), we get

$$\sum_{i=1}^{\infty} \frac{1}{R_0^{i+2}} \left(\frac{2i}{c} (f_{i+1})_t + i(i-1)f_i + \nabla_0^2 f_i \right) = 0. \quad (9.3)$$

By truncation and letting $R_0 \rightarrow \infty$, the approximate relation

$$(f_{i+1})_t = -\frac{c}{2} \left((i-1)f_i + \frac{1}{i} \nabla_0^2 f_i \right), \quad (9.4)$$

is solved (with $f_i(-\infty, \theta, \phi) = 0$)

$$f_{i+1}(t, \theta, \phi) = -\frac{c}{2} \int_{-\infty}^t (i-1)f_i(\tau, \theta, \phi) + \frac{1}{i} \nabla_0^2 f_i(\tau, \theta, \phi) d\tau. \quad (9.5)$$

From (9.2), we derive the relation

$$\begin{aligned} \frac{\partial u^{sc}}{\partial R_0} &= -\frac{1}{c} \frac{\partial u^{sc}}{\partial t} - \frac{u^{sc}}{R_0} - \frac{f_2(t - R_0/c, \theta, \phi)}{R_0^3} + \mathcal{O}(R_0^{-4}) \\ &= -\frac{1}{c} \frac{\partial u^{sc}}{\partial t} - \frac{u^{sc}}{R_0} + \frac{c}{2R_0^3} \int_{-\infty}^{t-R_0/c} \nabla_0^2 f_1(\tau, \theta, \phi) d\tau + \mathcal{O}(R_0^{-4}). \end{aligned} \quad (9.6)$$

From (9.5), we express f_1 in u^{sc}

$$f_1(t - R_0/c, \theta, \phi) = R_0 u^{sc}(R_0, \theta, \phi, t) + \mathcal{O}(R_0^{-1}), \quad (9.7)$$

which yields

$$\frac{\partial u^{sc}}{\partial R_0} = -\frac{1}{c} \frac{\partial u^{sc}}{\partial t} - \frac{u^{sc}}{R_0} + \frac{c}{2R_0^2} \int_0^t \nabla_0^2 u^{sc}(R_0, \theta, \phi, \tau) d\tau + \mathcal{O}(R_0^{-3}). \quad (9.8)$$

In order to compute the scattered field, we need to couple the incoming and scattered field on the scatterer boundary. In the coupling, we need the normal derivative

rather than the radial. By Jones, [15], we go to non-spherical coordinates by the substitutions

$$\frac{\partial u^{sc}}{\partial R_0} \rightarrow \frac{\partial u^{sc}}{\partial n}, \quad (9.9)$$

$$\frac{1}{R_0} \rightarrow H(\mathbf{r}), \quad (\text{Curvature at } \mathbf{r}), \quad (9.10)$$

$$\frac{1}{R_0^2} \nabla_0^2 u^{sc} \rightarrow \nabla_{\Gamma}^2 u^{sc}, \quad (9.11)$$

$$\frac{\partial u^{sc}}{\partial n}(\mathbf{r}, t) + \frac{1}{c} \frac{\partial u^{sc}}{\partial t}(\mathbf{r}, t) + H(\mathbf{r}) u^{sc}(\mathbf{r}, t) = \frac{c}{2} \int_0^t \nabla_{\Gamma}^2 u^{sc}(\mathbf{r}, \tau) d\tau \quad (9.12)$$

The condition (9.12) is used together with the Kirchhoff formula (2.3) to derive a method to compute the scattered field for both a Dirichlet and a Neumann boundary condition on the surface. A program is implemented for a Dirichlet sphere.

9.2 Dirichlet problem

For the Dirichlet problem, we have the boundary condition

$$u^{inc} + u^{sc} = 0, \quad \frac{\partial}{\partial t}(u^{inc} + u^{sc}) = 0 \quad (9.13)$$

on the boundary Γ . Together with the derived condition (9.12), we can write the Kirchhoff formula (2.3) (with $u_*^{inc} = u^{inc}(\mathbf{r}', t - R/c)$)

$$u^{sc}(\mathbf{r}, t) = \frac{1}{4\pi} \int_{\Gamma} K_1^D(R) \frac{\partial u_*^{inc}}{\partial t} + K_2^D(R, \mathbf{r}') u_*^{inc} + K_3^D[u^{inc}](R) d\Gamma', \quad (9.14)$$

$$K_1^D(R) = \frac{1}{cR} \left(1 - \frac{\partial R}{\partial n} \right), \quad (9.15)$$

$$K_2^D(R, \mathbf{r}') = \frac{\partial}{\partial n} \left(\frac{1}{R} \right) + \frac{1}{R} H(\mathbf{r}'), \quad (9.16)$$

$$K_3^D[u^{inc}](R) = -\frac{c}{2R} \int_0^{t-R/c} \nabla_{\Gamma}^2 u^{inc} d\tau. \quad (9.17)$$

We get a direct representation of the scattered field.

9.3 Neumann problem

For the Neumann problem, we have the boundary condition

$$\frac{\partial}{\partial n}(u^{inc} + u^{sc}) = 0, \quad (9.18)$$

on the boundary Γ . Together with the derived condition (9.12), the ODE

$$\frac{1}{c} \frac{\partial u^{sc}}{\partial t}(\mathbf{r}, t) + H(\mathbf{r})u^{sc}(\mathbf{r}, t) - \frac{c}{2} \int_0^t \nabla_{\Gamma}^2 u^{sc}(\mathbf{r}, \tau) d\tau = \frac{\partial u^{inc}}{\partial n}(\mathbf{r}, t) \quad (9.19)$$

is derived. Solving this ODE for each point $\mathbf{r} \in \Gamma$ yields $u^{sc}(\mathbf{r}, t)$ on Γ . Next we eliminate the time derivative

$$\frac{1}{c} \frac{\partial u^{sc}}{\partial t}(\mathbf{r}, t) = \frac{\partial u^{inc}}{\partial n}(\mathbf{r}, t) - H(\mathbf{r})u^{sc}(\mathbf{r}, t) + \frac{c}{2} \int_0^t \nabla_{\Gamma}^2 u^{sc}(\mathbf{r}, \tau) d\tau \quad (9.20)$$

which can be inserted in the Kirchhoff formula (2.3) and we get

$$u^{sc}(\mathbf{r}, t) = \frac{1}{4\pi} \int_{\Gamma} K_1^N(R) \frac{\partial u_*^{inc}}{\partial n} + K_2^N(R, \mathbf{r}') u_*^{sc} + K_3^N[u^{sc}](R) d\Gamma', \quad (9.21)$$

$$K_1^N(R) = \frac{1}{R} \left(\frac{\partial R}{\partial n} - 1 \right), \quad (9.22)$$

$$K_2^N(R, \mathbf{r}') = - \left(\frac{\partial}{\partial n} \left(\frac{1}{R} \right) + \frac{1}{R} \frac{\partial R}{\partial n} H(\mathbf{r}') \right), \quad (9.23)$$

$$K_3^N[u^{sc}](R) = \frac{c}{2R} \frac{\partial R}{\partial n} \int_0^{t-R/c} \nabla_{\Gamma}^2 u^{sc}(\mathbf{r}', \tau) d\tau. \quad (9.24)$$

A time stepping scheme is obtained, in which for each time step k

1. Solve the ODE in (9.19) to get $u^{sc}(\mathbf{r}, k\Delta t)$ on the scatterer Γ .
2. Compute $K_3^N[u^{sc}](R)$.
3. Compute the scattered field in the exterior, in (9.21).

9.4 Dirichlet test case on sphere

As a simple test case, we have chosen a sphere with radius R_0 . The sphere Γ is parameterized by

$$x = R_0 \cos \phi \sin \theta, \quad (9.25)$$

$$y = R_0 \sin \phi \sin \theta, \quad (9.26)$$

$$z = R_0 \cos \theta, \quad (9.27)$$

where $\phi \in [0, 2\pi]$ and $\theta \in [0, \pi]$. The sphere is discretized with a uniform mesh in θ and ϕ , with $M\Delta\theta = \pi$, $N\Delta\phi = 2\pi$ and

$$\theta_i = i\Delta\theta, \quad i = 1, \dots, M-1, \quad (9.28)$$

$$\phi_j = j\Delta\phi, \quad j = 1, \dots, N-1. \quad (9.29)$$

The curvature is constant

$$H(\mathbf{r}') = \frac{1}{R_0}$$

and the surface Laplace-Beltrami-operator is

$$\nabla_{\Gamma}^2 u^{inc} = \frac{1}{R_0^2} \nabla_0^2 u^{inc} = \frac{1}{R_0^2} \left(\frac{1}{\sin \theta} \frac{\partial}{\partial \theta} \left(\sin \theta \frac{\partial u^{inc}}{\partial \theta} \right) + \frac{1}{\sin^2 \theta} \frac{\partial^2 u^{inc}}{\partial \phi^2} \right) \quad (9.30)$$

For a sphere, we have

$$\sin \theta \nabla_0^2 u(R_0, \theta, \phi) = 0, \quad \theta = 0, \pi. \quad (9.31)$$

Moreover $\sin \theta \nabla_0^2 u$ is 2π -periodic in ϕ . Let $u_{i,j} = u(\theta_i, \phi_j)$ and the operator 9.30 can be discretized as

$$\begin{aligned} \sin \theta_i \nabla_0^2 u_{i,j} &= D_{0,i} \sin \theta_i D_{0,i} u_{i,j} + \frac{1}{\sin \theta_i} D_{+,j} D_{-,j} u_{i,j} + \mathcal{O} \left(\Delta \theta^2 + \frac{\Delta \phi^2}{\sin \theta_i} \right), \\ D_{0,i} \sin \theta_i D_{0,i} u_{i,j} &= \frac{\sin \theta_{i+1/2} u_{i+1,j} - (\sin \theta_{i+1/2} + \sin \theta_{i-1/2}) u_{i,j} + \sin \theta_{i-1/2} u_{i-1,j}}{\Delta \theta^2}, \\ D_{+,j} D_{-,j} u_{i,j} &= \frac{u_{i,j+1} - 2u_{i,j} + u_{i,j-1}}{\Delta \phi^2}. \end{aligned}$$

The discretization error is large for θ close to 0 and π . But for those values of θ , the expression $\sin \theta \nabla_0^2 u(R_0, \theta, \phi)$ is vanishing, and we can hope that the error does not destroy the expected second order accuracy.

9.4.1 Numerical experiments

We use the incoming field as in equation (7.1), with $T = 5$, $t_0 = 10$ and $\hat{k} = (1, 0, 0)$. The sphere with radius $R_0 = 5$ is discretized with 21×21 points in ϕ and θ and use $\Delta t = \frac{1}{8}$. As a reference solution, we use the solution obtained by the Dirichlet MOT solver in chapter 3 with a sphere with 92 nodes and 180 triangles. The computed solutions is presented in figure 9.1. The OSRC solution somewhat resembles the solution obtained by the MOT solver.

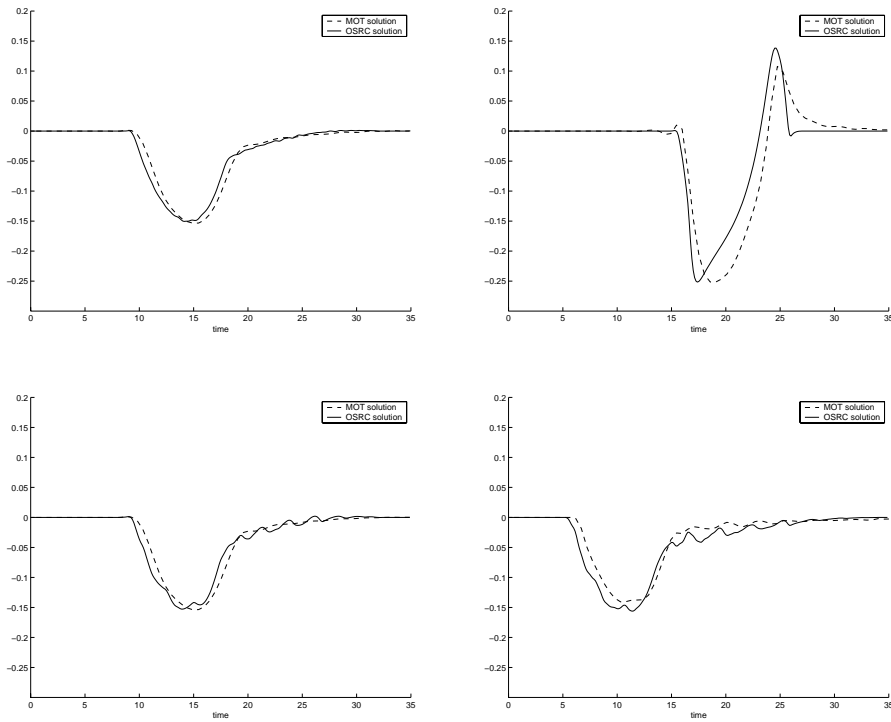


Figure 9.1. OSRC solution vs MOT solution of the scattered field for different observation points \mathbf{r} .
 Upper left: $\mathbf{r} = (0,0,10)$, Upper right: $\mathbf{r} = (10,0,0)$,
 Lower left: $\mathbf{r} = (0,10,0)$, Lower right: $\mathbf{r} = (-10,0,0)$

Appendix A

Numerical Integration

A.1 Numerical integration

During the assembly process, we need to evaluate some integrals numerically. This appendix, will discuss how to evaluate integrals over an interval, over a triangle and over a square. When integrating over a square, the domain is divided into two triangles, and the algorithm for a triangle is used. The goal is to develop high order adaptive methods. The integral over a line uses a 6th order Romberg method. The integral over a triangle uses a seven point Gaussian quadrature, proposed by Dunavant in [8]. This is also a 6th order method.

A.1.1 Numerical integration over an interval

The goal is to integrate

$$I_f = \int_0^1 f(x) dx \tag{A.1}$$

numerically, using a five point 6th order Romberg scheme

$$\int_{x_0}^{x_4} f(x) dx = \frac{x_4 - x_0}{90} (7f(x_0) + 32f(x_1) + 12f(x_2) + 32f(x_3) + 7f(x_4)), \tag{A.2}$$

where x_j are equidistant. In the adaptive Romberg method, we have a stack with elements consisting of the five x -values, their function values and the integral over the current segment. A stack consist of two operations:

- operation push adds an element to the top of the stack
- operation pop reads and removes an element from the top of the stack

Initially we push the whole interval to be integrated. In the refinement step, we pop an element and divide the current segment into two, with half the length. If the integrals on the refined segments differ from the integral over the current segment, then we push the two refined segments. If the integral over the segment is accurate enough, we add the integral value to the result. The result is extrapolated one time to get an eight order scheme. The procedure is repeated as long the stack is nonempty.

Algorithm 5 Adaptive Romberg method

```

1: {Initialization part}
2: res = 0
3: w =  $\frac{1}{90}[7, 32, 12, 32, 7]$ 
4: x =  $[0, \frac{1}{4}, \frac{1}{2}, \frac{3}{4}, 1]$ 
5:  $f_j = \text{fun}(x_j), j = 0, \dots, 4$ 
6: int = w·f
7: push(x, f, int)
8: {Divide and Conquer part}
9: while stack nonempty do
10:  [x, f, int] = pop
11:  {First half of segment}
12:   $x_{11} = \frac{1}{2}(x_0+x_1), f_{11}=\text{fun}(x_{11})$ 
13:   $x_{31} = \frac{1}{2}(x_1+x_2), f_{31}=\text{fun}(x_{31})$ 
14:   $\text{int}_1=(x_2-x_0)(w \cdot [f_0, f_{11}, f_1, f_{31}, f_2])$ 
15:  {Second half of segment}
16:   $x_{12} = \frac{1}{2}(x_2+x_3), f_{12}=\text{fun}(x_{12})$ 
17:   $x_{32} = \frac{1}{2}(x_3+x_4), f_{32}=\text{fun}(x_{32})$ 
18:   $\text{int}_2=(x_4-x_2)(w \cdot [f_2, f_{12}, f_3, f_{32}, f_4])$ 
19:  if  $|\text{int}_1+\text{int}_2-\text{int}| > (x_4-x_0) \cdot \text{TOL} \cdot \max\{1, f_2\}$  then
20:    {Further refinement needed, store results}
21:    x =  $[x_0, x_{11}, x_1, x_{31}, x_2]$ 
22:    f =  $[f_0, f_{11}, f_1, f_{31}, f_2]$ 
23:    push(x, f, int1)
24:    x =  $[x_2, x_{12}, x_3, x_{32}, x_4]$ 
25:    f =  $[f_2, f_{12}, f_3, f_{32}, f_4]$ 
26:    push(x, f, int2)
27:  else
28:    {Integrals are sufficiently accurate, add to result}
29:    res = res +  $\frac{1}{63}(64 \cdot (\text{int}_1 + \text{int}_2) - \text{int})$ 
30:  end if
31: end while

```

A.1.2 Numerical integration over a triangle

The goal is to integrate

$$I_f = \int_0^1 \int_0^{1-\alpha} f(\alpha, \beta) d\beta d\alpha \quad (\text{A.3})$$

numerically, using a seven point Gaussian quadrature, that is exact for polynomials up to order 5, [8]. The idea of our method is to divide the triangle into two parts as indicated by figure A.1. The ordering of the nodes of the refined triangles are important. If the node order is “wrong”, then we may divide the same side of the triangle in all refinements and we obtain triangles that is only refined in one dimension. Each subtriangle is integrated using the 7 point integration formula. We map the local coordinates to the global by

$$\alpha = a_0 + a_1\alpha^l + a_1\beta^l, \quad (\text{A.4})$$

$$\beta = b_0 + b_1\alpha^l + b_1\beta^l. \quad (\text{A.5})$$

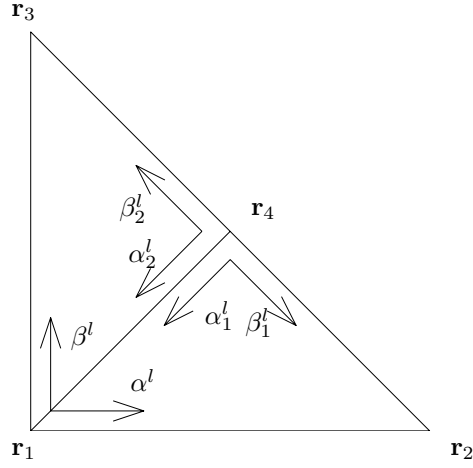


Figure A.1. Parametrization of triangle

The refined domains has the local mapping

$$\alpha^l = \frac{1}{2}(1 - \alpha_1^l + \beta_1^l), \quad (\text{A.6})$$

$$\beta^l = \frac{1}{2}(1 - \alpha_1^l - \beta_1^l), \quad (\text{A.7})$$

$$\alpha^l = \frac{1}{2}(1 - \alpha_2^l - \beta_2^l), \quad (\text{A.8})$$

$$\beta^l = \frac{1}{2}(1 - \alpha_2^l + \beta_2^l). \quad (\text{A.9})$$

Combining the two mappings yields the mapping of the refined to the global coordinates,

$$a_{01} = a_0 + \frac{1}{2}(a_1 + a_2), \quad (\text{A.10})$$

$$a_{11} = -\frac{1}{2}(a_1 + a_2), \quad (\text{A.11})$$

$$a_{21} = \frac{1}{2}(a_1 - a_2), \quad (\text{A.12})$$

$$a_{02} = a_0 + \frac{1}{2}(a_1 + a_2), \quad (\text{A.13})$$

$$a_{12} = -\frac{1}{2}(a_1 + a_2), \quad (\text{A.14})$$

$$a_{22} = -\frac{1}{2}(a_1 - a_2). \quad (\text{A.15})$$

The mapping for b_{ij} are exactly the same (up to the constants b_j).

In the adaptive integration method, we need a stack with elements consisting of these constants (a_j and b_j), the integral value and also the area of the triangle. The algorithm works similar to the algorithm used for an interval. We don't extrapolate the result in the triangle case.

A.1.3 Numerical integration over a square

The goal is to integrate

$$I_f = \int_0^1 \int_0^1 f(\alpha, \beta) d\alpha d\beta \quad (\text{A.16})$$

numerically. To evaluate this, perform a variable substitution and gets two integrals over a triangle,

$$I_f = \int_0^1 \int_0^{1-\alpha} f(\alpha, \beta) d\beta d\alpha + \int_0^1 \int_0^{1-\alpha} f(1-\alpha, 1-\beta) d\beta d\alpha. \quad (\text{A.17})$$

In the initialization phase of the adaptive method for the triangle, we push two elements with the constants

$$a_1 = [0, 1, 0], \quad (\text{A.18})$$

$$b_1 = [0, 0, 1], \quad (\text{A.19})$$

$$a_2 = [1, -1, 0], \quad (\text{A.20})$$

$$b_2 = [1, 0, -1], \quad (\text{A.21})$$

together with the area = 1 and the computed integral values.

Algorithm 6 Adaptive method for the triangle

```

1: {Initialization part}
2: res = 0
3: area = 1/2
4: a = [0, 1, 0]
5: b = [0, 0, 1]
6: int = integrate(fun, a, b)
7: push(area, a, b, int)
8: {Divide and Conquer part}
9: while stack nonempty do
10:  [area, a, b, int] = pop
11:  {First half of segment}
12:  area2 = area / 2
13:  a01 = a0 +  $\frac{1}{2}$  (a1+a2)
14:  a11 =  $-\frac{1}{2}$  (a1+a2)
15:  a21 =  $\frac{1}{2}$  (a1-a2)
16:  b01 = b0 +  $\frac{1}{2}$  (b1+b2)
17:  b11 =  $-\frac{1}{2}$  (b1+b2)
18:  b21 =  $\frac{1}{2}$  (b1-b2)
19:  int1 = area2·integrate(fun, [a01, a11, a21], [b01, b11, b21])
20:  {Second half of segment}
21:  a.2 = [a01, a11, -a21]
22:  b.2 = [b01, b11, -b21]
23:  int2 = area2·integrate(fun, [a02, a12, a22], [b02, b12, b22])
24:  if |int1+int2-int| > ar·TOL then
25:    {Further refinement needed, store results}
26:    push(area2, [a01, a11, a21], [b01, b11, b21], int1)
27:    push(area2, [a02, a12, a22], [b02, b12, b22], int2)
28:  else
29:    {Integrals are sufficiently accurate, add to result}
30:    res = res + int1 + int2
31:  end if
32: end while

```

A.1.4 L^2 -norm calculations using basis functions

In the Marching On in Time method with constant elements in time and linear elements in space, we should get a solution that is first order in time and second order in space. To verify this we need to specify a norm, to measure the order in. Our choice is to use the L^2 norm defined by

$$\|f\|_{L^2(\Gamma,(0,T))}^2 = \int_{\Gamma} \int_0^T f(\mathbf{r},t)^2 dt d\Gamma. \quad (\text{A.22})$$

Using linear basis functions in space, we have

$$f(\mathbf{r},t) = \sum_K \sum_{j=1}^3 f_j^K(t) \Phi_j^K(\mathbf{r}), \quad (\text{A.23})$$

$$\|f\|_{L^2}^2 = \sum_K \frac{2|K|}{12} (g_{11}^K + g_{22}^K + g_{33}^K + g_{12}^K + g_{13}^K + g_{23}^K), \quad (\text{A.24})$$

where

$$g_{jk}^K = \int_0^T f_j^K(t) f_k^K(t) dt. \quad (\text{A.25})$$

The integrand in (A.25) is a piecewise constant function.

Bibliography

- [1] A. Bamberger and T. Ha Duong. Formulation variationnelle espace-temps pour le calcul par potentiel retarde de la diffraction d'une onde acoustique. *Math. Meth. in the Appl. Sci.*, 8:405–435, 1986.
- [2] A. Bamberger and T. Ha Duong. Formulation variationnelle pour le calcul de la diffraction d'une onde acoustique par une surface rigide. *Math. Meth. in the Appl. Sci.*, 8:598–608, 1986.
- [3] C. L. Bennett and H. Mieras. Time domain integral equation solution for acoustic scattering from fluid targets. *J. Acoust. Soc. Am.*, 69(5):1261–1265, 1981.
- [4] J. J. Bowman, T. B. A. Senior, and P. L. E. Uslenghi. *Electromagnetic and Acoustic Scattering by Simple Shapes, revised printing*. A SUMMA Book, 1987.
- [5] P. J. Davies. Numerical stability and convergence of approximations of retarded potential integral equations. *SIAM J. Numer. Anal.*, 31:856–875, 1994.
- [6] P. J. Davies and D. B. Duncan. Averaging techniques for time-marching schemes for retarded potential integral equations. *Appl. Num. Math.*, 23:291–310, 1997.
- [7] Y. Ding, A. Forestier, and T. Ha Duong. A galerkin scheme for the time domain integral equation of acoustic scattering from a hard surface. *J. Acoust. Soc. Am.*, 86(4):1566–1572, 1989.
- [8] D. A. Dunavant. High degree efficient symmetrical gaussian quadrature rules for the triangle. *J. Num. Meth. Eng.*, 21:1129–1148, 1985.
- [9] J. Edlund. *A parallel, iterative method of moments and physical optics hybrid solver for arbitrary surfaces*. PhD thesis, Upsala University, 2001. Dissertation.
- [10] A. A. Ergin, B. Shanker, and E. Michielssen. Fast evaluation of three-dimensional transient wave fields using diagonal translation operators. *J. Comp. Phys.*, 146:157–180, 1998.

- [11] M.B. Friedman and R.P. Shaw. Diffraction of pulses by cylindrical obstacles of arbitrary cross section. *J. Appl. Mech.*, 29:40–46, 1962.
- [12] T. Ha Duong, B. Ludwig, and I. Terrasse. A galerkin bem for transient acoustic scattering by an absorbing obstacle. *J. Num. Meth. Eng.*, 57:1845–1882, 2003.
- [13] R. F. Harrington. *Time Harmonic Electromagnetic Fields*. Wiley, 1961.
- [14] J. D. Jackson. *Classical Electrodynamics, 3rd edition*. Wiley, 1998.
- [15] D. S. Jones. An approximate boundary condition in acoustics. *J. Sound and Vibration*, 121(1):37–45, 1988.
- [16] J. B. Keller. Geometrical theory of diffraction. *J. opt. soc. of Amer.*, 52(2):61–72, February 1962.
- [17] J. J. Knab. Interpolation of band-limited functions using the approximate prolate series. *IEEE Trans. on Information Theory*, 25:717–720, 1979.
- [18] G. A. Kriegsmann, A. Taflove, and K. R. Umashankar. A new formulation of electromagnetic wave scattering using an on-surface radiation boundary condition approach. *IEEE Trans. Antennas Propagat.*, AP-35 No. 2:153–161, 1987.
- [19] T.G. Moore, G.B. Baschak, A. Taflove, and G.A. Kriegsmann. Theory and application of radiation boundary operators. *IEEE Trans. Antennas Propagat.*, 36 No. 12:1797–1812, 1988.
- [20] J. C. Nedelec. *Acoustic and Electromagnetic Equations: Integral representations for Harmonic Problems*. Springer-Verlag Telos, 2001.
- [21] A. Peterson, S. Ray, and R. Mittra. *Computational Methods for Electromagnetics*. IEEE Press, 1998.
- [22] J. A. Stratton. *Electromagnetic Theory*. McGraw-Hill, 1941.
- [23] I. Terrasse. *Resolution mathématique et numérique des équations de Maxwell instationnaires par une méthode de potentiels retardés*. PhD thesis, L’Ecole Polytechnique, 1993.
- [24] D. A. Vechinski and S. M. Rao. A stable procedure to calculate the transient scattering by conducting surfaces of arbitrary shape. *IEEE Trans. Antennas Propagat.*, 40(4):157–180, 1992.
- [25] D. S. Weile, B. Shanker, and E. Michielssen. An accurate scheme for the numerical solution of the time domain electric field integral equation. *2001 IEEE International Sym.*, 4, 2001.